THERMAL RATCHETING OF THIN SHELLS: SIGNIFICANCE OF THERMOMECHANICAL INTERACTIONS

By

ASHUTOSH MISHRA

ENGG02201104012

Indira Gandhi Centre for Atomic Research, Kalpakkam

A thesis submitted to the

Board of Studies in Engineering Sciences

In partial fulfillment of requirements

for the Degree of

DOCTOR OF PHILOSOPHY

of

HOMI BHABHA NATIONAL INSTITUTE

February, 2016

HOMI BHABHA NATIONAL INSTITUTE

Recommendations of the Viva Voce Committee

As members of the Viva Voce Committee, we certify that we have read the dissertation prepared by **Mr. Ashutosh Mishra** entitled "**Thermal ratcheting of thin shells: Significance of thermomechanical interactions**" and recommend that it may be accepted as fulfilling the thesis requirement for the award of Degree of Doctor of Philosophy.

Chairman - **Dr. M. Sai Baba**	Date: 13-2-16
Guide / Convener - **Dr. P. Chellapandi**	Date: 13/2/16
Co-guide - **Dr. G. Sasikala**	Date: 13.2.2016
Examiner - **Prof. C. Lakshmana Rao**	Date: 13/2/16
Member 1- **Dr. K. Laha**	Date: 13.2.2016.
Member 2- **Dr. V.S. Srinivasan**	Date: 13/2/2016

Final approval and acceptance of this thesis is contingent upon the candidate's submission of the final copies of the thesis to HBNI.

I hereby certify that I have read this thesis prepared under my direction and recommend that it may be accepted as fulfilling the thesis requirement.

Date: 13.2.2016

Place: Kalpakkam

13/2/2016
Co-guide

Guide 13/2/16

STATEMENT BY AUTHOR

This dissertation has been submitted in partial fulfillment of requirements for an advanced degree at Homi Bhabha National Institute (HBNI) and is deposited in the Library to be made available to borrowers under rules of the HBNI.

Brief quotations from this dissertation are allowable without special permission, provided that accurate acknowledgement of source is made. Requests for permission for extended quotation from or reproduction of this manuscript in whole or in part may be granted by the Competent Authority of HBNI when in his or her judgment the proposed use of the material is in the interests of scholarship. In all other instances, however, permission must be obtained from the author.

Mishra

Ashutosh Mishra

DECLARATION

I, hereby declare that the investigation presented in the thesis has been carried out by me. The work is original and has not been submitted earlier as a whole or in part for a degree / diploma at this or any other Institution / University.

Ashutosh Mishra

LIST OF PUBLICATIONS

Journals

1. "Effect of frequency of free level fluctuations and hold time on the thermal ratcheting behavior", A. Mishra, P. Chellapandi, R. Suresh Kumar and G. Sasikala, *International Journal of Pressure Vessels and Piping,* **2015**, *Vol.*, 129-130, 1-11.
2. "Effect of Temperature Rate Term while Predicting Thermal Ratcheting of a Thin Cylinder due to Cyclic Temperature Variation", A. Mishra, P. Chellapandi, R. Suresh Kumar and G. Sasikala, *Transactions of the Indian Institute of Metals.* **2015**, *Vol.,* 68, 161-169.
3. "Comparative study of cyclic hardening behavior of SS 316L using time independent and dependent constitutive modeling: A simplified semi-implicit integration approach", A. Mishra, P. Chellapandi, R. Suresh Kumar and G. Sasikala, *Transactions of the Indian Institute of Metals,* **2015**, *Vol.*, 68, 623-63.
4. "Progressive deformation behaviour of thin cylindrical shell under cyclic temperature variation using Combined Hardening Chaboche Model", A. Mishra, R. Suresh Kumar, and P. Chellapandi, *Latin American Journal of Solids and Structure*, **2014**, *Vol.*, 11, 980-992.
5. "Influence of the frequency of level fluctuations with reference to progressive deformation of thin cylindrical shell", A. Mishra, R. Suresh Kumar, G. Sasikala and P. Chellapandi, *Procedia Engineering*, **2014,** *Vol.*, 86, 95 -102.
6. "Time dependent ratcheting of thin cylindrical shell due to axial temperature variation using visco-plastic model", A. Mishra, R. Suresh Kumar, and P. Chellapandi, *International Journal of Engineering and Technology*, **2014**, *Vol.*, 6, 234-237.
7. "Experimental and numerical simulation of thermal ratcheting behavior with thermomechanical interactions", A. Mishra, Kulbir Singh, R. Suresh Kumar and P. Chellapandi, *International Journal of Pressure Vessels and Piping* (**Under review**).

Conferences

1. A. Mishra, R. Suresh Kumar, G. Sasikala and P. Chellapandi. Significance of thermo-mechanical interaction in thermal ratcheting behavior. 7th International Conference on Creep, Fatigue and Creep-fatigue Interaction (CF-7), 19-22 January, **2016**, Indira Gandhi Centre for Atomic Research, Kalpakkam, India.
2. A. Mishra, P. Chellapandi, R. Suresh Kumar and G. Sasikala. Effect of temperature rate term while predicting thermal ratcheting of a thin cylinder due to cyclic temperature variation. International Symposium for Research Scholars on Metallurgy, Materials Science and Engineering (ISRS-2014), 11^{th}-12^{th} Dec, **2014**, IITM, India.
3. A. Mishra, R. Suresh Kumar, G. Sasikala and P. Chellapandi. Influence of the frequency of level fluctuations with reference to progressive deformation of thin cylindrical shell. First International Conference on Structural Integrity (ICONS-2014), 4^{th} -7^{th} Feb, **2014**, Kalpakkam.
4. A. Mishra, R. Suresh Kumar and P. Chellapandi. Shakedown study of thin cylindrical shell due to moving temperature distribution using combined hardening Chaboche model. Indian Conference on Applied Mathematics (INCAM 2013), 4^{th} -6^{th} July, **2013**, IIT Madras, India.
5. A. Mishra, R. Suresh Kumar and P. Chellapandi. Simulation of thermal ratcheting of thin cylindrical shell due to moving temperature distribution using combined hardening Chaboche model. International Conference on Pressure Vessel and Piping (OPE 2013), 13^{th} -16^{th} Feb, **2013**, Mamallapuram, Chennai, India.

(Ashutosh Mishra)

DEDICATED

TO

MY PARENTS

ACKNOWLEDGEMENTS

- To my guide **Dr. P. Chellapandi** (*Prof. HBNI, CMD Bhavini & Former Director, RDG, IGCAR*) for being my source of guidance. His strong opinions, questions and suggestions have significantly improved my work. His regular motivation, everlasting patience and technical advices helped me solving all the research related issues.
- To my doctoral committee chairman: **Dr. M. Sai Baba** (*Associate Director, RMG, IGCAR*) who acted as my troubleshooter, and Co-guide: **Dr. G. Sasikala** (*Dean HBNI*, *IGCAR & Head MMS, IGCAR*) for her guidance and mentoring.
- To the doctoral committee members: **Dr. K. Laha** *(Head, CSS, IGCAR)* and **Dr. V.S. Srinivasan (***SO/G, MDTG, IGCAR*) whose regular feedback brought improvement in the wok.
- To **Mr. Suresh Kumar** (*Head, SML, IGCAR*) for being my friendly reviewer of the research works and intensively helping me developing the new thermal ratcheting facility and carrying out the experiments.
- To **Shri P. Selvaraj** (*Associate Director, RAG, IGCAR*) and **Shri S. Jalaldeen** (*Head, SMS, IGCAR*) for providing a conducive and competitive research environment at my work place.
- To **Dr. S.A.V Satyamurthy** (*Director, IGCAR*), **Dr. Baldev Raj**, **Dr. S.C. Chetal** and **Dr. P.R. Vasudeva Rao,** (*Former Directors, IGCAR*), for providing the facilities and healthy research environment to pursue the research activities.
- To **Shri R. Jehadeesan** (*Computer Division, IGCAR*), and staff members for providing me the high performance computing facility, which has led to quicker results.
- To. **Dr. R.B. Grover** (*Director, HBNI, Mumbai*) and **Dr. B.K. Dutta**, (*Dean, HBNI, Mumbai*) for allowing me to continue my research and approving the financial assistance.

- To **Dr. R. Sandhya** (*Head, FSS, IGCAR*) and **Mr. Sunil Goyal** (*Scientific Officer, MMD, IGCAR*) for providing uniaxial test data required for parameter identification.
- To Scientific officers **Mr. R.P. Pandey**, **Mr. Kulbir Singh**, **Mr. Pavan Patel**, **Mr. B. Thilak**, **Mr. Gagan Gupta, Mr. Bhuwan Chnadra Sati, Mr. S.K. Pandey** and other RDG and SML staff members for all the encouragements, discussions, suggestions. To the administrative staff of RDG for timely assistance.
- Special thanks to **Dr. H-Y Lee** (*Principle researcher, Korea Atomic Research Institute*) for providing very useful technical suggestions that helped me carrying out time independent thermal ratcheting analysis.
- To the reviewers and editors of journals, conferences, and symposiums for reviewing my work.
- To my friends: **Anil, Srihari, Deepak, Zuber, Srinivas Srijan, Santhana, Navtesh, Atul, Shashwat, Subrat, Manas** and others for all the fun times we had and for *just being there* for me.
- To the **Department of Atomic Energy** (DAE) for providing me the generous fellowship to carry out the research as DGFS Ph.D fellow.

CONTENTS

Title	Page No.
ABBREVIATIONS	i
SYNOPSIS	iii
LIST OF FIGURES	v
LIST OF TABLES	x

CHAPTER 1	**INTRODUCTION**	**1-7**
1.1	BACKGROUND	3
1.2	PROBLEM STATEMENT	5
1.3	OBJECTIVE AND SCOPE OF THE WORK	6
1.4	THESIS STRUCTURE	7
CHAPTER 2	**LITERATURE REVIEW**	**9-36**
2.1	INTRODUCTION TO PLASTICITY	9
	2.1.1 Theory and formulation of ratcheting	10
	2.1.2 Time independent and dependent ratcheting models	22
2.2	THERMAL RATCHETING BECHMARKS	30
	2.2.1 Thermal ratcheting caused by primary and secondary loading	30
	2.2.2 Thermal ratcheting caused by secondary loading	32
2.3	SUMMARY	36
CHAPTER 3	**THERMAL RATCHETING ANALYSIS: ISOTHERMAL**	**37-76**
3.1	INTRODUCTION	37
3.2	NUMERICAL MODELING- DEVELOPMENT OF CODE FOR PREDICTION OF RATCHETING	38
	3.2.1 Governing equations	39
	3.2.2 Proposed simplified semi-implicit integration procedure	40

3.2.3 Flowchart for the adopted SSIP: Isothermal……….........................43

3.3 BENCHMARK ANALYSIS: TIME INDEPENDENT AND DEPENDENT MODELING...45

3.3.1 Time independent modeling..46

3.3.2 Time dependent modeling...49

3.4 NUMERICAL ANALYSIS AND RESULTS...50

3.4.1 Cyclic hardening behavior...50

3.4.2 Thermal ratcheting of cylindrical shell...55

3.4.3 Effect of frequency of free level variation in thermal ratcheting..64

3.4.4 Contribution of hold time in thermal ratcheting..............................69

3.5 SUMMARY...75

CHAPTER 4 THERMAL RATCHETING ANALYSIS: NON-ISOTHERMAL……………………………..………….....….....77-92

4.1 INTRODUCTION...77

4.2 NUMERICAL MODELING: DEVELOPMENT OF CODE FOR PREDICTION OF RATCHETING...78

4.2.1 Governing equations..79

4.2.2 Proposed simplified semi-implicit integration procedure…….…......79

4.2.3 Flowchart for the adopted SSIP: Non-isothermal……......................79

4.3 BENCHMARK ANALYSIS: TEMPERATURE RATE DEPENDENT MODELING...81

4.4 THERMOMECHANICAL INTERACTION STUDIES: TWO-BAR SYSTEM..84

4.4.1 Effect of phase shift in thermomechanical loading..........................85

4.4.2 Effect of thermal load rates..87

4.5 THERMOMECHANICAL INTERACTION STUDIES: CYLINDRICAL SHELL...88

4.5.1 Imposed thermal loading...88

4.5.2 Effect of concurrent change in the peak temperature with the moving temperature front...89

4.6 SUMMARY...92

CHAPTER 5 **EXPERIMENTAL AND NUMERICAL SIMULATIONS / APPLICATIONS**............ **93-110**

5.1 INTRODUCTION............ 93

5.1.1 Experiment and specimen details............ 95

5.1.2 Applied thermal loading............ 97

5.1.3 Test results............ 98

5.2 MATERIAL PARAMETER IDENTIFICATION............ 101

5.2.1 Specimen description and applied loading............ 101

5.2.2 Uniaxial tensile and cyclic hardening behavior............ 102

5.3 THERMAL RATCHETING: HARDENING RULES WITHOUT TEMPERATURE RATE TERMS............ 104

5.3.1 Numerically simulated thermal loading............ 104

5.3.2 Numerical results............ 105

5.4 THERMOMECHANICAL RATCHETING: HARDENING RULES WITH AND WITHOUT TEMPERATURE RATE TERMS............ 107

5.4.1 Effect of concurrent change in peak temperature with the moving temperature front............ 107

5.4.2 Numerical results............ 108

5.5 SUMMARY............ 110

CHAPTER 6 **CONCLUSIONS AND FUTURE SCOPE**............ **111-115**

6.1 CONCLUSIONS............ 111

6.1.1 Technical and scientific contribution............ 114

6.2 FUTURE SCOPE............ 115

REFERENCES............ **116-125**

ABBREVIATIONS

SFR	:	Sodium Cooled Fast Reactors
ISI	:	In-Service Inspection
FBTR	:	Fast Breeder Test Reactor
PFBR	:	Prototype Fast Breeder Reactor
IHX	:	Intermediate Heat Exchanger
SG	:	Steam Generator
PSP	:	Primary Sodium Pumps
DHR	:	Decay Heat Removal
SGDHR	:	Safety Grade Decay Heat Removal
IHX	:	Intermediate Heat Exchangers
TRT	:	Temperature Rate Terms
LKH	:	Linear Kinematic Hardening
AF	:	Armstrong and Frederick
CH3	:	Chaboche three tack stress
OW	:	Ohno and Wang
DSA	:	Dynamic Strain Aging
UVP	:	Unified Visco-plastic Constitutive Model
SPC	:	Plasticity-Creep Superposition Model
SSIP	:	Simplified Semi-implicit Integration Procedure
HT	:	550 °C
RT	:	27 °C
OD	:	Outer Diameter
SL	:	Stress Level
CT	:	Cycle Time

SVC	:	Visco-Plasticity-Creep Superposition Model
TLR	:	Thermal Load Rate
TML	:	Thermomechanical Loadings
TMF	:	Thermomechanical Fatigue
IP	:	In Phase
OP	:	Out of Phase
VFD	:	Variable-Frequency Drive
TC	:	Thermocouple

SYNOPSIS

The phenomenon of progressive deformation with increase in plastic strains cycle by cycle, such that collapse or failure of the structure occurs after gross plastic deformation, is termed as *Ratcheting*. Moreover, ratcheting in a cylindrical shell subjected to cyclic axial thermal gradients due to moving temperature front, with and without mechanical load, is a special category, termed as thermal ratcheting. It is an important failure criterion, which needs to be carefully considered while designing nuclear reactor components viz. Main vessel. Thermal ratcheting in the main vessel of Sodium cooled Fast Reactors (SFR) occur due to sodium free level variations.

The free level variations cause high thermal variations leading to high stress variations. This high temperature and stress loading for longer time introduce creep strain along with thermal ratcheting strain. Thermal ratcheting can cause dimensional instability due to excessive deformation beyond allowable limits prescribed by the design codes. Additionally, the accumulated inelastic strain in radial direction may affect the movement of in-service inspection (ISI) system between the gap of the main vessel and the safety vessel that assess the extent of damage if any to keep it under control. Therefore, the inelastic radial deformation is highly undesirable as it will pose problems during in-service inspection and satisfying safety criteria.

Robust design rules are not available in the design codes and realistic inelastic analysis is the only route to predict thermal ratcheting due to free level variations. During free level variations, the temperatures are different at different axial positions and hence, the constitutive model should consider temperature dependent material parameters. The ratcheting behavior of austenitic stainless steels exhibit plastic straining with cyclic hardening features beyond yield point. To simulate such inelastic behavior accurately, it is essential to involve sophisticated constitutive model. Out of various constitutive models reported in literatures, no single model is robust enough to cover the various aspects of mechanics and metallurgy to accurately predict the realistic ratcheting behavior. Further, it is quite challenging to perform numerical analysis by implementing different user defined constitutive models. Transformation of the complex constitutive rate equations of the chosen model into incremental equations to apply different integration procedure is another challenging task. Focusing these aspects, the present work addressed the thermal ratcheting behavior of smooth cylindrical shell using different constitutive models highlighting the significance of different loading methods. Especially, simplified expressions for plasticity integration for time independent and dependent constitutive models have been proposed. The simplified expressions can directly be used for UMAT coding in ABAQUS while predicting ratcheting strain. This work also presents the experimental and numerical simulation of thermal ratcheting with thermomechanical interaction effects in ratcheting behavior of two-bar system and cylindrical shell. The proposed approach can widely be implemented for studying deformation behavior under uniaxial or multiaxial ratcheting simulation under time independent, time dependent and temperature rate dependent loadings. The present work includes a critical design aspect of main vessel of SFR for its safe and reliable operating life.

LIST OF FIGURES

Figure No.	Figure Title	Page No.
Figure 1.1	Typical flow sheet of pool type fast breeder reactor	2
Figure 1.2	Typical sodium free levels in the main vessel of SFR	4
Figure 2.1	Typical stress-strain behavior of materials	10
Figure 2.2	Cyclic deformation behavior of hardening materials	11
Figure 2.3	Schematic response to various cyclic input variables [14]	12
Figure 2.4	(a) Schematics of the isotropic hardening in the deviatoric plane and the stress verses plastic strain response (b) Schematics of the linear kinematic hardening in the deviatoric plane and the stress verses plastic strain response [16]	14
Figure 2.5	The von Mises yield surface for conditions of plane stress, showing the increment in plastic strain $\mathbf{d\varepsilon^P}$ as per normality law	15
Figure 2.6	Predictions of cyclic behavior from Prager's rule for (a) strain-controlled stable hysteresis loop (b) axial strain at positive stress peaks of uniaxial cycles [19]	17
Figure 2.7	Predictions of cyclic behavior from Armstrong and Frederick rule for (a) strain-controlled stable hysteresis loop, (b) axial strain at positive stress peaks of uniaxial cycles [19]	18
Figure 2.8	Prediction of cyclic behavior using Chaboche three back stress (CH3) rule (a) strain controlled stable hysterisis loop (b) axial strain at positive stress peaks of uniaxial cycles [19]	20
Figure 2.9	Prediction using Ohno and Wang model (a) strain controlled stable hysterisis loop (b) axial strain at positive stress peaks of uniaxial cycles [19]	21
Figure 2.10	Stress-strain curve of material at different strain rates ε_1 and ε_2 is shown by dotted lines while continuous line is the response of material under sudden changes in the rates	25
Figure 2.11	Experimental and simulated monotonic tensile behavior: (a), (b) at room temperature (c), (d) at 700 ºC [36]	27
Figure 2.12	Evolution of ratcheting strain (78 ± 234 MPa) with number of cycles at room temperature for different stressing rates: (a) experiment and simulations by the UVP and SPC model (b) experiment and simulations by the SVC model [36]	27

Figure 2.13 Evolution of ratcheting strain (78 ± 234 MPa: at 2.6 MPa/s) with number of cycles at room temperature with and without peak/valley stress hold: (a) experiment and simulations by the UVP and SPC models (b) experiment and simulations by the SVC model [36] 28

Figure 2.14 Evolution of ratcheting strain (40 ± 100 MPa) with number of cycles at 700 ºC for different stressing rates: (a) experiment and simulations by the UVP and SPC models(b) experiment and simulations by the SVC model [36]..28

Figure 2.15 Evolution of ratcheting strain (40 ± 100 MPa: at 10 MPa/s) with number of cycles at 700 ºC with and without peak/valley stress hold: (a) experiment and simulations by the UVP and SPC models (b) experiment and simulations by the SVC model [36]....................................28

Figure 2.16 Bree's diagram for non-work hardening material and constant yield strength [38]..31

Figure 2.17 Temperature and stress distribution along the cylinder height [54]..............32

Figure 2.18 Temperature and level variations during decay heat removal operations [49]..35

Figure 3.1 Flowchart for the SSIP: Isothermal..44

Figure 3.2 (a) Schematic of the experimental setup for ratcheting and (b) Transient temperature profile measured by thermocouples as per Lee et al. [50]..47

Figure 3.3 Comparison of residual displacement (a) after 3rd cycle and (b) after 9th cycle..48

Figure 3.4 (a) Monotonic stress-strain curve at different strain rates (b) Comparison of cyclic stress-strain behavior of SS 316 L at strain rate of 6.67×10^{-4}/s (at 550°C). 49

Figure 3.5 (a) Schematic of stress controlled loading (b) Stress strain plots obtained using *Model-1* and *Model-2* at room temperature (RT)..................51

Figure 3.6 Evolution of axial strain (a) for *Model-1* at room temperature. (b) for *Model-2* at room temperature (c) for *Model-1* at 550 °C (d) for *Model-2* at 550 °C 52

Figure 3.7 Peak strain developed per cycle: at room temperature (a) for *Model-1* (b) for *Model-2*, at 550°C, (c) for *Model-1* (d) for *Model-2*..........................53

Figure 3.8 Variation in peak strain increment with no. of cycles: at room temperature (a) for *Model-1* (b) for *Model-2*: at 550°C, (c) for *Model-1* (d) for *Model-2* 55

Figure 3.9 Profile of residual radial displacements in outward direction (after 9th cycle upto 15th cycle)..57

Figure 3.10 (a) Temperature distribution along the axis of cylinder (b) Profiles of residual radial displacements in inward direction for 15 cycles....................58

Figure 3.11 Comparison of residual displacements for *Type-I* (radialy outward) and *Type-II* (radialy inward)..59

Figure 3.12 Temperature distribution along the axis of the cylinder after different time instances of 40 s interval. 60

Figure 3.13 (a) Profile of residual displacements for 20 cycles (b-d) Stress-Strain hysteresis loops at (b) 325 mm (c) at 345 mm and (d) at 390 mm from bottom of cylinder...61

Figure 3.14 (a) Residual radial displacement with no. of cycles (b) Radial displacement with time (outward direction)..63

Figure 3.15 Residual radial displacements for the cycle time 240 seconds for (a) *Model-1* (b) For *Model-2*..65

Figure 3.16 Comparison of residual radial displacement (outward) for *Model-1* and *Model-2* after 10th cycle (a) for CT-240 (b) for CT-320 (c) for CT-400 (d) for CT-480...66

Figure 3.17 Comparison of residual radial displacement with no of ratchet cycles for *Model-1* and *Model-2* (a) for CT-240 (b) for CT-320 (c) for CT-400 (d) for CT-480 67

Figure 3.18 Residual radial displacement (outward) with no. of ratchet cycles at various cycle times (a) For *Model-1* (b) For *Model-2*..................................69

Figure 3.19 Schematic of stress controlled uniaxial loading...71

Figure 3.20 Evolution of creep strain with hold time (a) At 100 MPa stress hold (b) At 120 MPa stress hold...72

Figure 3.21 Residual radial displacements for 10 cycles (a) At cycle time 250 seconds (CT-250) with 5 seconds hold time (b) At cycle time 260 seconds (CT-260) with 10 seconds hold time 73

Figure 3.22 Evolution of radial displacement with hold time and without hold time (a) At cycle time 250 seconds (CT-250) (b) At cycle time 260 seconds (CT-260) 74

Figure 4.1 Flowchart for the SSIP: Non-isothermal..80

Figure 4.2 (a) Two-bar system (b) Thermal loading for Test-A (c) Thermal loading for Test-B according to Kuhner et al. [73].......................................82

Figure 4.3 Comparison of the present analysis with the ratcheting results of two-bar system obtained by Kuhner et al. [73] experimentally and numerically using AF, Sievert, Chaboche rule and Kuhner's modified model (a) Corresponding to Test-A (b) Corresponding to Test-B 83

Figure 4.4 Loading schemes for *Study-A* and *Study-B* 85

Figure 4.5 Evolution of strain for IP/OP loadings (a) for *Study-A* load (b) for *Study-B* load (c) peak strain evolution with no. of cycles (d) plastic strain evolution with time 86

Figure 4.6 Evolution of strain for different thermal load rate (TLR) for *Study-C* 87

Figure 4.7 (a) Schematic of thermal ratcheting setup (b) Traveling temperature front along the axis after different time instances of 40 s 89

Figure 4.8 Residual radial displacements of cylinder for thermal load rates R1, R2 and R2 using constitutive model with temperature rate term and without temperature rate term 90

Figure 4.9 Evolution of residual radial displacements with the number of cycles (a) for rates R1 and R2 showing radial outward growth (b) for rate R3 showing radial inward growth 91

Figure 5.1 (a) Schematic of thermal ratcheting test setup (b) Actual thermal ratcheting test setup 96

Figure 5.2 Specimen geometry and location of thermocouples for thermal ratcheting test 97

Figure 5.3 Profiles of the moving temperature front recorded by thermocouples (TC) for *specimen 1* (Experimental): *Case-A Type-III* load 98

Figure 5.4 Measured residual radial displacements of the cylinder for *specimen 1* and *specimen 2* 99

Figure 5.5 (a) Hoop strain evolution for *specimen 1* and *specimen 2* (b) Residual radial displacement for *specimen 1* and *specimen 2* 100

Figure 5.6 Specimen geometry for the LCF tests 102

Figure 5.7 (a) Tensile stress-strain curve (450 °C) (b) Hysteresis loop at ±0.4 % strain range (c) Hysteresis loop at at ±0.6 % strain range (d) Hysteresis loop at ±0.8 % strain range (e) Stabilized hysteresis loop (450 °C) at strain rate 3×10^{-3}/s for ±0.8 % strain range 103

Figure 5.8 Profiles of the moving temperature front at different time instances for s*pecimen 1* (Numerical): *Case-A Type-III* load 104

Figure 5.9 Comparison of experimental and numerical prediction of residual radial displacements for *specimen 1* : *Case-A Type-III* load (a) after 10th cycle (b) after 20th cycle 105

Figure 5.10 Evolution of residual radial displacement with the number of cycles for AF and CH3 rules using SSIP: *Case-A Type-III* load 106

Figure 5.11 Moving temperature front with increasing peak temperature: *Case-B* load 107

Figure 5.12 Growth in residual radial displacements for *Case-B* load corresponding to CH3 rule with and without TRT after (a) 5 (b) 10 (c) 15 and (d) 20 cycles 108

Figure 5.13 Deformed cylinders after 20 cycles for *Case-B* load (a) corresponding to CH3 rule without TRT (b) corresponding to CH3 rule with TRT 109

LIST OF TABLES

Table No.	Table Title	Page No.
Table 2.1	Deformation behavior of SS 304 using three time dependent models	29
Table 3.1	Material parameters for *Model-1* and *Model-2*	46
Table 3.2	Cases for various cycle times (CT)	64
Table 3.3	Maximum residual radial displacements (U1) for various cycle times	67
Table 4.1	Non-isothermal material parameters for SS 316 LN [73]	81
Table 4.2	Thermomechanical loading for various cases	84
Table 4.3	Loadings for different temperature ranges and corresponding thermal load rates	89
Table 5.1	Summary of loading cases analyzed	95
Table 5.2	Identified material parameters at 450 ºC for AF and CH3 rules	104

INTRODUCTION 1

Energy is the key requirement of society to drive and improve the life. It is directly linked with the development of the mankind. With the growing population and rapid industrialization, the energy consumption rate is growing at a faster pace. This is creating a large energy deficit, which requires to be reduced to maintain demand-supply equilibrium. For a developing country such as India, there is a huge demand of energy. Among several energy generation methods, the non-conventional and renewable sources of energy being environment friendly are preferred globally. Nuclear energy is considered to be one of the clean and sustainable sources of energy. At present around 20% of electricity in US and 74% in France is generated through nuclear energy. India has an ambitious plan to extend its power generation capacity through nuclear energy to 20,000 MWe by 2020. Safety and reliability of energy through nuclear power plants with SFR are essential issues to be addressed to satisfy the public concern of danger besides the obvious economic viability.

SFR provide sustainable and environmentally acceptable energy and preferred worldwide over the years to come. SFR are very effective for handling actinides and long lived fission products in the waste management. They can be designed to incinerate high-level wastes arising from the reprocessing of spent fuel. In the concept of integrated SFR with co-located fuel cycle, it is possible to derive wealth from waste, i.e. fission products, such as ^{137}Cs, will be separated and used as a radiation source in various societal applications. This approach minimizes the quantity of waste to be immobilized on a long term basis. Further, SFR would provide critical liquid metal technology and high temperature design inputs for the future accelerated driven systems, fusion and high temperature reactor systems. These apart, they can provide electricity at competitive costs over long periods. Hence, SFR are the most preferred and inevitable option for providing sustainable energy systems.

In India, SFR are essential for effective utilization of limited natural uranium resource and converting the abundant thorium available to ^{233}U, required for third stage of Indian Nuclear Energy Programme. India needs Fast Breeder Reactors, in view of its ever-increasing energy requirements and limited availability of other energy resources. Fast Breeder Reactors provide energy security and diversity and form a large energy resource. Towards development of SFR, India developed a 40 MW thermal power *loop type* Fast Breeder Test Reactor (FBTR) in 1985 [1]. Afterwards, a 500 MW electric power *pool type* reactor called as Prototype Fast Breeder Reactor (PFBR) was designed and is under construction in India [2]. A typical flow sheet of pool type fast breeder reactor is shown in Figure 1.1.

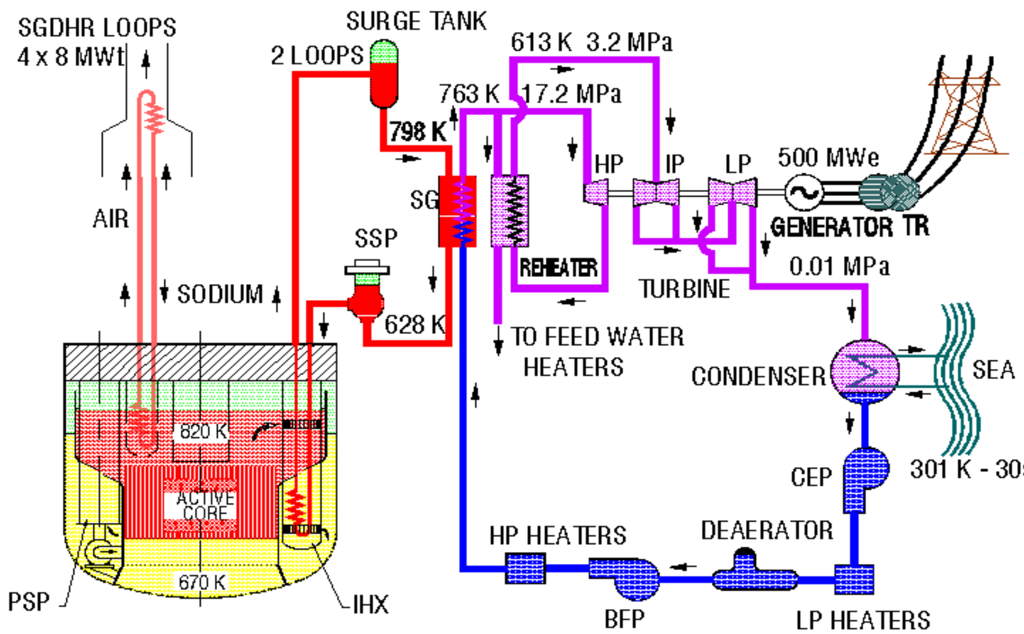

Figure 1.1 Typical flow sheet of pool type fast breeder reactor

Heat energy released during the fission process in the core is transported to steam generator by liquid sodium as a coolant in various steps. There are two loops for coolant flow, viz. primary and secondary loop. Pumps are provided to maintain the flow in these loops. Heat energy is first transferred to secondary sodium loop through the intermediate heat exchanger (IHX). Then the energy is used to convert the water into steam in steam generator (SG). The core, primary sodium pumps (PSP) and intermediate heat exchangers (IHX) are submerged in liquid sodium inside the main vessel in case of pool type reactors. The main vessel of reactor assembly houses the hot and the cold sodium pools, separated by an Inner vessel. Both the pools have a free sodium surface blanketed by argon. The nuclear heat generated in the core is removed by circulating sodium from the cold pool at 397 ºC to the hot pool, which is at 547 ºC. The sodium from hot pool transports the heat to four intermediate heat exchangers and joins back to the cold pool. Two primary sodium pumps maintain the circulation of sodium from the cold pool to the hot pool. The flow of sodium through intermediate heat exchangers is driven by a level difference (1.5 m of sodium) between the hot and the cold pool free surfaces. The heat from intermediate heat exchangers is transferred to eight steam generators by sodium in the secondary circuit while steam produced in steam generators is supplied to turbo-generator.

1.1 BACKGROUND

The main vessel of SFR is one of the most critical components that contain large quantities (~ 1150 t in PFBR) of radioactive liquid sodium at high temperature. Any failure or damage to the main vessel may lead to serious consequences, hence it is designed specially without any penetrations and the bottom closure shape is such that its buckling resistance is enhanced. Safety vessel is provided to collect the leaking sodium in the remote event of any sodium leakage from the main vessel. The inter vessel space between the main vessel and the safety vessel is filled with nitrogen. The gap is ~300 mm to permit robotic visual and ultrasonic inspection of the vessels and to keep the sodium level to about 250 mm minimum above the bottom of inlet windows of IHX which ensures continued cooling of the core in case of a main vessel leak. There are several possible modes of failure of the main vessel such as high cycle fatigue, low cycle fatigue, thermal stripping shell buckling, ratcheting etc. Ratcheting is one of the widely researched modes of failure to ensure safe functionality of the main vessel. Ratcheting is caused due to the sodium free level variations in the main vessel. The free levels according to the Figure 1.2 are hot pool level within an inner vessel, cold pool level between inner vessel and inner thermal baffle, restitution collector level between inner and outer thermal baffles, feeding collector level between outer thermal baffle and main vessel.

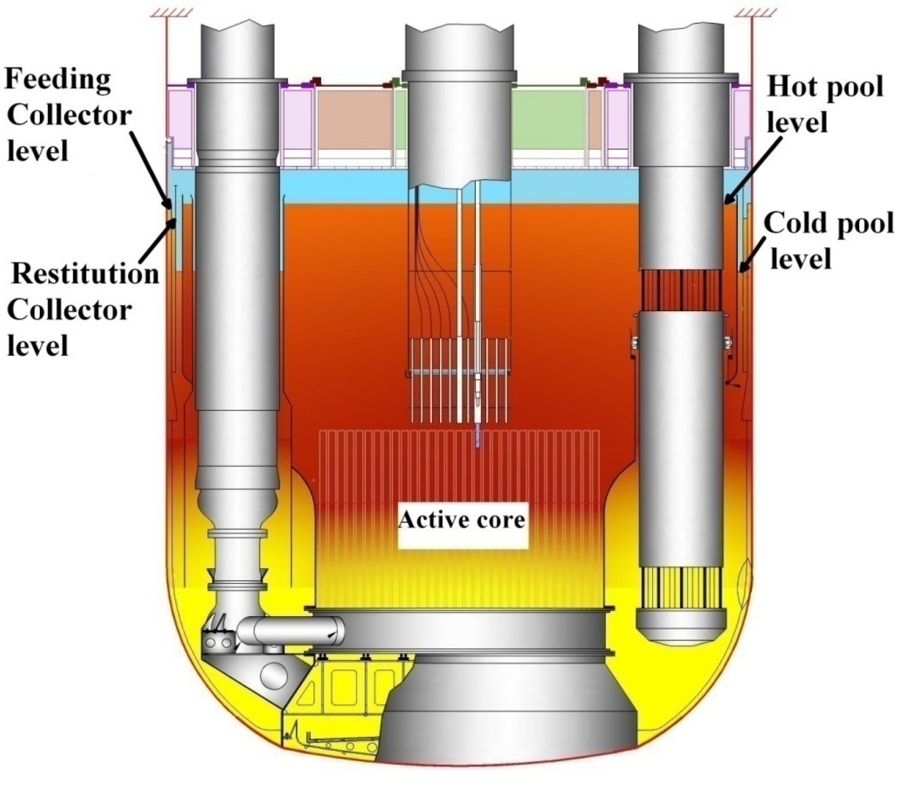

Figure 1.2 Typical sodium free levels in the main vessel of SFR

The sodium free level difference between the hot and cold pools is a function of sodium circulation rate through the PSP, which is also a function of reactor power. The sodium free level varies during normal operations and other operating conditions depending upon the temperatures of hot and cold pools. Significant free level variations occur during fuel handling and Decay

Heat Removal (DHR) operations as mentioned in next chapter. During normal operation, the upper cylindrical portion of the inner vessel (near the vicinity of hot pool sodium free level) is highly affected by the level variations. The wetting surface of the inner vessel experiences the temperature of sodium immediately without an appreciable film drop, because of the high heat transfer coefficient of sodium. On the contrary, heat transfer coefficient of argon contact surface is low and the temperature is approximately equal to the mean value (337 °C) between hot pool surface temperature (547 °C) and roof-slab bottom temperature (127 °C). This results in high temperature oscillations. However, the present work is focused to study the thermal ratcheting phenomenon in the main vessel, which is prominent during DHR operations rather during normal operation. The temperature changes approximately by 125 °C along with the sodium free level variation in feeding collector level when the reactor conditions varies from normal operation to DHR operation. This thermal loading is the cause of thermal stresses, which varies with position and time and may results in thermal ratcheting or shakedown.

1.2 PROBLEM STATEMENT

The problem of thermal ratcheting is complicated with possibility of thermomechanical coupling and creep effects. Until the present, no single constitutive model is robust enough to cover the various aspects of mechanics such as yield surface translation, thermomechanical interactions etc., during deformation to depict accurately the realistic ratcheting behavior. In addition, the implementation of these constitutive models to simulate highly nonlinear ratcheting response of cyclic hardening material is a complex task. In this connection, several variations of mathematical formulations and implementations procedures have been reported considering material anisotropy and yield surface distortion theories in conjunction with kinematic and isotropic hardening. Although, ratcheting behavior of material under cyclic mechanical loading have been investigated widely using several constitutive models, thermal ratcheting of shells have not been completely understood. The present work is intended to reveal the importance of using different mathematical correlations to account certain material behavior during complex mechanical, thermal or combined loading conditions.

1.3 OBJECTIVE AND SCOPE OF THE WORK

The present work is focused on the investigation of thermal ratcheting phenomenon in a thin hollow cylindrical shell of austenitic grade steels due to sodium free level variations. The primary objectives set for the present study are as follows:

- To deduce simplified plasticity integration procedure with the features of rapid convergence and improved accuracy while predicting uniaxial or multiaxial ratcheting strain.
- To develop the codes employing the simplified plasticity integration procedure for time dependent and independent constitutive models for direct implementation in ABAQUS FEA software to perform numeric analysis.
- To recognize the shakedown and ratcheting behaviour of the cylinder under applied loading cycles with different loading methods.
- Comparative study of cyclic hardening behavior of hardening steels by using time independent and dependent constitutive modeling.
- Effect of frequency of free level fluctuations and hold time with reference to time independent and dependent formulation of thermal ratcheting.

Besides, an experimental facility have been developed with improved features to predict the thermal ratcheting strain of a thin hollow cylindrical shell in order to compare the numerical results using present approach. To evaluate the life of some structural components involving the concurrence of ratcheting and fatigue, it is necessary to realize the interaction of ratcheting with fatigue during asymmetrical cyclic stressing. Concerning to this point, the study aims to predict ratcheting with thermomechanical interactions in self-constrained structures such as cylindrical shell and two-bar system subjected to thermomechanical loading. Thus, the study enhanced the understanding of contribution of ratcheting damage due to thermomechanical loading by employing modified hardening model having temperature rate terms (TRT). The development of codes, numerical simulation and investigation of ratcheting phenomenon by introducing different complexities sequentially and finally experimental simulation and application is the scope of the work.

1.4 THESIS STRUCTURE

The thesis has been organized as below having six chapters including Chapter 1 as introduction.

Chapter 2 details the work done by various researchers in the field of ratcheting. The experimental and numerical analysis performed so far with its significant contribution and importance for the development of various models is discussed here. The evolution of ratcheting theories leading to various time independent, time dependent, temperature rate dependent model is also included in this chapter.

Chapter 3 presents the investigation studies carried out to evaluate thermal ratcheting of cylindrical shell with isothermal approach. The detailed procedure adopted for development and the implementation of the code with benchmark analysis for the code validation is discussed. Comparative study of time independent and dependent models for ratcheting evaluation is also discussed here.

Chapter 4 is devoted to detailed analysis of thermal ratcheting behavior of two-bar system and cylindrical shell under thermomechanical loading considering Non-isothermal loading effects. The thermal cycling due to level variations in main vessel of SFR is transient in nature and hence involves temperature rate dependent modeling, which is discussed in this chapter.

Chapter 5 consists of the results of experimental and numerical simulation of ratcheting performed to illustrate the suitability of the proposed approach leading to enhanced understanding of thermal ratcheting behaviour with thermomechanical interactions. The identified material hardening parameters through uniaxial tests and a hardening rule with temperature rate terms is also discussed in this chapter.

Chapter 6 focuses on conclusion and future scope of the work

LITERATURE REVIEW 2

In order to develop a mechanistic understanding of thermal ratcheting behavior, a comprehensive review of plasticity in general is given in the first section of this chapter. The evolution of the plasticity theories and various other phenomena associated with it followed by a discussion on pertinent previous works on thermal ratcheting is presented in this chapter.

2.1 INTRODUCTION TO PLASTICITY

The modeling of inelastic deformation behavior of solids is complex and widely applicable in current scenario of advanced computational technologies, which needs few basic facts about uniaxial stress-strain relations for materials. For some initial deformation range, the increase in strain results in linear increase in stress, until a critical limit called the *elastic limit* is reached. Often the strain is such that the elastic limit is crossed and the material behaves in-elastically where elastic stress-strain idealization does not hold true. This behavior is termed as *plastic behavior*, which causes permanent deformation in the material and the ability of the material to deform permanently is termed as *plasticity.* The inelastic deformation and the corresponding stress are much higher than the values at yield limit for alloy materials. To model this behavior, sophisticated formulations of stress-strain are needed and the phenomenon of increase in the stress after the onset of yielding is termed as *hardening*. On the other hand, there are *softening* materials such as ceramics, rocks, masonry etc, which shows decrease in stress with the increase in strain. Figure 2.1 represents the typical deformation behavior of strain hardening, strain softening, brittle and elastic perfectly plastic materials. Basic analytical stress solutions for different materials are obtained by a simple tension or compression test from which stress-strain diagram can be plotted. Suitable numerical approximations of the actual uniaxial behavior however require the understanding of plasticity theories. The elementary concept of plasticity can be found some centuries back in Galileo's solution [3] for collapse load of a cantilever assuming uniform tensile stress distribution over the cross section. Realistic static failure analysis was first revealed by Coulumb's [4] introducing the concept of plastic slip and yield condition. The developments of different mathematical correlations called constitutive models, to represent or simulate the plastic behavior of materials under different loading conditions, numerous approach were adopted as mentioned below.

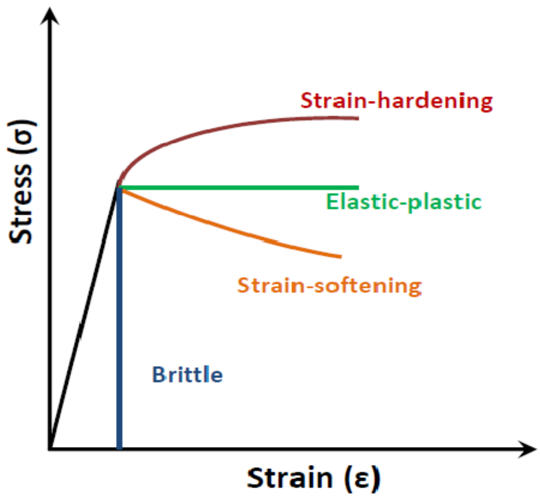

Figure 2.1 Typical stress-strain behavior of materials

2.1.1 Theory and formulation of ratcheting

Several theories regarding plastic deformation and failure were unfolded in the mid nineteenth century by researchers Tresca, Saint Venant and Levy [5], [6] and [7] . In the early twentieth century, von Mises [8] and Henky [9] unfolded some fundamental approach to yield surface, flow rules, slip lines. Gradual advancement of these plasticity theories and concepts gained importance in developing mathematical correlation to represent structural responses (elastic or plastic) under external loads. Plasticity theories are broadly classified into *physical theories of plasticity* and *mathematical theories of plasticity*. The former one quantifies plastic deformation at microscopic level where movements of atoms, crystals and grains deformation characterize the responses of material or structure. Whereas the later one represents the experimental observations neglecting the understanding of physics during deformation and based on the macroscopic phenomena involved in hypothesis hence are called as *phenomenological theories* [10]. Moreover, application of phenomenological theories for mathematical modeling concerning response of plastic solids under complex loading, involve several variables and parameters measured through experimental data. For metals and alloys under proportional monotonic loading, a simple tension-compression curve completely depicts the uniaxial behavior, but non-proportional loading or cyclic loading responses require deeper concepts of mechanics. It is quite complex to represent practical or realistic response of material subjected to cyclic loading. Under cyclic loading the structure or material undergoes progressive deformation leading to ratcheting.

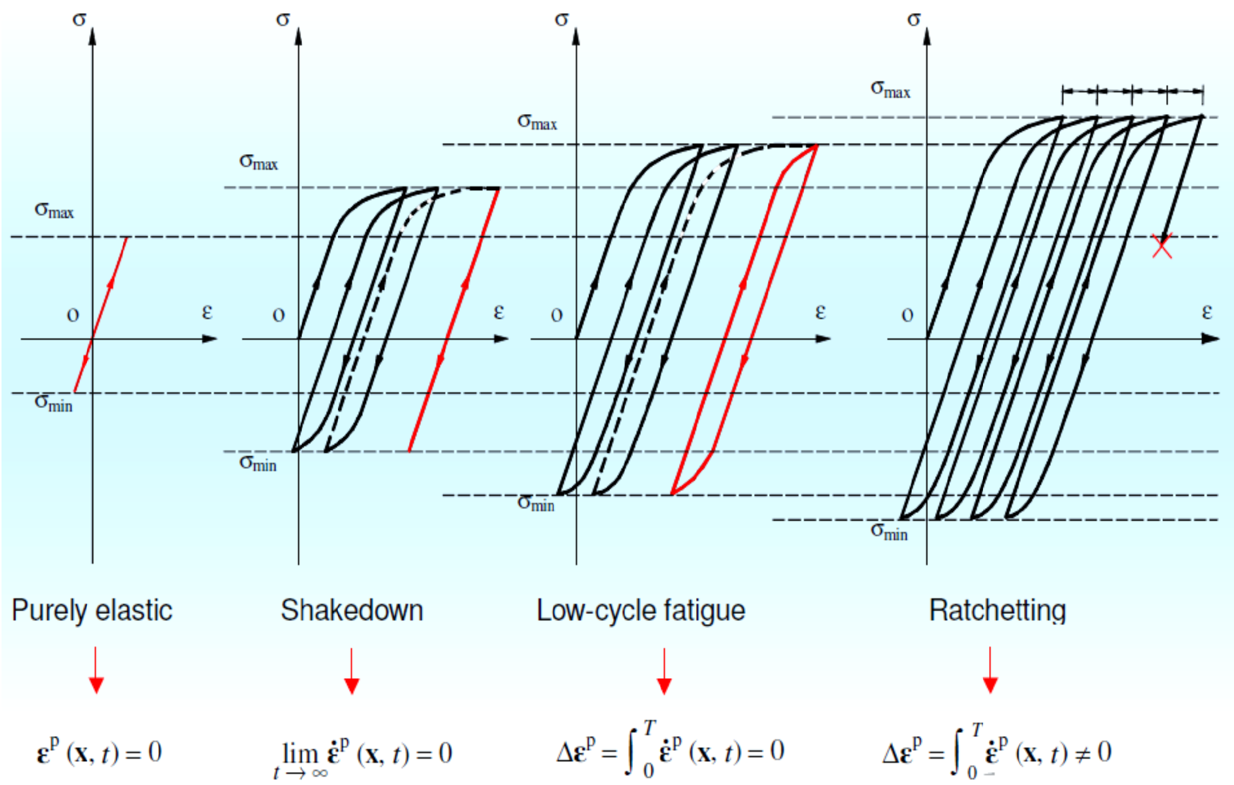

Figure 2.2 Cyclic deformation behavior of hardening materials

Ratcheting should be emphasized while safety assessment and life estimation of engineering structures. If the loading affects the elastic-plastic behaviour of the structure such that the structure achieves the steady state of plastic straining, the phenomenon is termed as *shakedown* and structure fails due to low cycle fatigue. Figure 2.2 shows the different deformation behavior of material under cyclic loading. The hardening and softening phenomenon, which occur under fully reversed strain controlled cyclic loading significantly govern the cyclic deformation behavior and hence ratcheting [11], [12], [13] for various steels under uniaxial and multiaxial loading cases. From these studies, it has been observed that different materials exhibit ratcheting behavior differently (hardening/softening). Schematic representations of cyclic deformation behavior [14] for cyclic hardening and softening materials are shown in Figure 2.3.

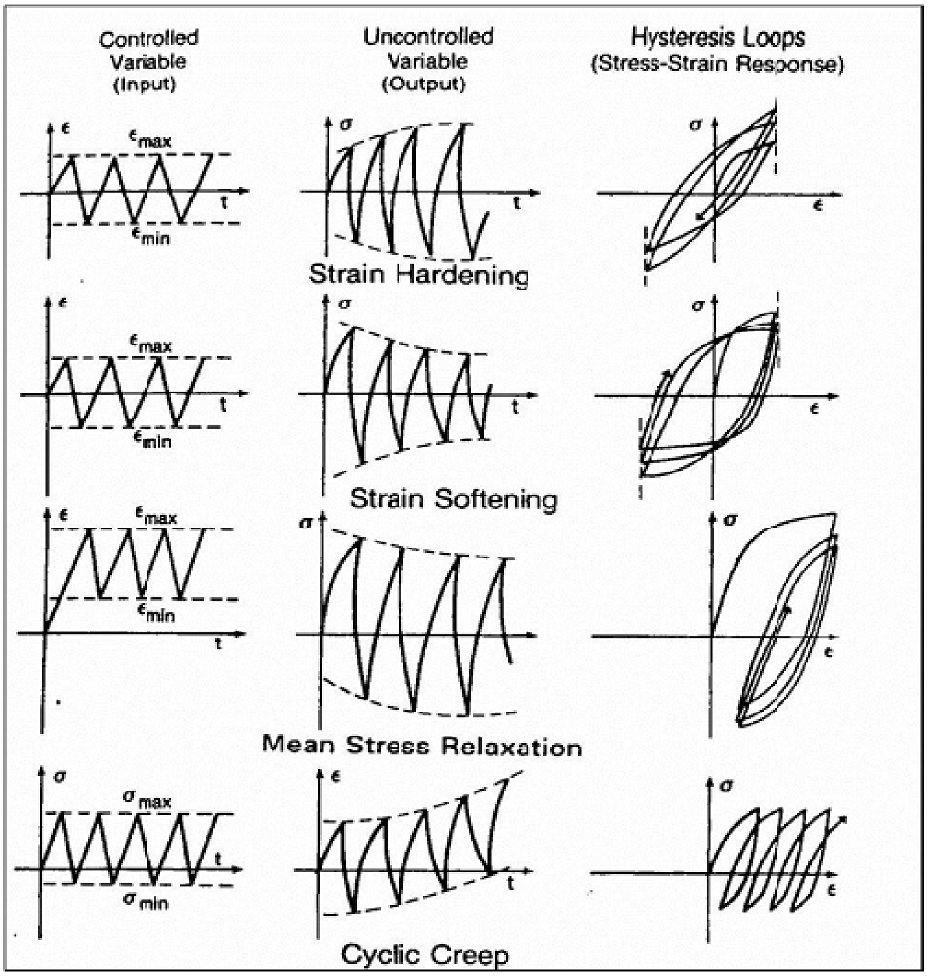

Figure 2.3 Schematic response to various cyclic input variables [14]

The cyclic deformation behavior of material involves loading followed by unloading or loading in the opposite direction. The cyclic deformation behavior of various steels employing linear and nonlinear constitutive model has been analyzed in detail in relevance to ratcheting phenomenon [15]. As a cyclic hardening material is loaded beyond yield limit, it hardens, making the material stronger. Using the isotropic hardening material model, during the unloading and reloading, material yields in compression after the same magnitude of stress is applied and the yield surface expands isotropically as shown in Figure 2.4 (a). However, hardening induced by plastic deformation may be described more appropriately by a combination of kinematic hardening and isotropic hardening. To understand the kinematic and isotropic hardening phenomenon, the graphical representation [16] is reproduced here in Figure 2.4 (b). These figures illustrate the transformation of the elastic domain and yield surface by the pure linear kinematic hardening such that the yield surface translates in the deviatoric stress plane. This led to a conclusion that, we need to define initial yield condition, flow rule and hardening rule in order to realize ratcheting behavior of hardening materials.

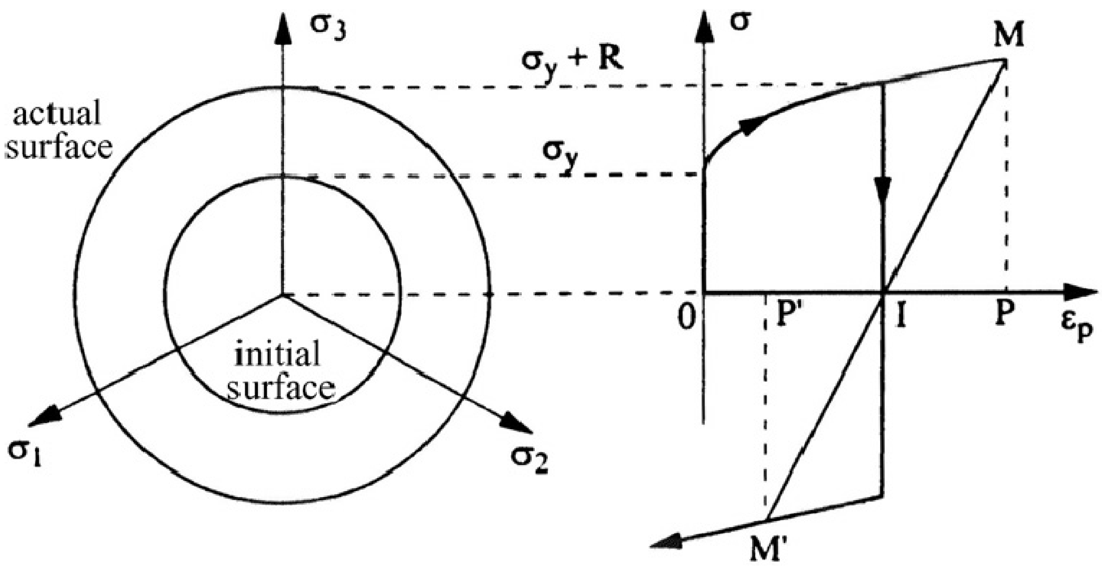

(a)

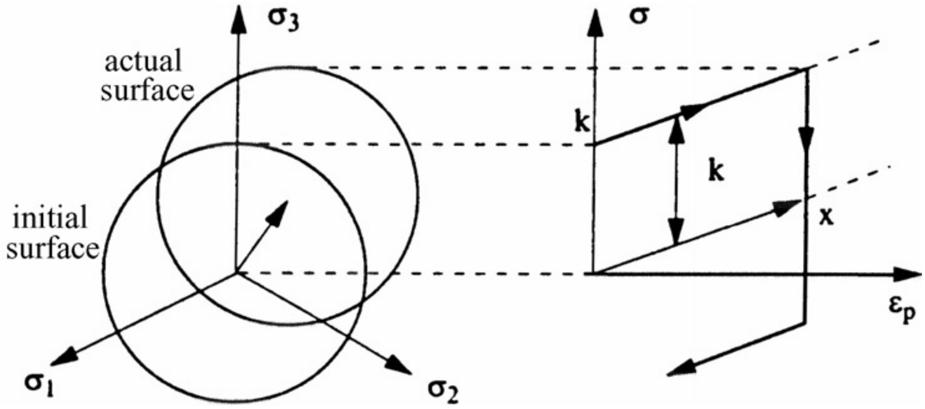

(b)

Figure 2.4 (a) Schematics of the isotropic hardening in the deviatoric plane and the stress verses plastic strain response (b) Schematics of the linear kinematic hardening in the deviatoric plane and the stress verses plastic strain response [16]

The formulation of initial yield condition is used to specify the state of stress after which plastic flow occurs while flow rule assumes the state of stress under plastic deformation condition. The hardening rule specifies the yield condition variation in the course of plastic deformation assuming the associated plasticity framework (the flow potential is identical with the yield surface) and the normality law. Yield condition for uniaxial, monotonically increasing load is quite simple and is checked by identifying if $\boldsymbol{\sigma} < \boldsymbol{\sigma}_y$, then the material is within elastic range or if $\boldsymbol{\sigma} >= \boldsymbol{\sigma}_y$, then the material has yielded. Here, σ is stress tensor, $\boldsymbol{\sigma}_y$ is yield stress. On the other hand, for a multiaxial state of stress, von Mises criteria is widely applied for the computation of yielding using effective stress concept in terms of principle stresses i.e.$\boldsymbol{\sigma}_1$, $\boldsymbol{\sigma}_2$ and $\boldsymbol{\sigma}_3$ as shown in Eq. (2.1) or in terms of direct and shear stresses shown in Eq. (2.2).

$$\sigma_{ef} = \frac{1}{\sqrt{2}}\left[(\boldsymbol{\sigma}_1 - \boldsymbol{\sigma}_2)^2 + (\boldsymbol{\sigma}_2 - \boldsymbol{\sigma}_3)^2 + (\boldsymbol{\sigma}_3 - \boldsymbol{\sigma}_1)^2 \right]^{1/2} \tag{2.1}$$

$$\sigma_{ef} = \left[\frac{3}{2}\left(\boldsymbol{\sigma}_{11}{}^2 + \boldsymbol{\sigma}_{22}{}^2 + \boldsymbol{\sigma}_{33}{}^2 + 2\boldsymbol{\sigma}_{12}{}^2 + 2\boldsymbol{\sigma}_{23}{}^2 + 2\boldsymbol{\sigma}_{31}{}^2 \right) \right]^{1/2} \tag{2.2}$$

The subscripts 1, 2 and 3 are used to represent the stress tensor in direction of X, Y and Z directions respectively and that the effective stress σ_{ef} comes out to be a scalar quantity. Let f be the yield function for isotropic non-porous material. This implies that the yield criterion can only depend on the deviatoric stress components and yielding only depend on the magnitudes of the principal stresses but cannot depend on the principal stress directions. Thus, the yield function f following von Mises criteria can be defined as Eq. (2.3).

$$f = \sigma_{ef} - \sigma_y = \left(\frac{3}{2}\boldsymbol{\sigma}' : \boldsymbol{\sigma}'\right)^{1/2} - \sigma_y \tag{2.3}$$

The yielding condition can be checked by identifying the value of f such that if $f < 0$, then the material is within elastic range or if $f >= 0$, then the material has yielded. Here, $\boldsymbol{\sigma}'$ is deviatoric stress tensor given by Eq. (2.4) and symbol ':' in Eq. (2.3) is called the double dot product of two second-order tensors and Tr ($\boldsymbol{\sigma}$) is the trace of a stress tensor.

$$\boldsymbol{\sigma}' = \boldsymbol{\sigma} - \frac{1}{3}\mathrm{Tr}(\boldsymbol{\sigma})\mathrm{I} \tag{2.4}$$

After the yield limit is reached, the state of stress lies on the yield surface. On further increase in load, the material hardening phenomenon can be observed in terms of the expansion of the yield surface along with its translation in the deviatoric stress space. The plastic flow and normality law are useful in determining the direction of the flow. For what is termed associated flow, the normality law says that any increment in the plastic strain is in direction, which is normal to the tangent to the yield surface at the load point as shown schematically in Figure 2.5.

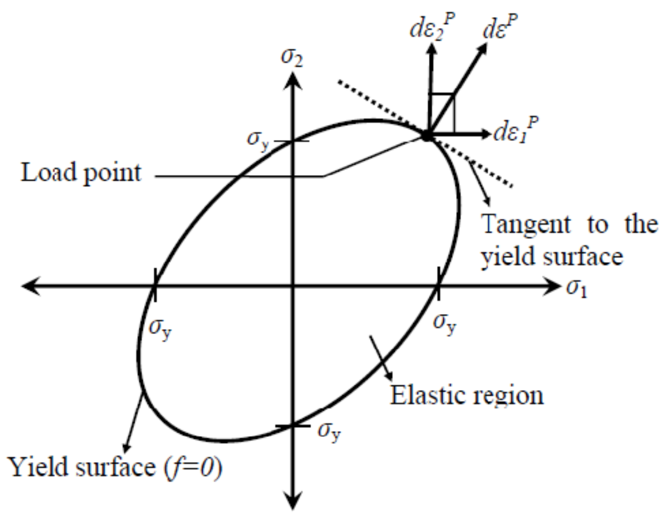

Figure 2.5 The von Mises yield surface for conditions of plane stress, showing the increment in plastic strain $\mathbf{d\varepsilon^P}$ as per normality law

The expression for normality law in terms of yield function can be written as Eq. (2.5),

$$\mathbf{d\varepsilon^P} = d\lambda \frac{\partial f}{\partial \boldsymbol{\sigma}} \tag{2.5}$$

or in terms of rate equations, we can write as Eq. (2.6), which is also called as flow rule.

$$\dot{\boldsymbol{\varepsilon}}^{\mathbf{P}} = \dot{\lambda} \frac{\partial f}{\partial \boldsymbol{\sigma}} \tag{2.6}$$

In the above expression, the direction of the plastic strain increment is given by $\partial f / \partial \sigma$, while the magnitude is computed for the plastic strain rate by using $\dot{\lambda}$ which is called the plastic multiplier. The yield condition given by Eq. (2.3) is dependent on effective stress and the yield stress only but during plastic flow for hardening material, yield stress is a function of plastic strain, hence yield condition can be expressed as Eq. (2.7),

$$f(\boldsymbol{\sigma}, p) = \sigma_{ef} - \sigma_y = \sigma_{ef}(\boldsymbol{\sigma}) - \sigma_y(p) = 0 \tag{2.7}$$

After establishing the yield condition considering hardening rules, the incremental change in stress and effective plastic strain can be computed by applying the consistency condition as shown below:

$$f(\boldsymbol{\sigma} + \mathrm{d}\boldsymbol{\sigma}, p + dp) = 0 \tag{2.8}$$

In other way, the above equation can be written as,

$$f(\boldsymbol{\sigma} + \mathrm{d}\boldsymbol{\sigma}, p + dp) = f(\boldsymbol{\sigma}, p) + \frac{\partial f}{\partial \sigma} : \mathrm{d}\boldsymbol{\sigma} + \frac{\partial f}{\partial p} dp = 0 \tag{2.9}$$

The detailed procedure of formulation of yielding condition with hardening rules employing appropriate integration method is described in subsequent chapters for different constitutive models. While many researchers have intensively investigated several factors affecting ratcheting behavior, the extensive studies in the past decades report that the kinematic hardening is the primary reason for material ratcheting [17]. Therefore, some important kinematic hardening models have been discussed here under along with their advantages and shortcomings in order to appreciate the advantages of the proposed models.

2.1.1.1 *Prager model*

Prager [18] proposed the simplest rule, which describes the translation of the yield surface. According to his rule, the plastic response of materials is linearly varies with the plastic strain and thus it is called as *Linear Kinematic Hardening* (LKH) rule. The model proposed by Prager to describe the evolution of the kinematic hardening is expressed as,

$$\mathbf{dX} = \frac{2}{3} C \mathbf{d\varepsilon^P} \tag{2.10}$$

where C is a constant derived from a simple monotonic uniaxial curve and X is back stress tensor, $\mathbf{d\varepsilon^P}$ is plastic strain increment. Though, it is simpler to implement, the accuracy of prediction is compromised as reported in literature [19]. It is clear from the cyclic behavior of CS 1026 grade steels in Figure 2.6 that Prager's model cannot represent the experimental hysteresis curve during the initial nonlinear part.

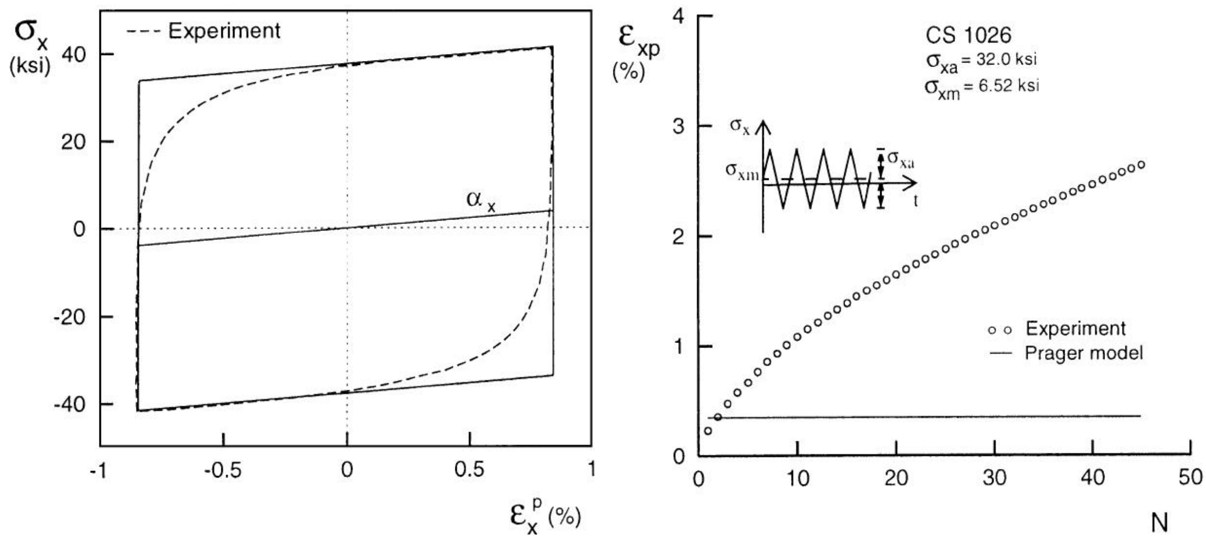

(a) (b)

Figure 2.6 Predictions of cyclic behavior from Prager's rule for (a) strain-controlled stable hysteresis loop (b) axial strain at positive stress peaks of uniaxial cycles [19]

In addition, for a prescribed uniaxial stress cycle with a mean stress, this model fails to distinguish between the shapes of the loading and reverse loading hysteresis curves and consequently produces a closed loop with no ratcheting. Although being simpler to apply, this model underestimates the ratcheting strain significantly and thus not used for ratcheting computations.

2.1.1.2 *Armstrong and Frederick model*

Armstrong and Frederick (AF) introduced a rule [20] that simulates the multiaxial Bauschinger effect. Predictions by AF rule were more accurate than Prager's rule when compared to the experimental observations for the cyclic behavior of CS 1026 grade steels shown in Figure 2.7. Despite being complex to calculate strain increments from stress and stress increments [21], the coding with this rule improve the numerical results than the ones calculated using Prager's rule. For uniaxial loading condition, the ratcheting strain predicted by this rule deviates largely from experimental results. Constant rate of ratcheting in Figure 2.7 demonstrate an over prediction of strain leading to highly conservative results. However, the performance of this rule is satisfactory while evaluating thermal ratcheting behavior of cylindrical shells as described in subsequent section of this chapter.

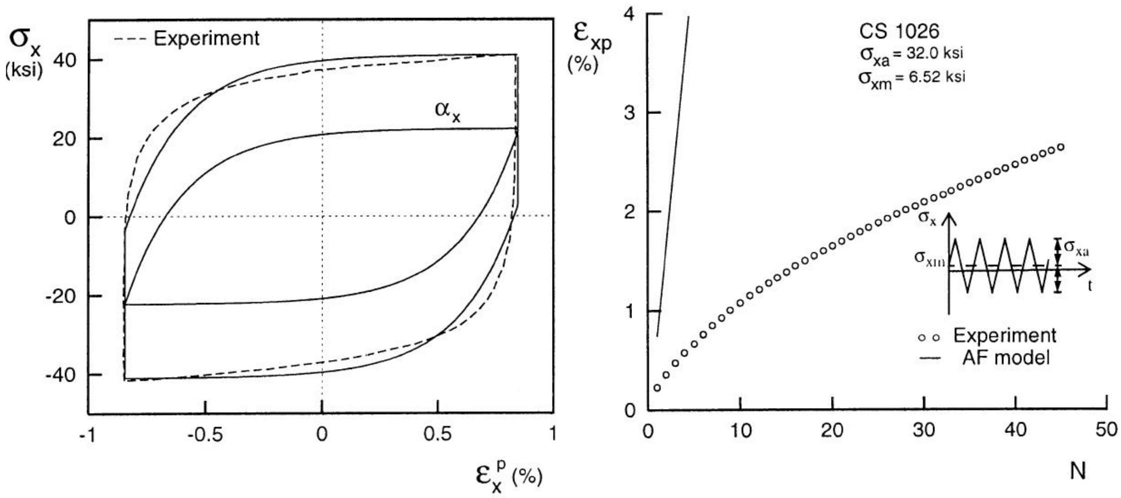

(a) (b)

Figure 2.7 Predictions of cyclic behavior from Armstrong and Frederick rule for (a) strain-controlled stable hysteresis loop, (b) axial strain at positive stress peaks of uniaxial cycles [19]

Therefore, the kinematic hardening rule by Armstrong and Frederick has been applied extensively in the current study and its mathematical expression for the rate of change of back stress is given Eq. (2.11).

$$\dot{\mathbf{X}} = \frac{2}{3} C \mathbf{d\varepsilon^{P}} - \gamma \mathbf{X} \dot{P} \tag{2.11}$$

Here *C, γ* are material parameters defining kinematic hardening, $\dot{P}$ is accumulated plastic strain rate.

2.1.1.3 *Chaboche model*

For the better description of the nonlinear portion of the hysteresis loop, Chaboche and his coworkers [22], [23] came up with a new form of kinematic hardening rules obtained by the superposition of several Armstrong and Frederick models. They divided the stabilized hysteresis loop in three segments to describe the hardening curve. The first segment starts showing hardening behavior rapidly and stabilizes very quickly for small strain range while the second segment simulates the transient nonlinear portion of the stable hysteresis curve. Finally, the third segment represents the subsequent linear portion of the curve at a high strain range. For each decomposed rule, the choice of values of different constants is made in such a way that the stabilized hysteresis curve can be reproduced accurately. The overall hardening is represented by the following expression is named as Chaboche three back stress (CH3) rule, where M is number of back stresses to be considered such that 'i' varies from 1 to M.

$$\mathbf{\Delta X} = \sum_{i=1}^{M} \mathbf{dX_i}, \mathbf{dX_i} = \frac{2}{3} C_i \mathbf{d\varepsilon^{P}} - \gamma_i \mathbf{X_i} \Delta P \tag{2.12}$$

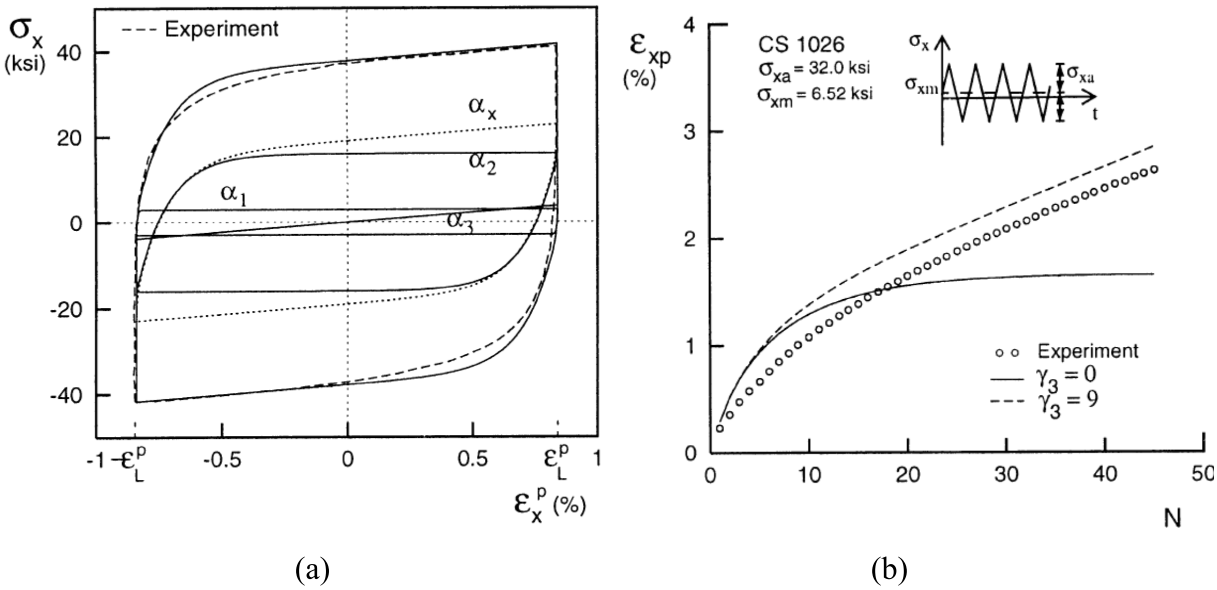

Figure 2.8 Prediction of cyclic behavior using Chaboche three back stress (CH3) rule (a) strain controlled stable hysterisis loop (b) axial strain at positive stress peaks of uniaxial cycles [19]

The simulation of the hysteresis curve using this rule shows significant improvement in uniaxial ratcheting prediction. The deviation in experimental and simulation results is governed by choosing the appropriate value of the parameters for the third segment of the stable hysteresis curve. The capability of this rule was demonstrated earlier [19] as shown in the Figure 2.8. It showed that the progressive ratcheting behavior is due to a non-zero positive value of γ_3 (at γ_3 = 9) whereas shakedown is achieved if γ_3 is zero. The uniaxial ratcheting result by this rule is highly promising and thus used for thermal ratcheting prediction in chapter 5.

2.1.1.4 *Ohno and Wang model*

Similar to Chaboche rule of ratcheting prediction, Ohno and Wang (OW) superposed several AF rules with the assumption that the component of back stress reaches a critical state before dynamic recovery term activates [24]. The non-linear portion of stabilized curve is very well reproduced (Figure 2.9) using OW rule for strain controlled cyclic behavior.

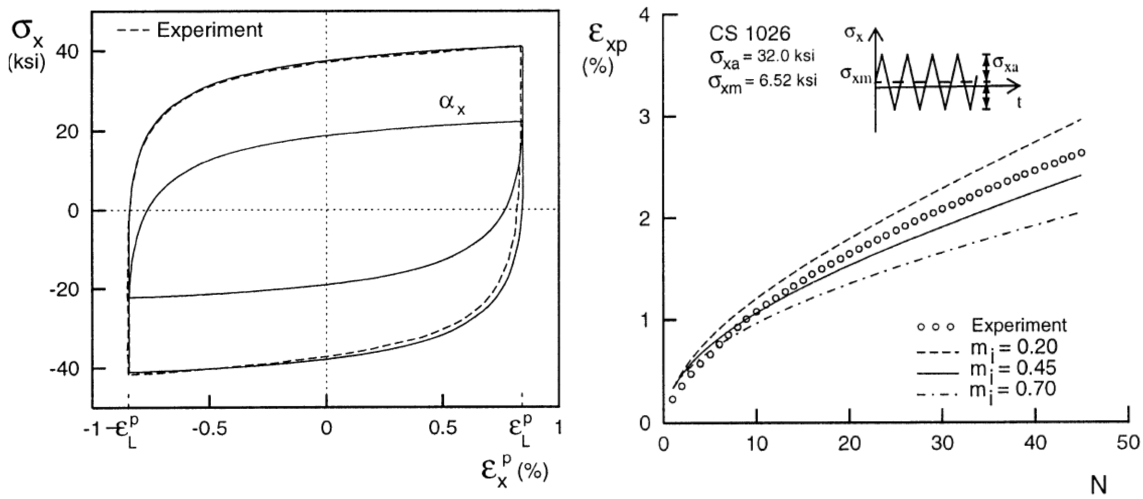

(a) (b)

Figure 2.9 Prediction using Ohno and Wang model (a) strain controlled stable hysterisis loop (b) axial strain at positive stress peaks of uniaxial cycles [19]

Depending upon the concept of critical state of dynamic recovery term, Ohno and Wang models had two forms: the first being the form expressed by Eq. (2.13), which used a critical state by introducing a surface $f_i = \|X_i\| - C_i/\gamma_i$. Here $\tilde{\mathbf{n}}$ is the plastic strain rate direction and $\mathbf{k_i} = X_i / \|X_i\|$ is the unit direction of the back stress in Eq. (2.13). The other form uses the power function in place of Heaviside step function as shown in Eq. (2.14). The nonlinear portion of the stabilized curve is governed by adjusting the values of power multiplier m_i, however determination of large number of constants in this rule is a cumbersome process. While the uniaxial ratcheting prediction using this rule is very accurate, the least conservative estimation of thermal ratcheting strain [25] through this rule has decreased its suitability for present analysis. Here $\Delta\mathbf{X}$, ΔP and H are back stress increment tensor, effective plastic strain increment and Heaviside's step function. 'M' is the number of back stresses to be considered and 'i' varies from 1 to M.

$$\mathbf{\Delta X} = \sum_{i=1}^{M} \mathbf{dX_i}, \mathbf{\Delta X_i} = \frac{2}{3} C_i \mathbf{d\varepsilon^P} - \gamma_i H(f_i) \langle \tilde{\mathbf{n}} : \mathbf{k_i} \rangle \mathbf{X_i} \Delta P \qquad (2.13)$$

$$\Delta \mathbf{X_i} = \frac{2}{3} C_i \mathbf{d\varepsilon^P} - \gamma_i \frac{\|\mathbf{X_i}\|^{m_i}}{C_i/\gamma_i} \langle \tilde{\mathbf{n}} : \mathbf{k_i} \rangle \mathbf{X_i} \Delta \mathrm{P} \tag{2.14}$$

2.1.1.5 *Sievert model*

In many areas of engineering applications, the material experience cyclic mechanical and thermal loadings concurrently. The cyclic behavior of materials under such loading conditions can be described better by using temperature dependent constitutive models. Furthermore, the quantitative prediction of cyclic strain accumulation due to ratcheting under thermomechanical loadings requires temperature dependent material parameters to reduce over-estimation. Chaboche [23] reported that, under varying temperature condition, the plastic flow of materials is significantly affected by (a) initial yield surface size or yield stress k, and (b) evolution equation for the yield surface centre. Sievert [26] modified the temperature dependent Chaboche hardening model to obtain better description of deformation behavior under Non-isothermal loading conditions. Sievert replaced the dynamic and static recovery term from the Chaboche temperature dependent hardening model of Eq. (2.15) by a new term maintaining the thermodynamic consistency of hardening formulation as shown in Eq. (2.16). Here B and M in Eq. (2.15) are material and temperature dependent model parameters, while X_s = C/γ. The influence of the new term and temperature dependent material parameters on ratcheting behavior has been analyzed separately in chapter 4.

$$\dot{\mathbf{X}} = \frac{2}{3} C \mathbf{d\varepsilon^P} - \gamma \mathbf{X} \dot{P} - B \mathbf{X}^M + \frac{\partial C}{\partial T} \frac{\mathbf{X}}{C} \dot{T} \tag{2.15}$$

$$\dot{\mathbf{X}} = \frac{2}{3} C \mathbf{d\varepsilon^P} + \frac{\partial C}{\partial T} \frac{\mathbf{X}}{C} \dot{T} - \frac{\mathbf{X}}{X_s} \left\langle \frac{2}{3} C \dot{P} + \frac{\partial C}{\partial T} \frac{\|\mathbf{X}\|}{C} \dot{T} \right\rangle \tag{2.16}$$

2.1.2 Time independent and dependent ratcheting models

Materials subjected to asymmetric cyclic loading beyond yield limit undergo progressive deformation which may lead to excessive deformation beyond acceptable limits. Hence, pre-assessment of strain and limiting the excessive deformation is an important task carried out by designers to ensure safe and reliable operation of mechanical components/engineering structures. It is well known that the austenitic stainless steels and their nitrogen containing alloys are widely used in various industries for high temperature applications. Cyclic hardening or ratcheting behavior of austenitic stainless steels such as SS 304 and SS 304 LN has been studied at room temperature and high temperature [27], [28]. It demonstrated that, the cyclic hardening behavior varies with mean stress variations and hence fatigue life at different temperatures. Additionally, the uniaxial and biaxial ratcheting behavior analyzed by many researchers [11], [29] also substantiate the same. Parallel to experiments, various models have been developed considering hardening and visco-plasticity to predict the cyclic response of materials using different plasticity theories. Time independent constitutive theories [23], [30] have been widely applied for predicting ratcheting behavior, although the overestimation of strain is obtained. The applicability of these theories is restricted to loadings when rate effect is negligible. Rate effect has to be considered while developing the constitutive models to predict cyclic deformation behavior of structural components under cyclic load at different rates at high temperature. Kang and Gao [31] adopted time dependent constitutive model for mechanical loading and verified it by simulating the uniaxial or multiaxial ratcheting of U71Mn rail steel at room temperature. Different types of time dependent constitutive models have been studied [32] for SS 304, which characterize the features of different phenomena such as rate effect, creep during ratcheting behavior. At high temperature, the significance of creep and possible effects of dynamic strain aging (DSA) phenomena should also be considered [33]. The influence of DSA on the ratcheting behavior of SS 316 LN in the temperature range of 300 to 900 K was discussed in the context of effects of mean stress and stress amplitude [33]. It shows that the real material behavior can be depicted by using appropriate constitutive models considering other important phenomena, environmental and metallurgical effects (creep, DSA etc.). However, DSA is not considered in the present work. Most of the time independent and dependent constitutive models overestimate ratcheting strain. The solution to these nonlinear equations involves large computational time and advance or improved finite element integration techniques. Concerning these points, some numerical methods and integration techniques were employed earlier depending upon its suitability for different material behavior [34], [35]. Nevertheless, the need for the improvement in the accuracy and simpler formulation procedures remained in the mind of researchers. The present work is a contribution to provide an improved approach of implementing the constitutive models in time independent and dependent framework.

In the context of modeling the ratcheting behavior in time independent framework, the rate independent plasticity theories are applied with standard strain partitioning method and appropriate yield criteria. In this framework, the effect of loading rate (strain or stress controlled) is insignificant and considered as the limiting case of classical visco-plasticity with the infinitely slow process. The material is assumed *inviscid plastic* and corresponding deformation due to inelastic behavior after yielding is denoted as ε^P instead of ε^{In} during strain partitioning as shown in Eq. (2.17) for isothermal conditions. The relation of incremental form of stress with the strain tensors can be expressed as a column vector using Hooke's law as in Eq. (2.18) while the yield condition, flow criteria and hardening rule described earlier can be applied to the analysis.

$$\boldsymbol{\varepsilon} = \boldsymbol{\varepsilon}^{\mathbf{e}} + \boldsymbol{\varepsilon}^{\mathbf{P}} \tag{2.17}$$

$$\mathbf{d}\boldsymbol{\sigma} = D_{ijkl}(\mathbf{d}\boldsymbol{\varepsilon} - \mathbf{d}\boldsymbol{\varepsilon}^{\mathbf{P}}) \tag{2.18}$$

On the other hand, in the framework of time dependent ratcheting, the plasticity of materials exhibit rate dependence and hence the mechanical response is called as *visco-plasticity*. For visco-plastic materials, the crystallographic slip is the dominant mechanism of deformation, which is a temperature dependent phenomenon. The strain partitioning as in case of the time independent framework still stands valid. The plastic flow rule can also be applied using same normality hypothesis as defined by Eq. (2.6) after the onset of yielding. The major difference between time independent and dependent approach is the consistency condition, which in the later case cannot be applied as before because the load point may cross the yield surface and lie outside. Therefore, visco-plastic models are often referred to as *over-stress* models and the changes in the loading rates results into a change in stress response as shown schematically in Figure 2.10.

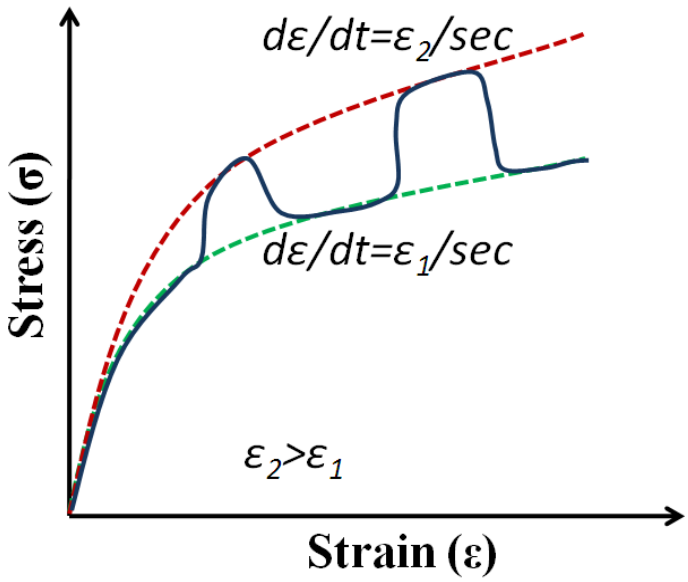

Figure 2.10 Stress-strain curve of material at different strain rates ε_1 and ε_2 is shown by dotted lines while continuous line is the response of material under sudden changes in the rates

The other important feature of visco-plastic framework is that it may exhibit permanent deformations after the application of loads and the material may undergo creep deformation with time. The thermal ratcheting behavior due to moving temperature front being thermal stress driven, hence visco-plastic modeling is of greater interest for the present work. Therefore, it is worth mentioning here that for a better insight of visco-plastic framework, we can refer an important contributory work by Kang et al. [36]. His work highlights the features of different time dependent models and is extensively used in the present analysis. The deformation behavior of SS304 stainless steels and the illustrations that demonstrate the capability of his models are reproduced hereunder and important finding are tabulated afterwards in Table 2.1.

(a) *Unified Visco-plastic constitutive model (UVP model):* As proposed by Kang et al. [36] employing Abdel-Karim and Ohno kinematic hardening rule [37], *UVP* model fairly reproduced the uniaxial ratcheting behavior of SS 304 stainless steels at room temperature and 700 ºC. The uniaxial time dependent deformation behaviors at different loading rates and with or without hold time are shown in Figure 2.11-Figure 2.13. It is observed that, (a) There exist rate dependence in monotonic tensile response of the material and the responded stress at higher strain rate is higher than that at smallest one. (b) Remarkable rate dependence at 700 ºC is observed because of the enhanced viscous effect. At room temperature, decrease in stressing rate significantly increased the ratcheting strain.

(b) *Plasticity-Creep Superposition model (SPC model):* For lower stressing rate and longer hold time at peak/valley stress, larger ratcheting strain was obtained experimentally both at room temperature and 700 ºC. It was due to the effect of creep, which the UVP model failed to describe satisfactorily because of no static recovery term in it. To overcome this drawback of UVP model, the strain partitioning in SPC model was done such that the strains due to cyclic plasticity and creep were computed separately. This improved the prediction capability by accounting the strains caused by the slight opening of hysteresis loop and the viscosity of the material described fairly by Ohno-Abdel-Karim kinematic hardening rule with dynamic recovery term and hyperbolic sine creep law respectively as illustrated in Figure 2.11-Figure 2.13. This model lacked in representing the rate dependence, but hold time effect was reasonably predicted.

(c) *Visco-Plasticity-Creep Superposition model (SVC model):* SPC model shown in Figure 2.11-Figure 2.15 did not satisfactorily simulate the rate dependence of material observed in the experimental results. Therefore, to account rate dependent and creep effect, partitioning of strain was done to evaluate these effects separately in case of SVC model. Thus, the SVC model successfully determined both the time dependent deformations at low stressing rates and short duration peak / valley stress hold at room temperature and 700 ºC. The comparative performances of widely popular time dependent models discussed here motivated to carry out the present work using the strain partitioning approach of UVP and SVC models.

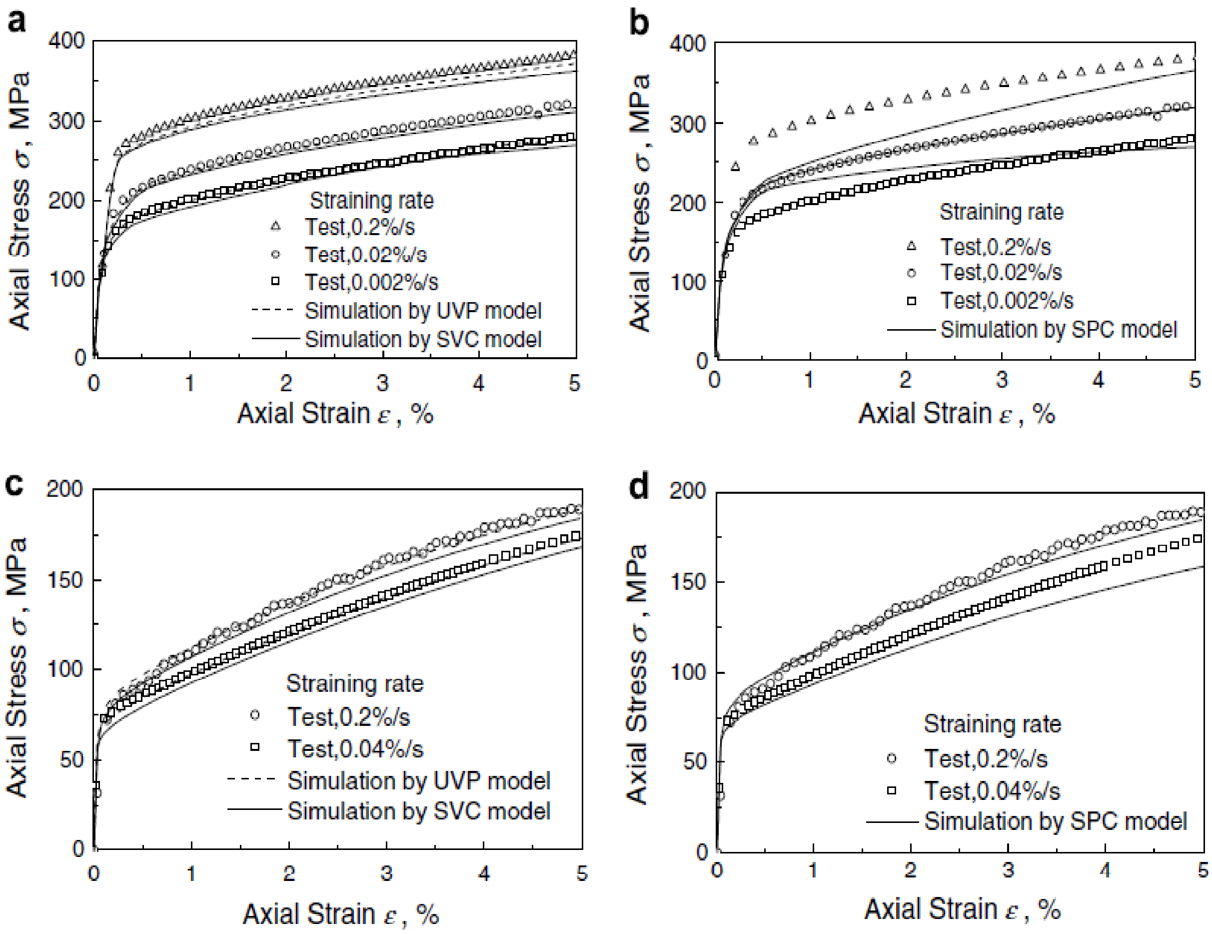

Figure 2.11 Experimental and simulated monotonic tensile behavior: (a), (b) at room temperature (c), (d) at 700 ºC [36]

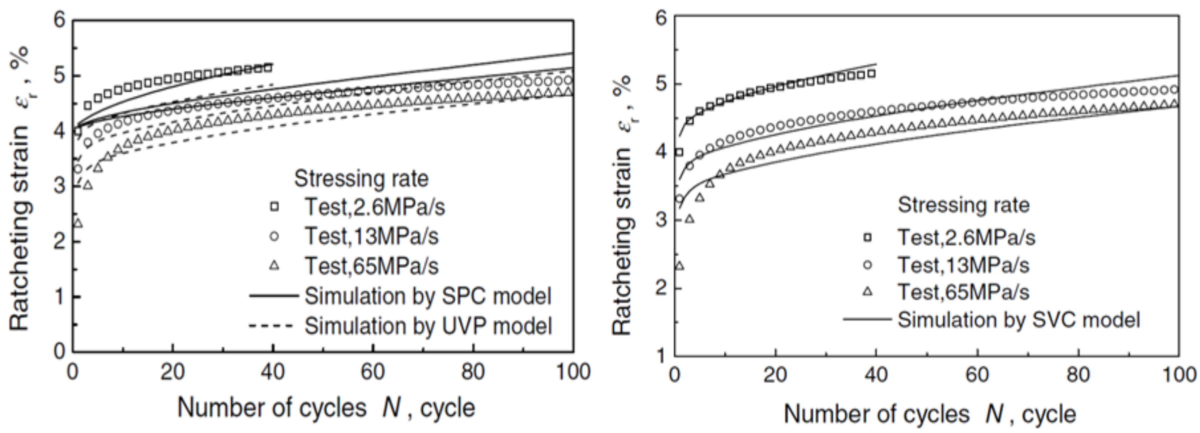

(a) (b)

Figure 2.12 Evolution of ratcheting strain (78 ± 234 MPa) with number of cycles at room temperature for different stressing rates: (a) experiment and simulations by the UVP and SPC model (b) experiment and simulations by the SVC model [36]

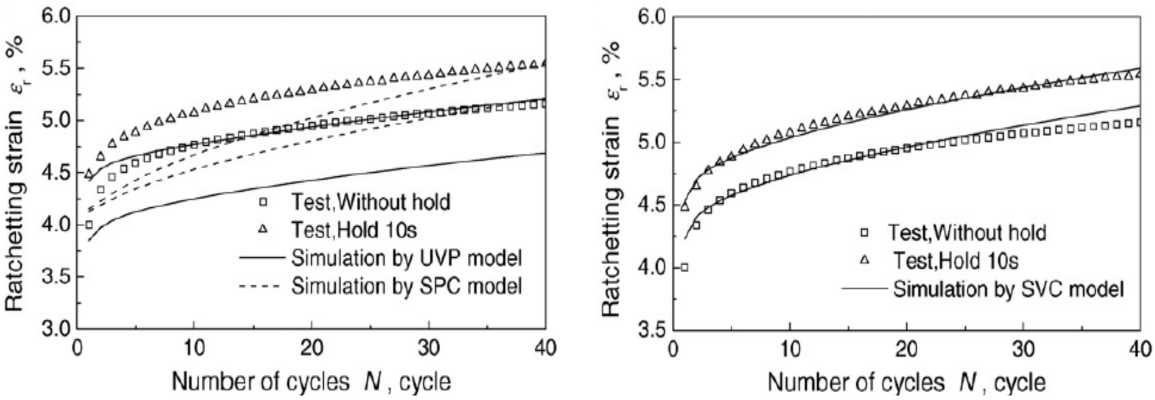

(a) (b)

Figure 2.13 Evolution of ratcheting strain (78 ± 234 MPa: at 2.6 MPa/s) with number of cycles at room temperature with and without peak/valley stress hold: (a) experiment and simulations by the UVP and SPC models (b) experiment and simulations by the SVC model [36]

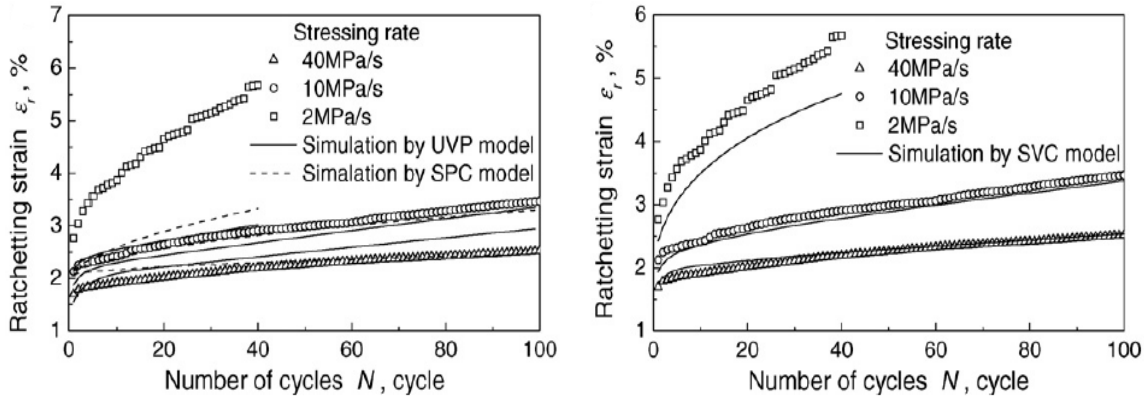

(a) (b)

Figure 2.14 Evolution of ratcheting strain (40 ± 100 MPa) with number of cycles at 700 ºC for different stressing rates: (a) experiment and simulations by the UVP and SPC models(b) experiment and simulations by the SVC model [36]

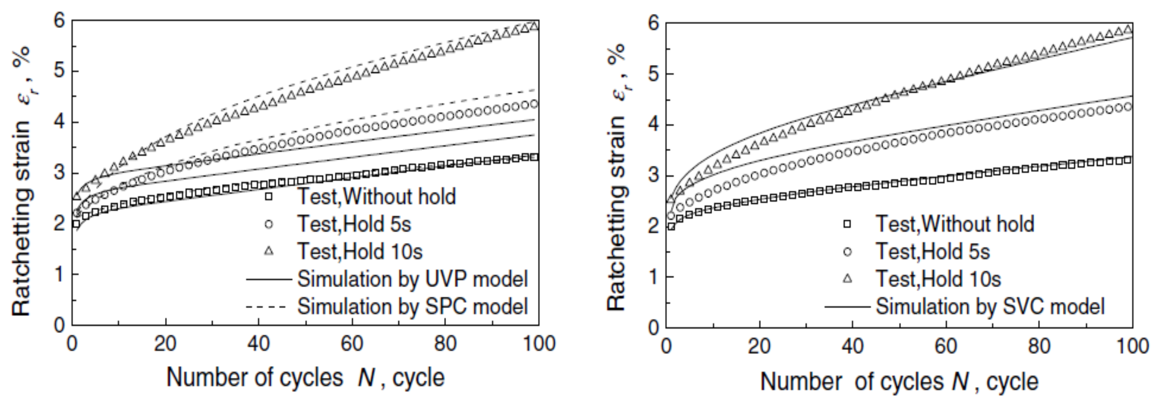

(a) (b)

Figure 2.15 Evolution of ratcheting strain (40 ± 100 MPa: at 10 MPa/s) with number of cycles at 700 ºC with and without peak/valley stress hold: (a) experiment and simulations by the UVP and SPC models (b) experiment and simulations by the SVC model [36]

Table 2.1 Deformation behavior of SS 304 using three time dependent models

	Behavior	UVP Models	SPC Models	SVC Models
Room temperature	Uniaxial tensile behavior	Satisfactory simulation at varied strain rates in Figure 2.11 (a)	Cannot provide well simulations at varied strain rates in Figure 2.11 (b)	Slightly lower simulation at varied strain rates in Figure 2.11 (a)
	Ratcheting behavior	Provided well simulations at moderate stressing rates with or without hold-times in Figure 2.12. (c) and Figure 2.13 (c)	Cannot provide well simulations at the beginning of the cyclic stressing caused by various stressing rates or hold times in Figure 2.12 (c) and Figure 2.13 (c)	Can provide Well simulations at varied stressing rates in Figure 2.12 (d)
	Creep behavior	Provided well simulations at lower stressing rates with peak valley stress holds due to little effect of creep at room temperature in Figure 2.13 (c)	Creep insignificant so cannot provide well simulation of peak valley stress hold in Figure 2.13 (c)	Satisfactory simulations of peak valley stress hold in Figure 2.13 (d)
High temperature (700° C)	Uniaxial tensile behavior	Satisfactory simulation at varied strain rates in Figure 2.11 (c)	Cannot provide well simulations at varied strain rates in Figure 2.11 (d)	Slightly lower simulation at varied strain rates in Figure 2.11 (c)
	Ratcheting behavior	Cannot provide well simulations even at moderate stressing rates in Figure 2.14 (c) and Figure 2.15 (c)	Satisfactory simulation at varied stressing rates in Figure 2.14 (c) and Figure 2.15 (c)	Satisfactory simulation at varied stressing rates in Figure 2.14 (d)
	Creep behavior	Creep significant so it can provide well simulation of peak valley stress hold in Figure 2.14 (c) and Figure 2.15 (c)	Creep significant so it can provide well simulation of peak valley stress hold in Figure 2.14(c) and Figure 2.15 (c)	Creep significant so it can provide well simulation of peak valley stress hold in Figure 2.15 (d)

2.2 THERMAL RATCHETING BECHMARKS

The phenomenon of ratcheting was known to the designers several decades ago, but its conceptual application by Bree [38] while evaluating the thermal ratcheting behavior of a *thin cylindrical can* become a widely referred work. Large numbers of works were carried out afterwards, and some of which are discussed below including Bree's work to develop better understanding of thermal ratcheting behavior of cylindrical shells.

2.2.1 Thermal ratcheting caused by primary and secondary loading

Bree proposes an approach for determining the deformation behavior of the cladding material of fuel pins under the effects of both pressure and thermal stress. He considered a thin walled *can* subjected to a high through wall thermal gradient at the operating and shutdown conditions of nuclear reactors. Thus, the *can* experiences cyclic thermal loading and a pressure loading due to the release of gaseous fission products from the fuel, which increases with fuel burn-up. For simplicity, the pressure (primary) load was assumed constant. This cyclic thermal and constant pressure load causes yielding of the material, which can result in accumulation of plastic strain until fatigue failure. This fatigue failure should be prevented for safe operation of nuclear reactors.

According to Figure 2.16, the *can* made up of non-work hardening material exhibit different behavior under the combination of primary and secondary loads as per stress regimes R1, R2, S1, S2, P and E. Here E is the purely elastic region, S1 and S2 are the plastic shakedown regions which represent initial plastic strain accumulation for few cycles and leading stabilization due to elastic response. P is the plastic stability region, where plastic strain cycles between the maximum and minimum stresses without strain accumulation. R1 and R2 are the regions of ratcheting which represent the condition of stresses that may lead to the failure due to excessive deformation.

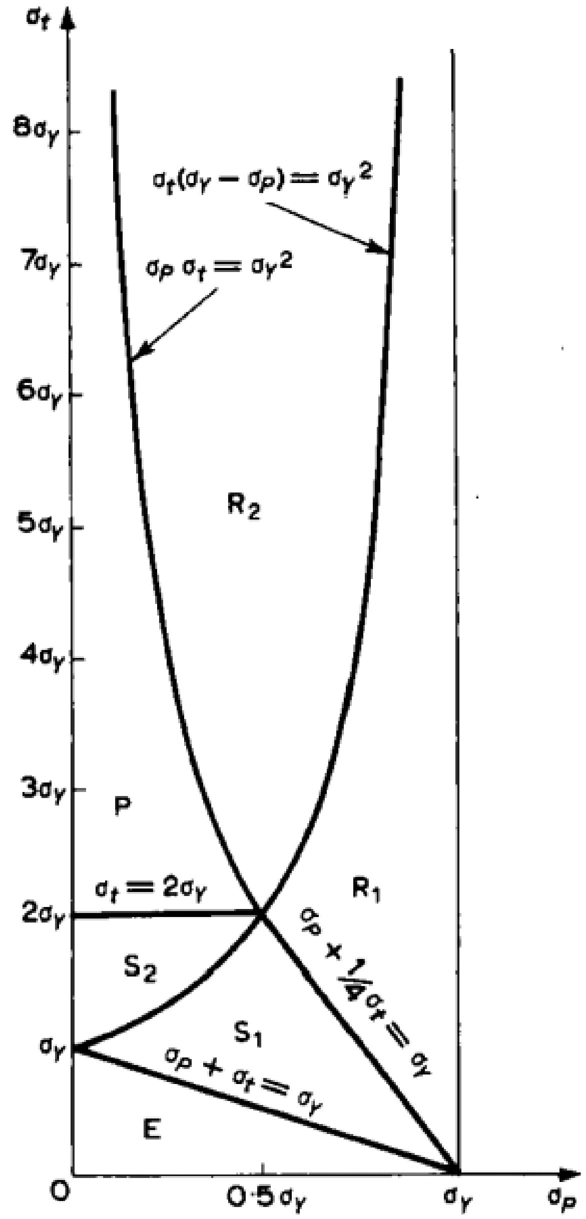

Figure 2.16 Bree's diagram for non-work hardening material and constant yield strength [38]

Bree's assumption of a constant primary load (pressure) and cyclic secondary load hold reasonably valid for the above mentioned application. However, there may be some conditions, where the primary load cycles with secondary load. Bradford [39] has reported one of such cases recently, which demonstrated that the in-phase cycling of primary with the secondary loading is considerably benign than that of the original Bree's loading. Consequently, the more conservative results by Bree's diagram will remain valid for such case of loadings.

2.2.2 Thermal ratcheting caused by secondary loading

On one hand, ratcheting in the presence of primary and secondary load has been researched widely. On the other hand, the studies of ratcheting in absence of primary load also gained importance with the increasing global concern for the nuclear safety by various regulatory bodies. This type of ratcheting is an important concern while designing the main vessel of fast breeder reactors (FBR), which experiences axial movement of temperature distribution due to free level variations.

Wada et al. [40] proposed the predictive equations of the ratcheting strains for two types of temperature distribution (a) step change, (b) linear change. His mechanism was based on the hoop membrane ($\sigma_{\theta,el}$) stress strain behavior of the cylinder by elastic analysis. Igari et al. [41] proposed an evaluation procedure for a representative case of thermal ratcheting of a hollow cylinder (Figure 2.17) subjected to moving temperature distribution with the work hardening of materials taken into account. Igari's work was an improvement on the previous one, which described the thermal ratcheting behavior of a cylinder of SU 304 stainless more appropriately.

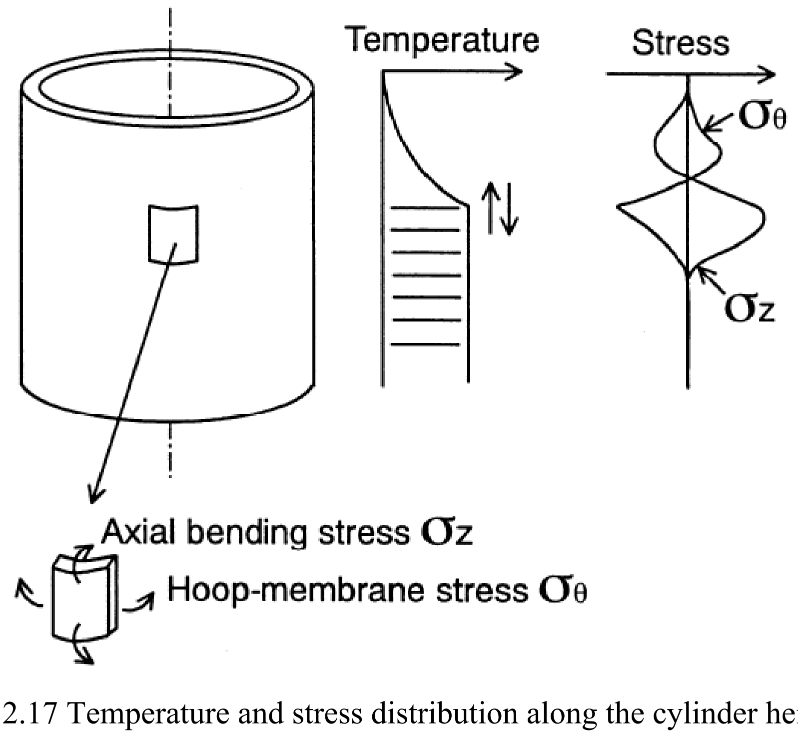

Figure 2.17 Temperature and stress distribution along the cylinder height [54]

In order to propose more advanced and reliable methods of analysis, experimental work at CEA Cadarache termed as VINIL tests were carried out [42]. Long and short mock-ups were conducted on cylinders (800 mm diameter and 1.2 mm thickness) with moving sodium free level at about 620 °C. It was a challenging task to operate and record the effect of sodium free level variations. Further, the deformation measurement was not possible in continuous mode of operation due to high temperature sodium and its high affinity with oxygen, which may result in accidents. The temperature of 620 °C was to accelerate the creep effect and reduce the duration of hold time. After this test, it was concluded that the progressive deformation does in fact occur, which depend on the size, geometry and free or embedded condition of the cylindrical specimen. With the progress in thermal ratcheting studies, the existing codes [43], [44], [45] updated the analysis procedures to evaluate thermal ratcheting strain. Ratcheting following inelastic analysis route for different combination of loads [46] is explained in DDS (Demonstration plant Design Standard). Japanese design code DDS [47] evaluated ratcheting strain considering a combination of primary and secondary stresses with imposition of secondary membrane and bending stresses.

Kobayashi and Ohno [25] presented the significant role of the procedure or constitutive models adopted for evaluation of ratcheting. They examined the effect of choosing perfectly plastic model (PP), the LKH, the classical nonlinear AF rule and the rule proposed by Ohno and Wang. They assumed the material to have only kinematic hardening with no isotropic and cyclic hardening component. The analysis was performed with a hollow cylinder of SS 304 material with radius 170 mm, length 200 mm and thickness 1 mm. The cylinder was thermally loaded in three stages viz., (a) At the beginning in each cycle, temperature (say T_o) distributes uniformly in the cylinder and then increased by ΔT, (b) The temperature front moves by a distance of 100 mm and (c) The temperature of the cylinder is recovered back to T_o. He concluded that, out of the four models, AF and OW may be used for thermal ratcheting estimation, though there was over prediction by AF and under estimation by OW model. With the OW model, the thermal ratcheting strain saturated after few numbers of cycles when ΔT was smaller. On the other hand, the thermal ratcheting strain using LKH and AF models, developed more constantly when ΔT was smaller.

Igari and co-authors [48] performed a detailed inelastic analysis of thermal ratcheting due to a moving temperature front. His work was to find out an appropriate inelastic constitutive equation, which can simulate the effect of traveling distance, stress level and hold time on thermal ratcheting behavior of a cylinder. Experimental data of ten specimens made of SUS 316 and 316FR stainless steels was obtained and the ratcheting results were compared with the corresponding inelastic analysis using different models. For this type of thermal ratcheting, two kinds of stresses are important which are induced by the axial temperature distribution; (a) the hoop-membrane stress (b) the axial bending stress. The axial temperature distribution was produced by the combination of induction heating from outside and water-cooling from inside the specimen. Thus, the developed stresses may cause expansion or contraction in cylinder near the vicinity of free level. The amount of radial displacement was compared for different cases of traveling length and was obtained lesser for short traveling length of temperature profile. Furthermore, great amount of experiments were conducted to study the effect of temperature variations and hold time during strain controlled loading. For different conditions of traveling distance, stress level and hold time, analysis results were presented taking account of creep and thermal aging. It was also concluded that, for the applied loading there was little influence of the hold time on thermal ratcheting behavior.

Chellapandi et al. [49] demonstrated the thermal ratcheting behavior of hollow cylinder ($1/17^{th}$ scaled down model of PFBR main vessel) subjected to a more realistic traveling temperature profile. According to his studies, when the reactor conditions changes from shutdown to normal operation as well as normal operation to DHR or Safety Grade Decay Heat

Removal (SGDHR) conditions, the sodium free level vary in accordance with the associated temperatures.

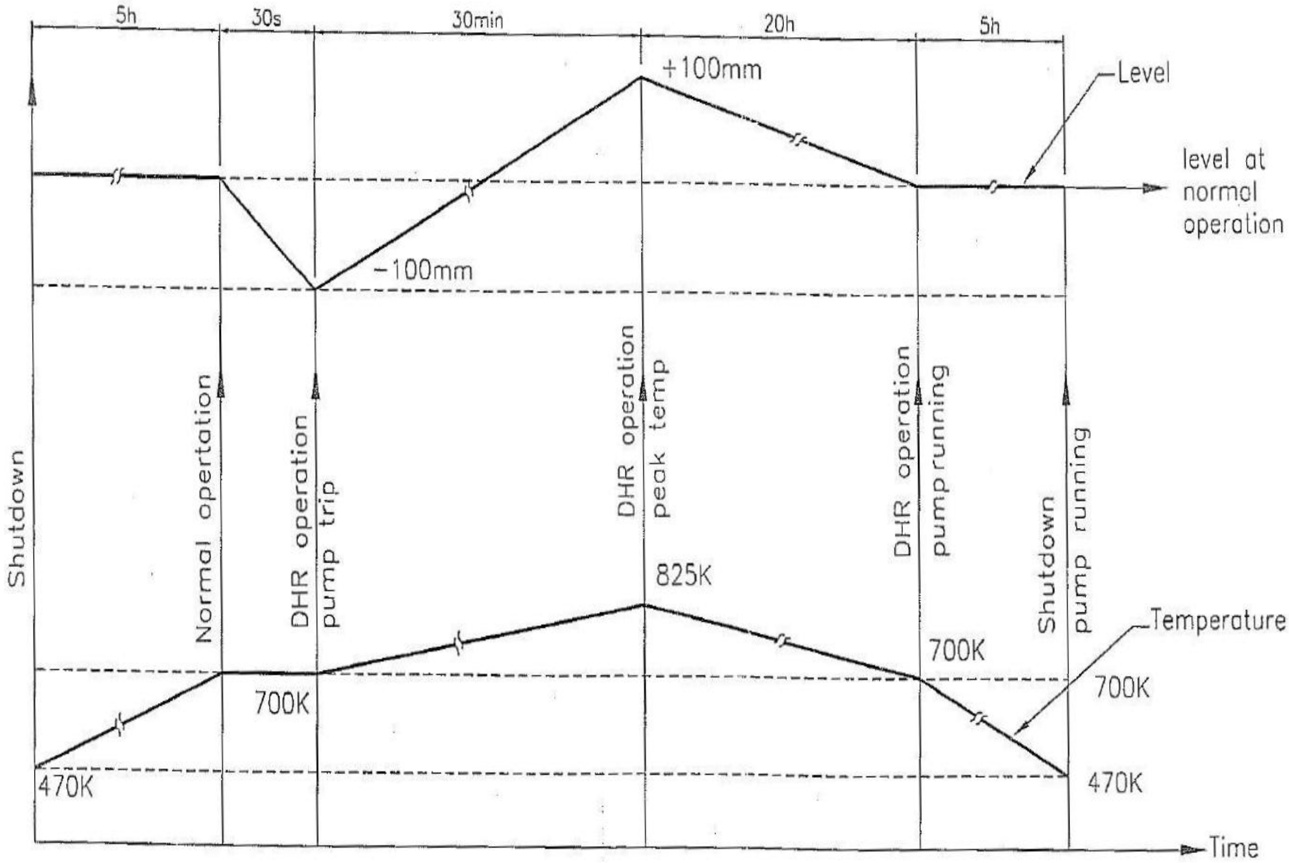

Figure 2.18 Temperature and level variations during decay heat removal operations [49]

Figure 2.18 illustrates an idealized load cycle of temperature and level variation. This is to be noted that, there is a considerable changes in rate of level variation as well as temperature variation, which requires rate dependent modeling for ratcheting prediction accurately. He used '23-parameter Chaboche visco-plastic model' for the analysis and the results so obtained after validating the proposed formulation with VINIL test results, were reasonably conservative. The amount of radial deformation in the main vessel came out to be 15 mm in radial inward direction after an assumed 120 number of SGDHR cycles. However, lesser deformation may be possible if the realistic constitutive model is employed.

Through the above discussed works on thermal ratcheting, it is observed that VINIL tests are used widely to validate the numerical results, which are quite complex and difficult to conduct due to the involvement of sodium based system. Thus, problems in performing the thermal ratcheting tests and validation of the numerical procedure still exist. Hence, we require some simplified test setups and computationally simple formulation procedure to bring improvement in thermal ratcheting estimation. In this connection, the present work focused on proposing a simplified experimental setup and computationally effective procedure for ratcheting evaluation and finally addressing some unattended features of thermal ratcheting behavior. For this purpose the experimental and numerical simulation of thermal ratcheting by Lee et al. [50] described in the next chapter as a benchmark analysis, is used extensively.

2.3 SUMMARY

The detailed discussion on plasticity theories and different variations of the constitutive models applied to represent ratcheting behavior unveil some important features of ratcheting. To represent ratcheting behavior of hardening material, time independent or time dependent constitutive models have been described. It can be noted that the applicability of these models depends largely on the loading conditions for accurate prediction of ratcheting. It is also evident that no single model is robust enough to represent ratcheting phenomenon for varied loading conditions. Further, the thermal ratcheting phenomenon addressed by the researchers adopting different modeling approach has revealed that simplification of loadings (short or long traveling temperature front, ignoring temperature variation during free level change) also affect thermal ratcheting behavior. This suggests that, rate dependence, hold time and rate of change in temperature during sodium free level variation play an important role in progressive strain accumulation of the cylindrical shell. Another factor which leads to over prediction of thermal ratcheting is the choice of constitutive models used. This motivates to further investigate thermal ratcheting phenomenon considering realistic loading and appropriate modeling approach to reduce the overestimation.

THERMAL RATCHETING ANALYSIS: ISOTHERMAL 3

3.1 INTRODUCTION

The findings of the previous knowledge suggest that there is a remarkable effect of choice of constitutive models. Various models have been developed considering the effect of hardening and visco-plasticity to predict the cyclic response of materials using different plasticity theories. As described earlier, the linear hardening rule [18] is the simplest kinematic hardening rule which considers the Bauschinger effect, but fails to show the plastic strain accumulation in the presence of mean stress. The non-linear kinematic hardening model [20] has been found suitable to simulate ratcheting after modifications by researchers [22] showed improved results. Chaboche kinematic hardening model with single back stress, due to its simplicity and conservative results has been used for ratcheting behavior of cylindrical pipes [51]. The applicability of these theories is restricted to loadings when rate effect is negligible. Rate effect has to be considered while developing the constitutive models to predict cyclic deformation behavior of structural components under cyclic load at different rates at high temperature. It has been reported [32] that plasticity-creep superposition model (SPC) is suitable when hold time and creep effects are significant while unified visco-plastic constitutive model (UVP) is preferred to account for visco-plasticity without hold time and creep. Further, the implementation of hardening rules and complex constitutive models in FEM package invites another complexity while using the implicit or explicit technique for the plasticity integration.

A simpler approach can be a semi-implicit scheme of plasticity integration. All these studies addressed various phenomena concerning ratcheting behavior of material through isothermal approach, which is widely applied owing to its simplicity and cost effectiveness. However, isothermal approach is an idealization of dynamic behavior of material under transient thermal loading such that the temperature dependence of material properties is neglected. It can be stated, therefore, that a careful consideration of three basic factors may yield improved ratcheting results. These are: (i) Constitutive models for ratcheting (ii) Integration procedure (iii) Isothermal or non-isothermal approach. In this chapter, the governing equations considered for the present work and the derivation of integrations procedure are described first, and the implementation and validation of the code are described subsequently. Further, the chapter addresses the cyclic hardening and the thermal ratcheting behavior of SS 316 L austenitic steels using time independent and dependent constitutive models for ratcheting employing the proposed integration procedure with isothermal approach.

3.2 NUMERICAL MODELING- DEVELOPMENT OF CODE FOR PREDICTION OF RATCHETING

Numerical modeling is performed using the concept of radial return technique to ensure the unconditional stability during plastic deformation. For effective plastic strain increment, Newton's method of integration is used, while all other quantities are integrated explicitly with self-developed FORTRAN coding employed in UMAT subroutine [52]. In implicit scheme, momentum balance or equilibrium equations require the determination of Jacobian that comprises the tangent stiffness matrix and load stiffness matrix. Since the tangent stiffness matrix is dependent on material behavior, hence the choice of governing equations for constitutive modeling should be realistic to yield accurate results for strain calculation. The governing equations in the framework of time independent and time dependent approach are henceforth called as *Model-1* and *Model-2* respectively.

3.2.1 Governing equations

The equations for *Model-1* describing time independent material ratcheting with the normality hypothesis and associated flow rule obeying the von Mises yield criteria [53], [54] are reproduced below in Eqs. (3.1) - (3.5).

$$\mathbf{d\varepsilon^P} = d\lambda \frac{\boldsymbol{\sigma}' - \mathbf{X}'}{J_2(\boldsymbol{\sigma} - \mathbf{X})} \tag{3.1}$$

$$d\lambda = \frac{H(f)}{h} \left\langle \frac{3}{2} \frac{\boldsymbol{\sigma}' - \mathbf{X}'}{J_2(\boldsymbol{\sigma} - \mathbf{X})} \mathbf{d\sigma} \right\rangle \tag{3.2}$$

$$J_2(\boldsymbol{\sigma} - \mathbf{X}) = \sqrt{\frac{3}{2}(\boldsymbol{\sigma} - \mathbf{X}):(\boldsymbol{\sigma} - \mathbf{X})} \tag{3.3}$$

$$f = J_2(\boldsymbol{\sigma} - \mathbf{X}) - R - k \tag{3.4}$$

$$h = C - \frac{3}{2}\gamma \mathbf{X} \frac{\boldsymbol{\sigma}' - \mathbf{X}'}{J_2(\boldsymbol{\sigma} - \mathbf{X})} + b(Q - R) \tag{3.5}$$

where $d\lambda$ is plastic multiplier, $\boldsymbol{\sigma}'$ is deviatoric stress tensor, $\mathbf{X}'$ is the deviatoric back stress tensor, $\mathbf{X}$ is back stress, $J_2(\boldsymbol{\sigma}-\mathbf{X})$ is the second invariant of the deviatoric stresses, R is the drag stress in isotropic hardening, P is accumulated plastic strain, $\mathbf{d\varepsilon^P}$ is plastic strain increment. The other symbol such as f, h, $H(f)$ and k are yield function, hardening modulus, Heaviside step function and initial yield stress respectively. $\langle \bullet \rangle$ is the Macaulay's bracket, which means that, $\langle x \rangle = 0$ for $x \leq 0$ and $\langle x \rangle = x$ for $x > 0$.

Governing equations for *Model-2* describing time dependent material ratcheting using unified visco-plastic theory [55] are given below in Eqs. (3.6) - (3.10).

$$\boldsymbol{\varepsilon}_{ij} = \boldsymbol{\varepsilon}_{ij}^{e} + \boldsymbol{\varepsilon}_{ij}^{In} + \boldsymbol{\varepsilon}_{ij}^{T} \tag{3.6}$$

$$\boldsymbol{\varepsilon}_{ij}^{e} = D_{ijkl}^{-1}\boldsymbol{\sigma}_{kl} \tag{3.7}$$

$$\dot{\boldsymbol{\varepsilon}}_{ij}^{In} = \sqrt{\frac{3}{2}}\left\langle \frac{F_y}{K} \right\rangle^{n} \frac{\boldsymbol{\sigma}' - \mathbf{X}}{\left\| \boldsymbol{\sigma}' - \mathbf{X} \right\|} \tag{3.8}$$

$$\dot{\boldsymbol{\varepsilon}}_{ij}^{T} = C_{ij}\dot{T}\boldsymbol{\delta}_{ij} \tag{3.9}$$

$$F_y = \sqrt{1.5(\boldsymbol{\sigma}' - \mathbf{X})(\boldsymbol{\sigma}' - \mathbf{X})} - R \tag{3.10}$$

where $\boldsymbol{\varepsilon}_{ij}, \boldsymbol{\varepsilon}_{ij}^{In}, \boldsymbol{\varepsilon}_{ij}^{e}, \boldsymbol{\varepsilon}_{ij}^{T}$ and $\dot{\boldsymbol{\varepsilon}}_{ij}^{In}$ are total strain, inelastic strain, elastic strain, thermal strain and inelastic strain rate respectively. $\dot{\boldsymbol{\varepsilon}}_{ij}^{T}$ is the thermal strain rate caused by $\dot{T}$ and D_{ijkl} is the matrix of elasticity. K and n are material parameters representing the viscous characteristics. F_y is loading function and C_{ij} is the coefficient of thermal expansion while δ_{ij} is Kronecker delta where $\delta_{ij} = 0$ for $i \neq j$ and $\delta_{ij} = 1$ for $i = j$.

$$\dot{R} = b(Q - R)\dot{P} \tag{3.11}$$

Here Q is the asymptotic value, which corresponds to a regime of stabilized cycles and b indicates the speed of stabilization. Nonlinear kinematic and isotropic hardening variables are updated explicitly for (t) to $(t+1)^{th}$ increment as follows:

$$\mathbf{X}_{(t+1)} = \mathbf{X}_{(t)} + \Delta\mathbf{X} \tag{3.12}$$

$$R_{(t+1)} = R_{(t)} + \Delta R \tag{3.13}$$

3.2.2 Proposed simplified semi-implicit integration procedure

An implicit integration procedure, unlike the explicit procedure does Newton iterations to enforce equilibrium of the internal structure forces with the externally applied loads. This feature of implicit procedure is more suitable for cyclic loading cases in nonlinear analysis resulting in better accuracy and equilibrium with improved convergence. The procedure for plasticity integration performed implicitly while updating stresses and other parameters explicitly at the end of time increment is termed as semi-implicit procedure [56]. The semi-implicit procedure adopted in this work requires expressions for infinitesimal effective plastic strain increment. The expressions are derived for the plasticity integration using the closed and the rapid converging feature of implicit procedure while simplicity of explicit procedure is retained. Hence, the proposed procedure is named as Simplified Semi-implicit Integration Procedure (SSIP) for present constitutive models. Another reason for its simplicity is the expression of infinitesimal effective plastic strain increments ($d\Delta P$) which involves scalar operation for its update and tolerance check during yielding. The expression of $d\Delta P$ derived for *Model-1* and *Model-2* can be used directly in UMAT subroutine for sub-incrementation avoiding tedious algebra to implement the Newton's iteration. Although powerful, the Newton's iteration is difficult to implement for complex constitutive relations because it requires second order derivatives of the yield function and plastic potential. Implicit procedure is unconditionally stable and a quadratic rate of convergence is achieved with Newton's iterations. This advantageous feature of Newton's method saves computational time. Therefore, in comparison to the conventional numerical procedure (Fully implicit or explicit procedure), the SSIP is proved to be both simple and time saving for present numeral analysis.

3.2.2.1 *Infinitesimal plastic strain increment formulation for Model-1*

Trial effective stress (σ_{ef}^{Tr}) assumed initially using effective stress (σ_{ef}) for predictor-corrector step using Eq. (3.3), and then flow criteria using von Mises yielding condition are checked by Eq. (3.14).

$$f = \sigma_{ef} - R - k = \sigma_{ef}^{Tr} - 3G\Delta P - R - k = 0 \tag{3.14}$$

The above expression is nonlinear in terms of ΔP (effective plastic strain increment). G: is the shear modulus. Applying the Newton-Rapson method using Eq. (3.15)

$$\Delta P_{t+1} = \Delta P_t - \frac{f(\Delta P)}{f'(\Delta P)} \tag{3.15}$$

we get, $$d\Delta P = -\frac{f(\Delta P)}{f'(\Delta P)} = \frac{f(\Delta P)}{3G + (\partial R / \partial \Delta P) - (\partial \sigma_{ef}^{Tr} / \partial \Delta P)} \tag{3.16}$$

Now referring Eq. (3.11) while partially differentiating Eq. (3.13), we get:

$$\frac{\partial R}{\partial \Delta P} = b(Q - R) = H_i \tag{3.17}$$

Here the subscript *'i'* corresponds to isotropic hardening. Similarly, considering Eqs. (2.11) and (3.12), we get H_k ,where *'k'* corresponds to kinematic hardening while obtaining the derivative of effective trial stress with respect to plastic strain increment as shown below:

$$\frac{\partial \sigma_{ef}^{Tr}}{\partial \Delta P} = \frac{\partial \sigma_{ef}^{Tr}}{\partial \mathbf{X}} : \frac{\partial \mathbf{X}}{\partial \Delta P} = -\eta : \frac{2}{3} C\eta - \gamma \mathbf{X} = -\eta : H_k \tag{3.18}$$

Thus, the combined hardening modulus and infinitesimal plastic strain increment can be evaluated using the implicit integration method by considering Eqs. (3.19) and (3.20) respectively.

$$h = (-\eta : H_k) + H_i \tag{3.19}$$

$$d\Delta P = \frac{\sigma_{ef}^{Tr} - 3G\Delta P - R - k}{3G + h} \tag{3.20}$$

3.2.2.2 *Infinitesimal plastic strain increment formulation for Model-2*

Unified visco-plastic theory is discussed in its general form, so that after further simplification, it can be reduced to time independent constitutive model as a limiting case. To maintain consistency with time independent constitutive model, plastic multiplier concept is adopted such that Eq. (3.8) can be expressed in terms of accumulated plastic strain rate [11]. Thus, expression for $\dot{P}$ can be expressed as a function of stress and hardening variables as below:

$$\dot{P} = \left(\frac{V_f}{K} \right)^n = \varphi(\boldsymbol{\sigma}, \mathbf{X}, R) \tag{3.21}$$

The time dependence is accounted by introducing the following function:

$$\psi = \Delta P - \varphi \Delta t = 0 \tag{3.22}$$

Now applying consistency condition, we get Eq. (3.23).

$$\psi+\frac{\partial\psi}{\partial\Delta P}d\Delta P+\frac{\partial\psi}{\partial X}:dX+\frac{\partial\psi}{\partial R}dR=0 \tag{3.23}$$

$$\Delta P-\varphi\Delta t+\left((1-\frac{\partial\varphi}{\partial\Delta P}\Delta t)d\Delta P\right)-\left(\frac{\partial\varphi}{\partial\Delta X}\Delta t\right):dX-\left(\frac{\partial\varphi}{\partial\Delta R}\Delta t\right)dR=0 \tag{3.24}$$

$$\Delta P-\varphi\Delta t+\left\{1-\varphi_{(\Delta P)}\Delta t\right\}d\Delta P-\left\{\left(\varphi_{(\Delta X)}\Delta t\right):H_k\right\}d\Delta P-\left\{\left(\varphi_{(\Delta R)}\Delta t\right)H_i\right\}d\Delta P=0 \tag{3.25}$$

$$d\Delta P=\frac{\varphi\Delta t-\Delta P}{1-\left[\left\{\varphi_{(\Delta P)}\Delta t\right\}+\left\{\left(\varphi_{(\Delta X)}\Delta t\right):H_k\right\}+\left\{\left(\varphi_{(\Delta R)}\Delta t\right)H_i\right\}\right]} \tag{3.26}$$

where, $$\frac{\partial\varphi}{\partial\Delta P}=\varphi_{(\Delta P)};\frac{\partial\varphi}{\partial\Delta X}=\varphi_{(\Delta X)};\frac{\partial\varphi}{\partial\Delta R}=\varphi_{(\Delta R)} \tag{3.27}$$

Considering von Mises flow criteria, we assume V_f (yield function) in terms of loading function F_y i.e. Eq. (3.10) as below:

$$V_f(F_y)=\sqrt{1.5(\sigma'-X):(\sigma'-X)}-R-k=0 \tag{3.28}$$

$$\varphi=\left(\frac{V_f}{K}\right)^n=\left(\frac{\sigma_{ef}^{Tr}-3G\Delta P-R-k}{K}\right)^n \tag{3.29}$$

Now from Eqs. (3.27) and (3.29), we get:

$$\varphi_{(\Delta P)}=\frac{n}{K^n}(V_f)^{n-1}-3G;\varphi_{(\Delta X)}=-\frac{n}{K^n}(V_f)^{n-1};\varphi_{(\Delta R)}=-\frac{n}{K^n}(V_f)^{n-1} \tag{3.30}$$

We find that, infinitesimal effective plastic strain increment as in Eq. (3.26) for Newton's method using unified visco-plasticity can be expressed as below:

$$d\Delta P=\frac{\varphi\Delta t-\Delta P}{1+\Delta t\frac{n}{K^n}(V_f)^n\left[3G+\eta:H_k+H_i\right]} \tag{3.31}$$

3.2.3 Flowchart for the adopted SSIP-Isothermal

The flow chart of the code for SSIP in the UMAT subroutine for the computation of ratcheting behavior is shown in Figure 3.1 and the steps for its implementation is provided subsequently.

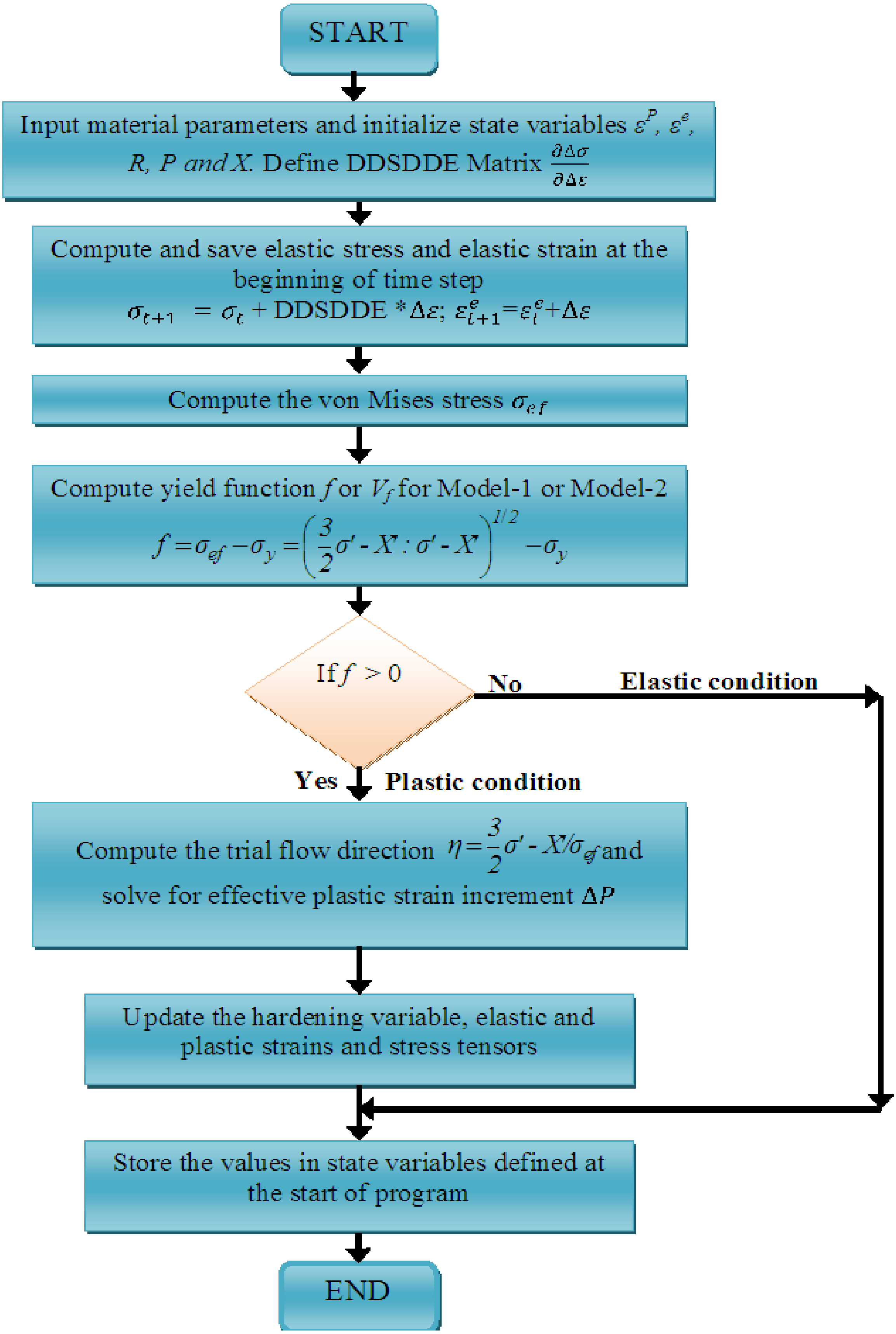

Figure 3.1 Flowchart for the SSIP: Isothermal

The implementation of the coded involves following steps:

(i) Determination of elastic stress.

(ii) Determination of elastic strain.

(iii) The equivalent stress by von Mises stress criteria is calculated.

(iv) Yield function determination.

(v) Yielding condition is checked.

(vi) If yielding condition is met, Newton's method is applied for effective plastic strain increment otherwise the effective plastic strain increment is zero.

(vii) Elastic and plastic strain and stress increment is computed.

(viii) All the quantities such as stress, strain, isotropic and kinematic hardening variables are updated.

3.3 BENCHMARK ANALYSIS: TIME INDEPENDENT AND DEPENDENT MODELING

In order to validate the present procedure and developed code for *Model-1* and *Model-2*, the benchmark studies of ratcheting behavior of SS 316 L austenitic steel performed by Lee et al. [50] and Kang and Gao [57] respectively are chosen. The analyses have been conducted at high temperature (HT) i.e. 550 ºC and room temperature (RT). The material parameters listed in

Table 3.1 for *Model-1* HT case are taken from Lee's work while the parameters for *Model-2* HT case are identified by comparing present analysis with Lee's strain controlled cyclic hardening test results. The tensile test data by Kang and Gao [57] is used to identify the material parameters for *Model-2* RT case assuming the kinematic and isotropic hardening parameters same for *Model-1* and *Model-2*. This assumption stands true at room temperature for small strain range applications under low strain rate loading conditions.

Table 3.1 Material parameters for *Model-1* and *Model-2*

Models	Cases	*C* (MPa)	*γ*	*b*	*Q* (MPa)	*k* (MPa)	*K*	*n*
Model-1	HT	92400	1390	14.6	51.1	59.4	---	---
	RT	131200	860	38	123	138	---	---
Model-2	HT	98400	880	8.7	119	64	38	2.2
	RT	131200	860	38	123	138	42	5.6

3.3.1 Time independent modeling

Thermal ratcheting analysis of a cylinder with dimensions 600 mm outer diameter (OD), 500 mm height and 3 mm thickness as per Lee et al. [50] is performed using a finite element model having 600 axisymmetric four noded quadratic elements. Figure 3.2 (a) shows the schematic diagram of the thermal ratcheting experimental setup that simulates the loading due to free level variation by generating a moving temperature distribution. Lee et al. have applied the thermal loading due to moving temperature distribution as shown in Figure 3.2 (b) for 9 cycles. This case of loading simulates the up and down movement of the thin, hollow cylinder in a water filled container with the cylinder being heated using a fixed induction heater while moving down into the water.

The evaluation of progressive inelastic strain due to level variation has been computed by introducing user-defined subroutines (UMAT) in ABAQUS. It includes FILM subroutine [52] to take care of thermal and heat transfer properties for thermal cycling and material subroutine UMAT for material behavior definition. The material subroutine is formulated such that it takes care of isotropic and kinematic hardening behavior of material following Chaboche nonlinear combined hardening model (i.e. *Model-1*).

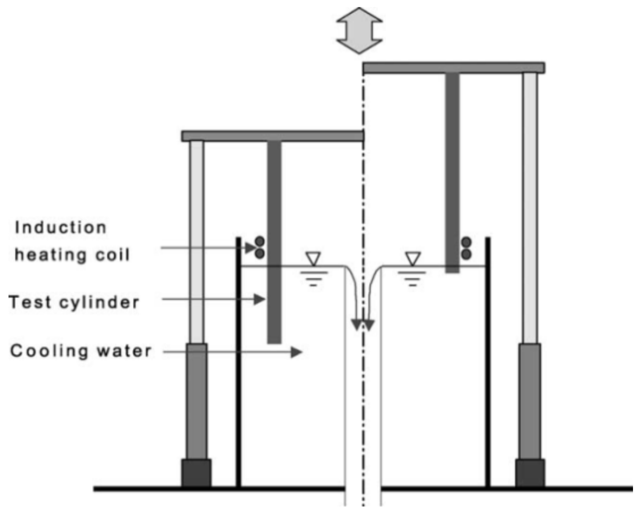

(a)

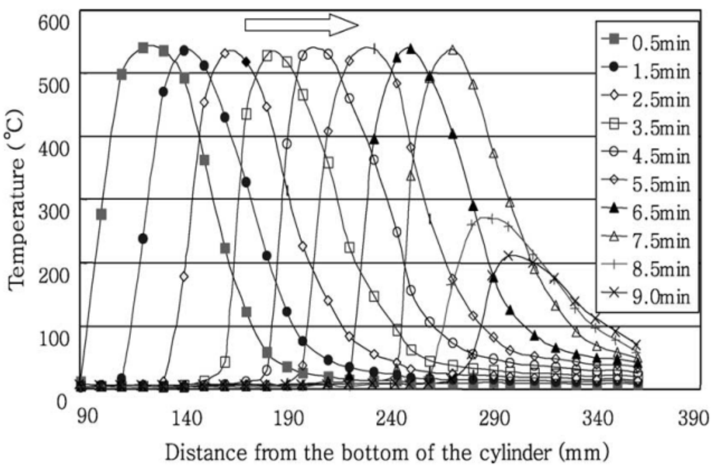

(b)

Figure 3.2 (a) Schematic of the experimental setup for ratcheting and (b) Transient temperature profile measured by thermocouples as per Lee et al. [50]

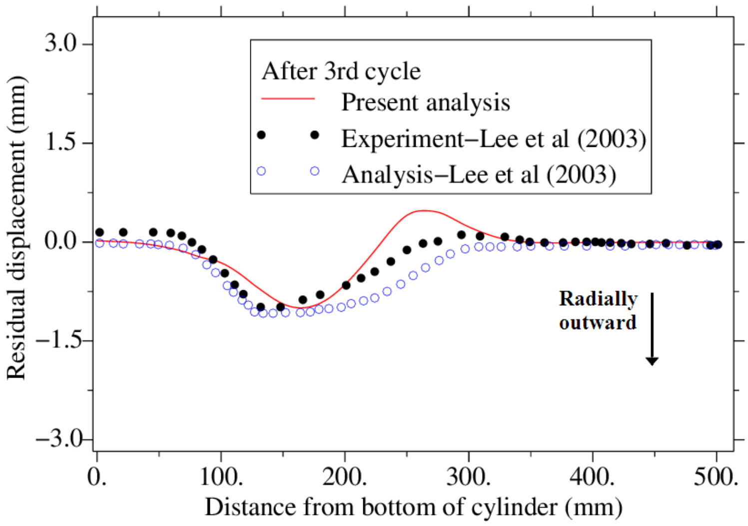

(a)

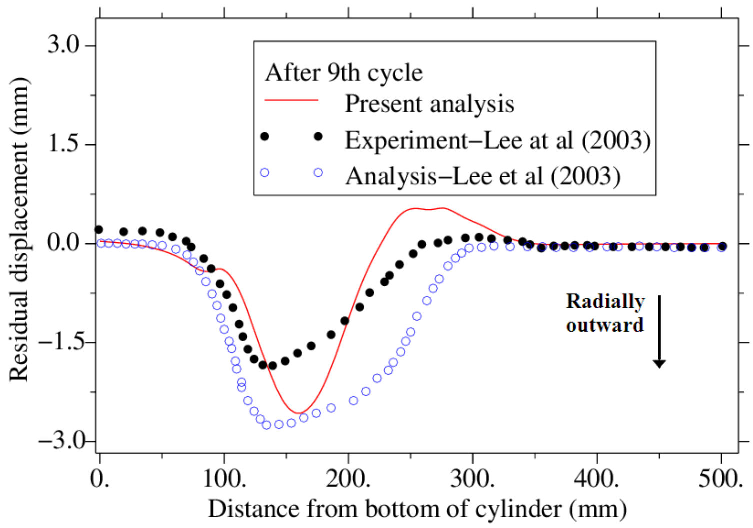

(b)

Figure 3.3 Comparison of residual displacement (a) after 3rd cycle and (b) after 9th cycle.

The progressive inelastic deformation at the end of each cycle is measured for 9 loading cycles with 150 mm of level variations. The displacements after 3 cycles and 9 cycles are −0.98 mm and −2.57 mm, respectively (−ve sign is for radially outward displacement). Figure 3.3 compares the residual radial displacements after the 3rd and 9th cycle obtained by present analysis and literature data. The values obtained by time independent formulation with SSIP are reasonably close to the values obtained by the experiment at the end of 9 load cycles. The present analysis yielded −2.57 mm radial displacements which is in reasonable agreement to the experimental value of 1.79 mm and numerical analysis value of 2.74 mm predicted by Lee et al. [50]. This improvement in the prediction of ratcheting is observed by adopting SSIP for the present analysis, although four node elements were used instead of eight node elements which were used by Lee et al. considering explicit midpoint procedure. However, a slight shift in location of peak displacement is noticed while comparing the radial displacements. Nevertheless, the high value of displacement in the radial direction is a matter of concern for ratcheting analysis because ratcheting strain limit should be 1% for base metal and 0.5% for weld metal as per RCC-MR [44] so the observed difference in location of peak displacement can be ignored.

3.3.2 Time dependent modeling

Results of uniaxial tensile tests at room temperature at strain rates of 2.0×10^{-4}/s and 2.0×10^{-3}/s as in Kang and Gao [57] whereas strain controlled cyclic loading test at 550 °C as in Lee et al. [50] at 6.67×10^{-4}/s strain rates are compared with present analysis in Figure 3.4. It satisfactorily validates the present analysis results for time dependent visco-plastic formulations (*Model-2*). Thus, the multiaxial and uniaxial ratcheting strain predicted by the developed code agrees well with the reported results for both the time independent and dependent models hence used for further analysis in subsequent sections.

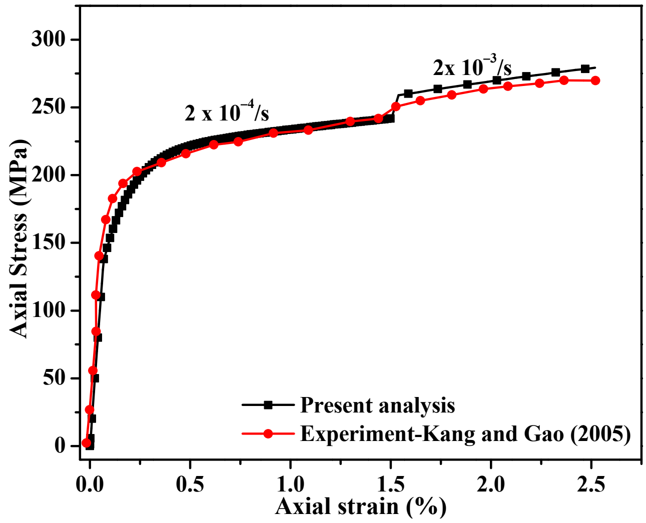

(a)

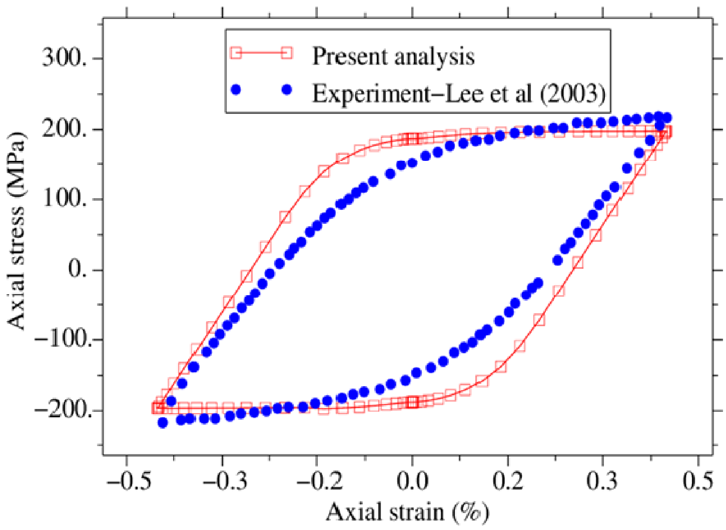

(b)

Figure 3.4 (a) Monotonic stress-strain curve at different strain rates (b) Comparison of cyclic stress-strain behavior of SS 316 L at strain rate of 6.67×10^{-4}/s (at 550°C).

3.4 NUMERICAL ANALYSIS AND RESULTS

In order to understand the significance of choice of constitutive models and integration procedure, the application studies of *Model-1* and *Model-2* have been performed for different mechanical and thermal cyclic loading conditions. On the one hand, investigation of cyclic hardening behavior of SS 316 L at ambient and elevated has been carried out at various mean stresses under uniaxial cyclic mechanical loading. On the other hand, detailed investigation of ratcheting behavior of cylindrical shell subjected to travelling temperature front due to free level variations as in the main vessel of SFR has been carried out. Effects of various loading methods on ratcheting or shakedown behavior, contribution of rate dependence, contribution of hold time on thermal ratcheting are discussed subsequently in the following section of the chapter. Influence of time independent and dependent modeling approach is also highlighted by investigating the effect of frequency of free level fluctuations on thermal ratcheting strain. The discussion throughout this section is on the analysis performed on SS 316 L austenitic steels, which is a widely used structural material for high temperature applications in chemical, automobile and nuclear industries.

3.4.1 Cyclic hardening behavior

Strengthening due to constant amplitude strain cycling is a characteristic feature of austenitic steels and hence they are called as cyclic hardening materials. This section describes the cyclic hardening behavior of SS 316 L at room temperature (RT) and 550 ºC (HT). Furthermore, influence of mean stress increase on cyclic accumulation of strain is analyzed by implementing *Model-1* and *Model-2* in UMAT code. For this analysis, a finite element model of solid bar specimen with test section diameter of 10 mm and gauge length 30 mm is subjected to uniaxial stress controlled loading. Schematic of applied load is shown in Figure 3.5Figure 3.5 (a) where σ_m and σ_a are mean stress and stress amplitude respectively. The effect of mean stress variation is investigated by varying σ_m while keeping σ_a constant. Time to reach the maximum stress is 9.5 s for each loading case.

Stress controlled loading (MPa) for 40 cycles with the stress histories at different Stress Levels (SL): at room temperature (a) RT-SL-1: 22±195 (b) RT-SL-2: 37±195 (c) RT-SL-3: 52±195 and at 550 °C (d) HT-SL-1: 10±70 (e) HT-SL-2: 20±70 (f) HT-SL-3: 30±70 are analyzed. It is observed from the Figure 3.5 (b) that the ratcheting strain predicted by *Model-2* shows higher strain compared to that obtained by *Model-1* (for RT-SL-3: 52±195). The maximum ratchet strain of 0.82 % is seen from Figure 3.5 (b) which is in agreement with the experimental value ~0.79 % maximum strain for *Model-2* [57]. This again confirms the validity of time dependent formulations using *Model-2*. The cyclic response of SS 316 L under various loading condition at room temperature and 550 °C shows strong influence of mean stress variations. Significant initial hardening is noticed in the first few cycles for both room temperature and high temperature conditions

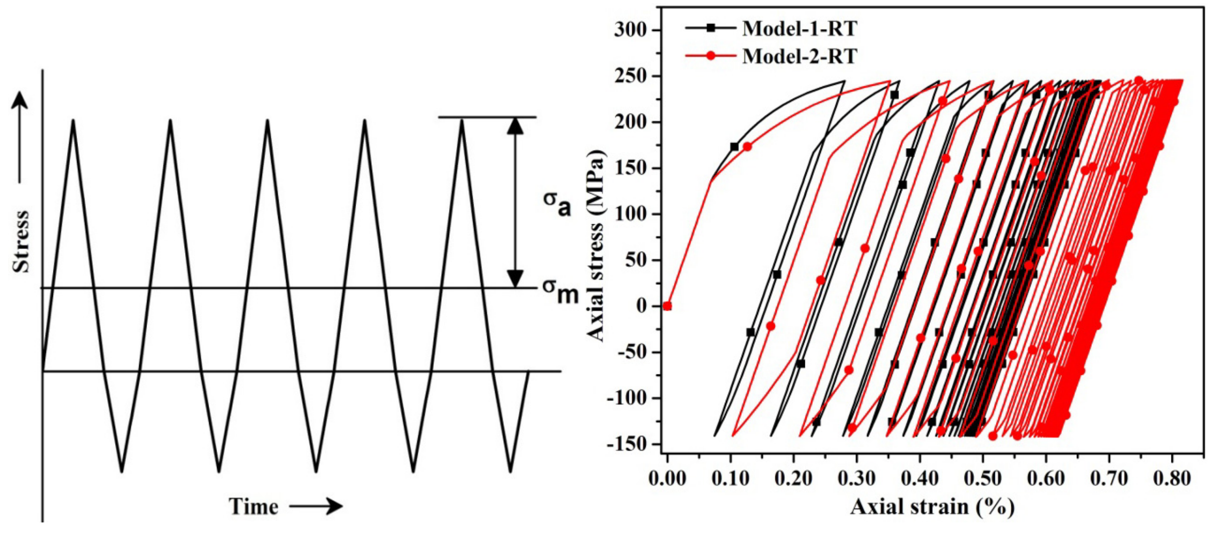

(a) (b)

Figure 3.5 (a) Schematic of stress controlled loading (b) Stress strain plots obtained using *Model-1* and *Model-2* at room temperature (RT).

3.4.1.1 *Effect of mean stress on ratcheting behavior*

The underlying effect of mean stress on ratcheting behavior is investigated by conducting the finite element analysis using self developed code employing formulations for *Model-1* and

Model-2 in UMAT code. Uniaxial asymmetric cyclic stress loadings mentioned in section 2.4 are applied to record the effect of increase in mean stress.

Figure 3.6 (a) and (b) shows the evolution of axial strain using *Model-1* and *Model-2* respectively, at room temperature, while, Figure 3.6 (c) and (d) show the evolution of axial strain using *Model-1* and *Model-2* respectively at 550 °C. Mean stress increase results into an increase in accumulated strain at room temperature and high temperature for both the models and shakedown state is noticed in Figure 3.6 (a) and (b) while near shakedown state in Figure 3.6 (c) and (d).

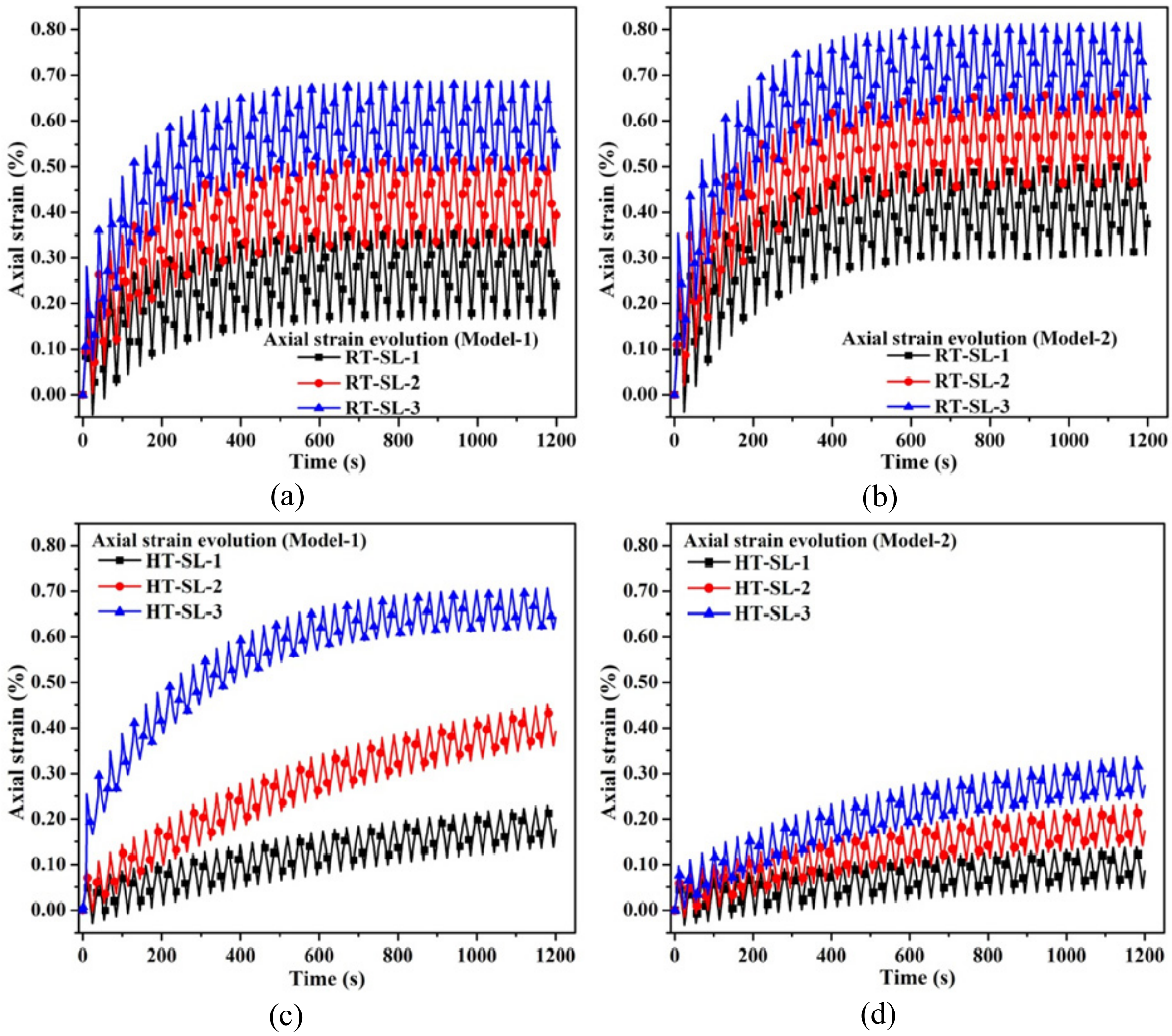

Figure 3.6 Evolution of axial strain (a) for *Model-1* at room temperature. (b) for *Model-2* at room temperature (c) for *Model-1* at 550 °C (d) for *Model-2* at 550 °C

The prediction of strain accumulation with loading cycles is compared by plotting peak strain values vs number of loading cycles in Figure 3.7 (a) - (d). The results indicate montonic increase in strain with increasing no. of cycles. The increase in mean stress lead to increase in accumulated strain both for *Model-1* and *Model-2* but difference of simulation in corresponding results of *Model-1* and *Model-2* at room temperature is negligible. Therefore, it may be proposed to use *Model-1* having less material parameters for room temperature ratcheting analysis at stressing rates below 26 MPa/s.

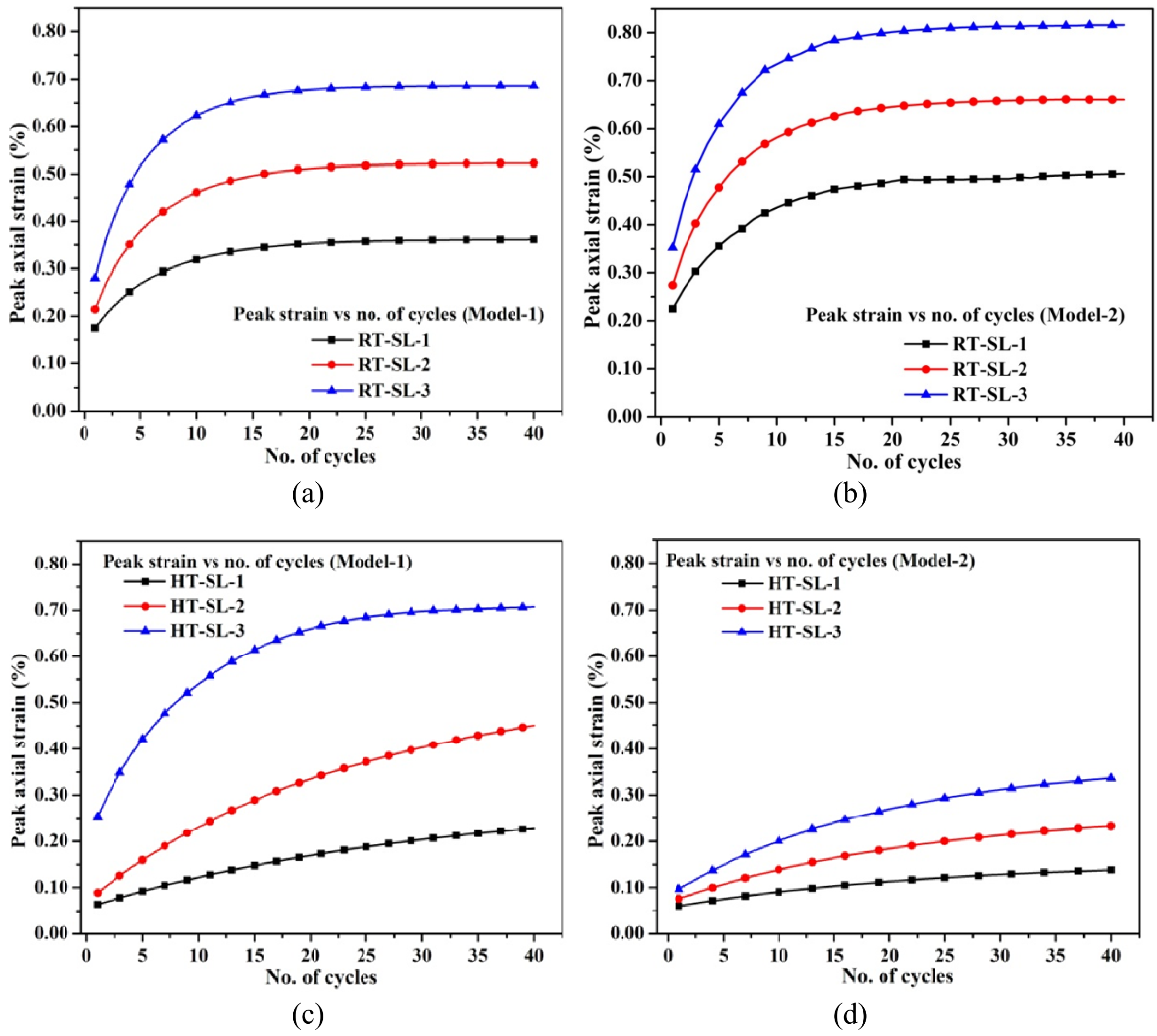

Figure 3.7 Peak strain developed per cycle: at room temperature (a) for *Model-1* (b) for *Model-2*, at 550°C, (c) for *Model-1* (d) for *Model-2*

Alternatively, *Mode1-2* may be used for moderate or higher stressing rates since the remarkable rate dependence of austenitic steels have been reported in literatures [57], [58]. At high temperature, increase in strain with the mean stress is suppressed in case of time dependent (*Model-2*) constitutive modeling. Moreover, *Model-2* predicts less strain accumulation compared to corresponding results for *Model-1*. This shows the influence of visco-plasticity/rate dependence which is accounted in *Model-2* and is prominent at high temperature condition. Therefore, it is inferred that *Model-2* simulate satisfactorily the ratcheting behavior for the loading rates of ~8.5 MPa/s and above, since rate dependent deformation of the material is overestimated by *Model-1* compared to *Model-2* at 550 °C.

3.4.1.2 *Increment in peak strain after each loading cycles*

Variation of peak strain increments ($\Delta\varepsilon_R$ % =Peak strain $_{nc+1}$− Peak strain $_{nc}$) after each loading cycle is used here as a measure to indicate the rate of cyclic hardening where nc denotes no. of cycles. Increment in peak strain decreases for cyclic hardening material and plots are made between each incremental value corresponding to no. of loading cycle. Plots are divided into two phases, Phases-I and –II, depending upon the % peak strain increment value (assumed 0.01 %) attained after a certain number of cycles. Thus, Phase-I represent a zone with high rate of hardening while Phase-II refers to a zone with low rate of hardening.

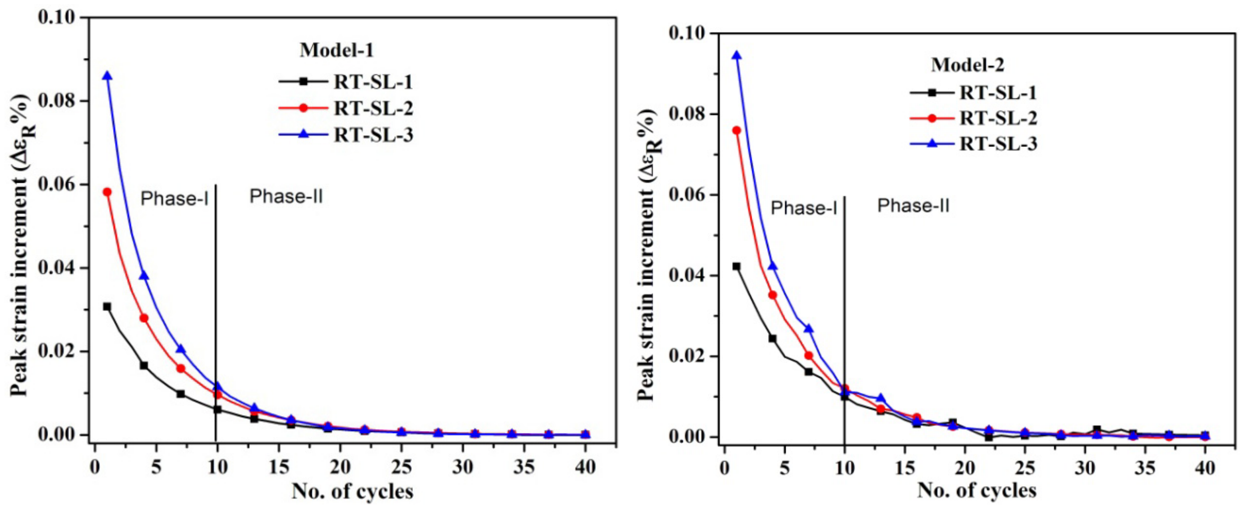

(a) (b)

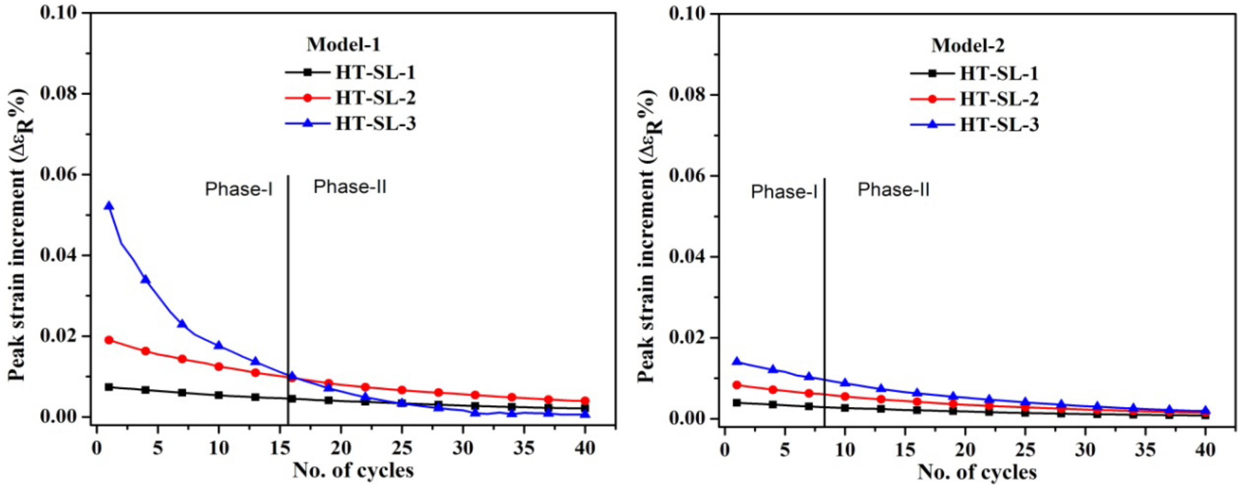

(c) (d)

Figure 3.8 Variation in peak strain increment with no. of cycles: at room temperature (a) for *Model-1* (b) for *Model-2*: at 550°C, (c) for *Model-1* (d) for *Model-2*

Figure 3.8 (a) and (b) shows peak strain increment value of 0.01 % is attained after a maximum of 10 loading cycles at room temperature for both the models. This reveals that severity of damage due to ratcheting which effects fatigue life is high up to 10 cycles for both the models. On further cycling, fatigue damage theories govern the life estimation. On the contrary, at high temperature, Figure 3.8 (c) shows greater than 15 cycles are required to attain 0.01 % peak strain increment for *Model-1* while Figure 3.8 (d) shows less than 10 cycles are required for *Model-2*. Greater contribution of ratcheting damage from Figure 3.8 (c) would results in reduced life compared to that from Figure 3.8 (d).

3.4.2 Thermal ratcheting of cylindrical shell

The cyclic hardening phenomenon in austenitic steels governs the extent of damage due to ratcheting behavior. The rapid and slow saturation of strain accumulation behavior is responsible to bring *shakedown* and *finite ratcheting state* respectively that may in turn lead to excessive deformation or failure. Aforementioned study figured out the effect of cyclic hardening on ratcheting or shakedown behavior of round steel bar under cyclic mechanical loading conditions. It is quite complex to understand ratcheting or shakedown behavior of cylindrical shells under thermal cycling. Cyclic strain accumulation due to thermal ratcheting may lead to localized progressive deformation in radial inward or outward direction resulting into bulge inward or outward. This inelastic deformation can cause contraction or expansion depending upon loading conditions and geometry of the cylinder specimen. The loading also affects the elastic-plastic behaviour of the structure such that the structure may achieve the steady state of plastic straining called as shakedown and fails due to low cycle fatigue. Alternatively, the phenomenon is termed as ratcheting if the structure undergoes progressive deformation leading to increase in plastic strain cycle by cycle and the structure collapses after gross plastic deformation.

In order to illustrate the shakedown and thermal ratcheting deformation due to cyclic thermal loading caused by free level variations in sodium pool, the work done by Lee et al. [50] is considered which reported a ratcheting strain for 9 cycles of thermal loading. However, according to a review study by Abdel-Karim [17], 9 loading cycles were not sufficient to recognize shakedown or progressive ratcheting. In this context *Type-I* and *Type-II* loadings are discussed in the following sections to recognize shakedown and ratcheting behavior respectively. The cylindrical shell is subjected to thermal cycling by applying different loading methods for *Type-I* and *Type-II*.

3.4.2.1 *Type-I: The test cylinder was heated only when moving down into the pool*

Thermal loading condition: Thermal loading similar to that as mentioned in the Figure 3.2 (b) is applied only when cylinder moves down into the pool for 15 cycles and the displacement is recorded cycle by cycle to recognize the phenomenon of shakedown. ABAQUS FILM subroutine is formulated to produce cyclic temperature variation on the curved surface of cylinder by imposing moving temperature profile along the axis of cylinder. Temperature profile was generated by varying the film coefficient along the axis of cylinder. Film coefficients considered for water is 1100 W/m^2 K and of heater is 800 W/m^2 K. The rate of change of the film coefficient with respect to the surface temperature is kept equal to zero.

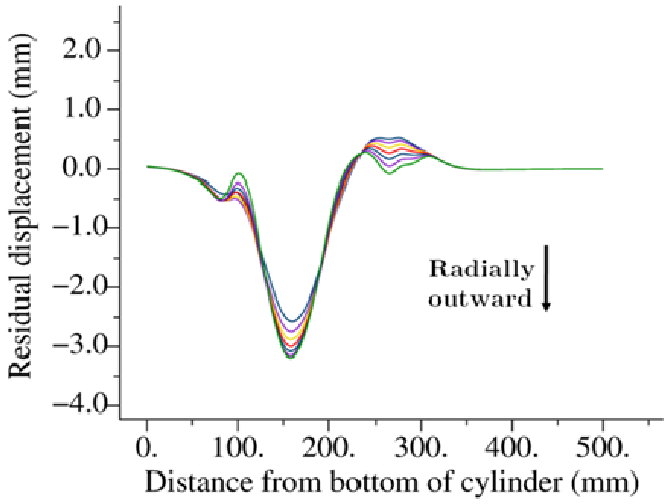

Figure 3.9 Profile of residual radial displacements in outward direction (after 9th cycle upto 15th cycle).

Residual radial displacement- Shakedown: After the 15th cycle, the residual radial displacement of −3.2 mm in radial outwards direction is observed. Residual radial displacement in outward direction (i.e. Expansion) cycle by cycle is shown in Figure 3.9 for the 9th cycle up to 15th. Buckling is also noted at critical locations of the cylinder, since the outward radial displacement exceeds the thickness of the cylinder considered.

3.4.2.2 *Type-II: The test cylinder was heated when moving up and down into the pool*

Thermal loading condition: Thermal loading as in *Type-I* is applied such that the thermal gradient ($\Delta T/\Delta Z$) along the axis of the cylinder is the same during up and down movement of the cylinder. Figure 3.10 (a) shows the transient thermal loading at different instances of time.

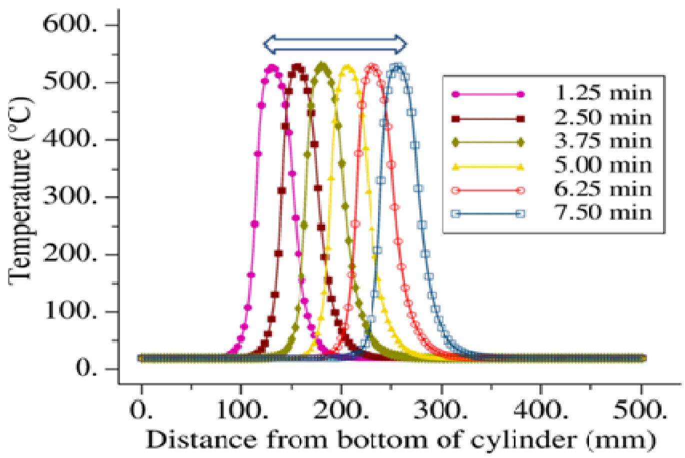

(a)

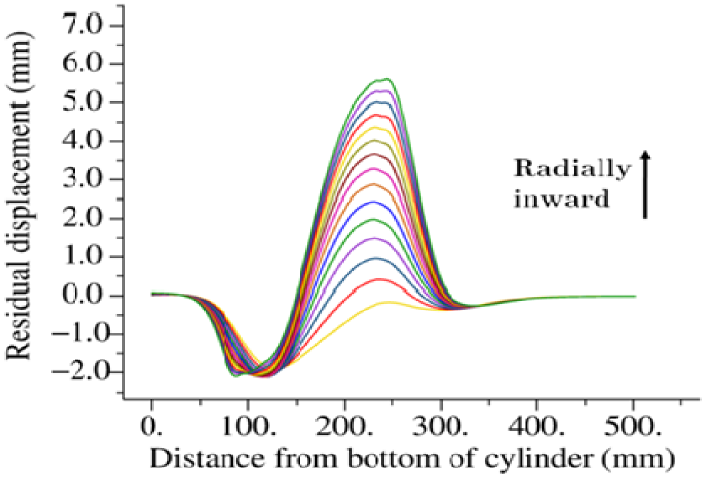

(b)

Figure 3.10 (a) Temperature distribution along the axis of cylinder (b) Profiles of residual radial displacements in inward direction for 15 cycles

Residual radial displacement- Ratcheting: The analysis is done for 15 cycles and the residual displacements are recorded cycle by cycle as shown in Figure 3.10 (b). The cyclic thermal loading due to level variations leads to the residual radial displacement of 5.6 mm (radially inwards) at the end of 15th cycle. Figure 3.10 (b) shows ratcheting with slow rate of decrease in progressive deformation, which may lead to infinite ratcheting as discussed by Hubel [59] and may eventually lead to collapse due to excessive deformation after large number of cycles. From the plot, it can be inferred that the deformation mode (expansion or contraction) of the cylinder also depends on the loading method apart from geometry and traveling speed of the temperature front. Expansion in the first few cycles is observed, while the cylinder contraction mode of deformation dominates resulting into net inward deformation for this case of loading method.

3.4.2.3 *Comparison of Type-I and Type-II*

Results for *Type-I* and *Type-II* loading are compared with the help of a plot between residual radial displacement and no. of ratchet cycles. The total residual strain accumulated at the end of 9 cycles due to cyclic thermal loading is recorded and outward radial displacement of −2.57 mm in the cylinder can be seen in the Figure 3.11. The recorded value of the present analysis is an improvement and in reasonable agreement with −1.79 mm as experimental value, and −2.74 mm as the value of inelastic analysis in ABAQUS obtained by Lee et al. [50].

Further, the analysis is continued to recognize the total number of loading cycles required to bring shakedown state. 15 load cycles in *Type-I* are required to attain shakedown, with rapid saturating behavior of the curve. Total outward radial displacement after 15 cycles is estimated to be −3.2 mm. Curve for *Type-II* (Figure 3.11) shows slow saturating behavior of the cylinder compared to the curve for *Type-I*. Change in deformation mode (expansion or contraction) is also observed on comparing *Type-I* and *Type-II*. Total inward radial displacement after 15 cycles is estimated to be 5.6 mm for *Type-II*.

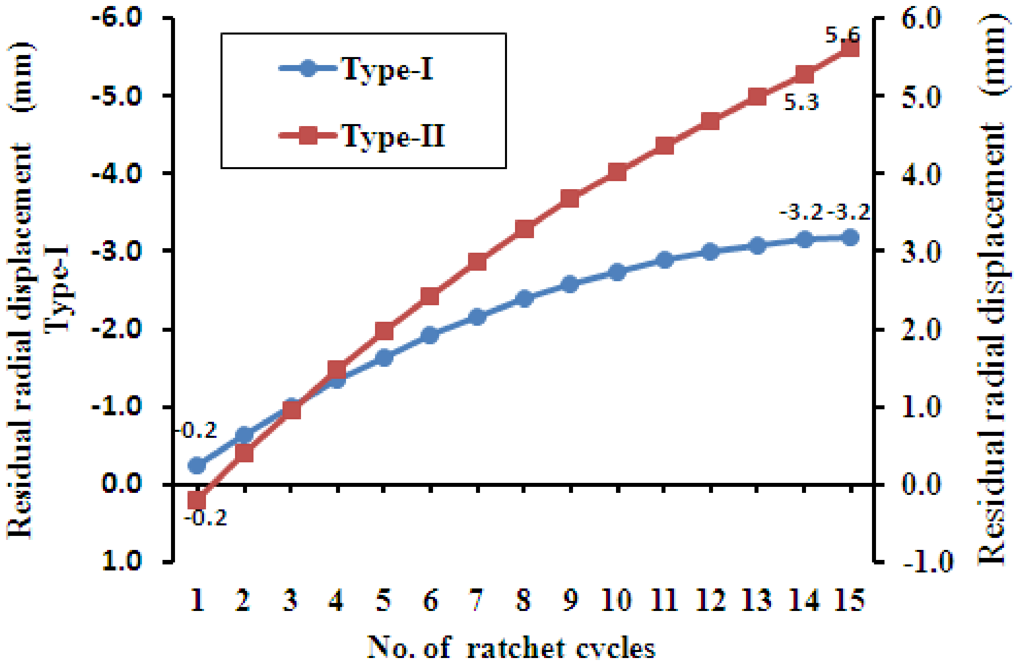

Figure 3.11 Comparison of residual displacements for *Type-I* (radialy outward) and *Type-II* (radialy inward)

3.4.2.4 *Ratcheting analysis of main vessel of PFBR for simplified loading*

Cylinder of dimensions 600 mm height, 500 mm outer diameter and 1 mm thickness is considered to simulate 1/25th scaled down model of the main vessel for PFBR. Thermal loading applied in this section will simulate the upward and downward movement of the locally heated cylinder specimen in water-filled container with the help of stepper motor. Temperature distribution along the axis of the cylinder is considered for a travel distance of 50 mm from 275 mm to 325 mm height of cylindrical shell instead of long travelling distance of 150 mm as in *Type-I* or *Type-II*. This is to avoid buckling, since thin cylinder may buckle for large travel distance.

Thermal loading condition: Thermal loading is imposed using user defined FILM subroutine, which takes care of the temperature variation along the surface of the cylinder. A peak temperature of about 550°C is imposed. The typical temperature variations along the inner surface of the cylinder at different time instances of 40 s interval are shown in Figure 3.12. Temperature profile move with a speed of 0.31 mm/s. Range of horizontal axis (i.e. distance from the bottom of the cylinder) is considered to be 250 mm to 600 mm for the better readability of the temperature profile in the region of level variations.

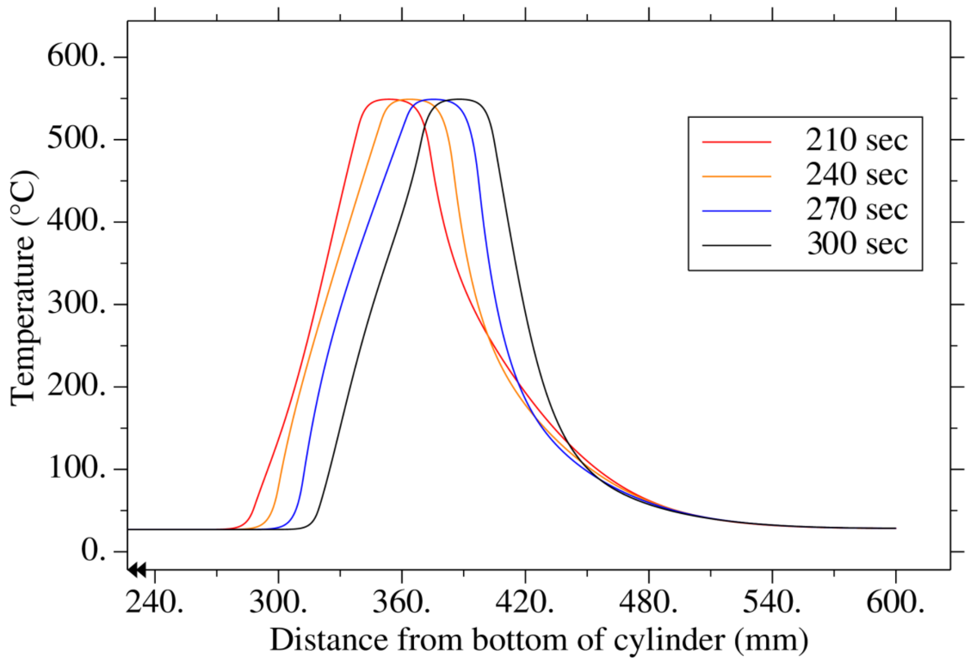

Figure 3.12 Temperature distribution along the axis of the cylinder after different time instances of 40 s interval.

Residual radial displacement- Ratcheting: The value of residual radial displacement of the inner surface of the cylinder is plotted against axial coordinate of the cylinder (i.e. distance from the bottom of the cylinder) at the end of each cycle for 20 cycles. Range of horizontal axis in Figure 3.13 (a) is 300 mm to 440 mm to represent the region of radial deformation clearly. Figure 3.13

(a) shows a maximum displacement of −0.75 mm (radially outward) at a distance of 367.5 mm while maximum inward displacement is 0.17 mm at 405 mm.

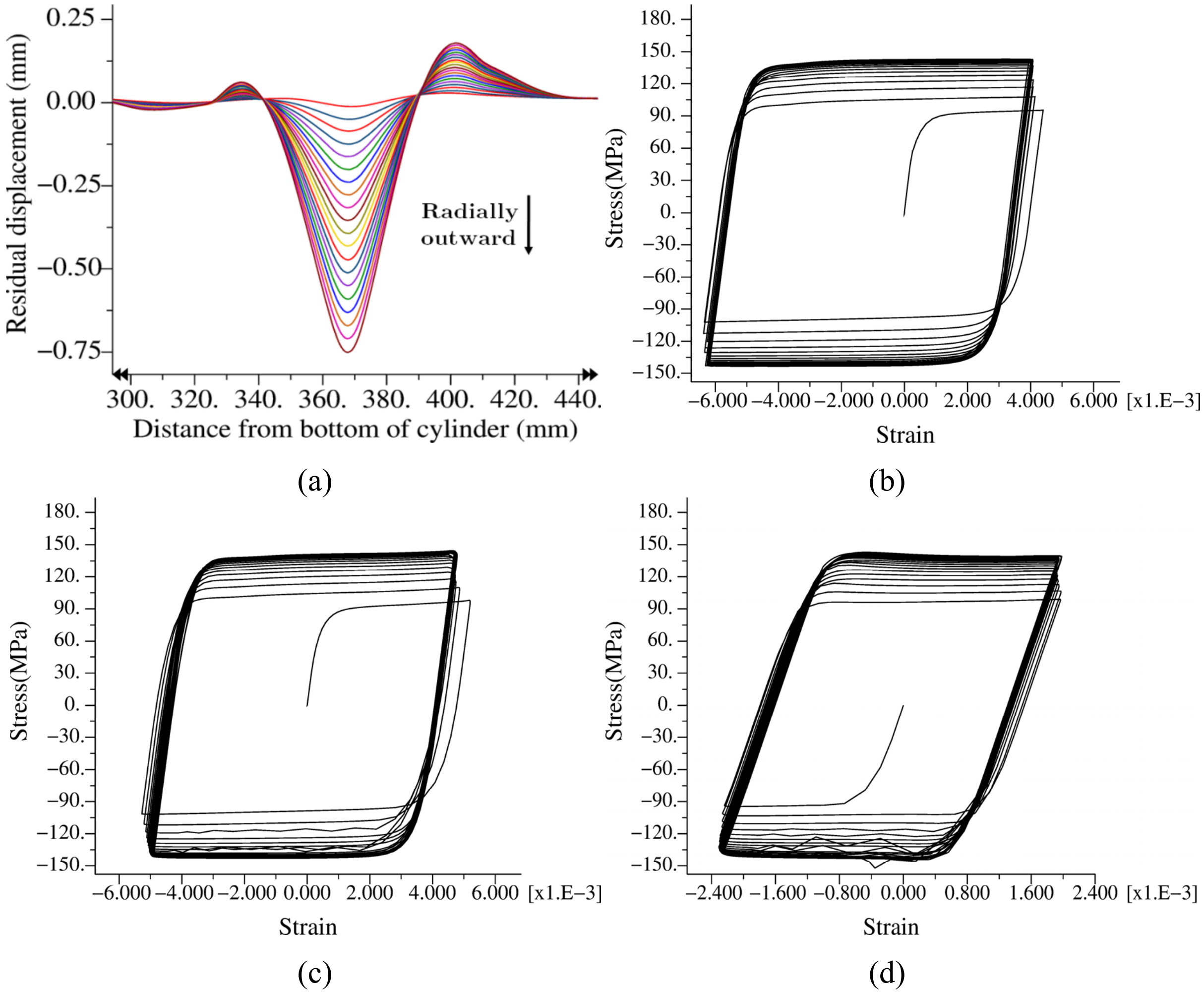

Figure 3.13 (a) Profile of residual displacements for 20 cycles (b-d) Stress-Strain hysteresis loops at (b) 325 mm (c) at 345 mm and (d) at 390 mm from bottom of cylinder

The progressive inelastic ratcheting strain is very important in the circumferential direction because excessive deformation beyond acceptable limit can cause dimensional instability. The positions corresponding to the transition region of changing the mode of contraction to expansion or vice-versa is identified and the nodal positions at 325 mm, 345 mm and 390 mm from bottom of cylinder are considered to evaluate hoop strain. Stress-strain hysteresis loops at different nodal positions of high von Mises stress are shown in Figure 3.13 (b), (c) and (d). The above nodal positions achieved saturation after a few load cycles. The saturated stress-strain curves shown here establish the fact that radial deformation is bounded by saturated regions along the axis of cylinder. Figure 3.14 (a) shows the evolution of residual radial displacements with number of ratchet cycles. It illustrates strain accumulation at a constant rate with no sign of saturation at the end of twenty load cycles. The behavior of the curve indicates a possible case of progressive ratcheting instead of shakedown. Radial displacement at a critical location of maximum deformation is plotted against time in Figure 3.14 (b) to show the progressive increase in radius. The estimated value of residual radial displacement after twenty cycles is −0.75 mm (−ve sign for radially outward displacement). For greater no. of cycles, the progressive deformation can be estimated by the extrapolation method available in RCC-MR Appendix A10 [44] as discussed in the previous work [49]. The equation for extrapolation method is reproduced here for the sake of completeness.

$$\varepsilon_N = \varepsilon_n + (\delta\varepsilon_n/(m-1)) * [1-4^{1-m}] + (\delta\varepsilon_n/4^m) * [N-4n] \tag{3.32}$$

where N = Total number of imposed cycles

n = Number of load cycles analyzed

ε_n = Strain predicted at end of 'n' th cycle

ε_{n-1} = Strain predicted at end of '$n-1$' th cycle

ε_{n-2} = Strain predicted at end of '$n-2$' th cycle

$\delta\varepsilon_n$ = $\varepsilon_n - \varepsilon_{n-1}$: $\delta\varepsilon_{n-1}$ = $\varepsilon_{n-1} - \varepsilon_{n-2}$: $\delta\varepsilon_{n-2}$ = $\varepsilon_{n-2} - \varepsilon_{n-3}$

m_1 = $\log(\delta\varepsilon_n/\delta\varepsilon_{n-1})/\log((n-1)/n)$

m_2 = $\log(\delta\varepsilon_n/\delta\varepsilon_{n-2})/\log((n-2)/n)$

m_3 = $\log(\delta\varepsilon_n/\delta\varepsilon_{n-3})/\log((n-3)/n)$

m = $0.9 \times \min(m_1, m_2, m_3)$

Using the above equation, the radial growth is evaluated after 20 cycles by considering the values of deformation for the first 5 cycles. The radial displacements (mm) at the end of 1st, 2nd, 3rd, 4th and 5th cycles are −0.012, −0.05, −0.086, −0.125 and −0.162 respectively. Value predicted by applying Eq. (3.32) for radial growth is −0.74 mm for 20 cycles, which closely matches with the ABAQUS result of −0.75 mm obtained for 20 cycles. The procedure of extrapolation is used to evaluate the total accumulated strain after 50 load cycles. A value of 1.90 mm of radial displacement is predicted for the temperature cycling having amplitude of 550 °C. The temperature difference in PFBR sodium pool is about 200 °C. Hence, the corresponding value of displacement due to accumulated ratcheting strain will be 0.69 mm for the 1/25th model. This can be scaled up to the PFBR main vessel resulting in a radially outward displacement of 17.25 mm.

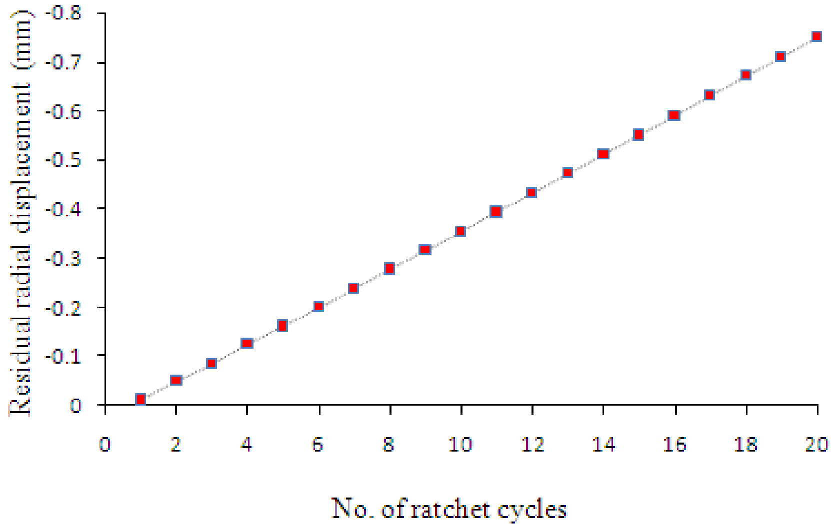

(a)

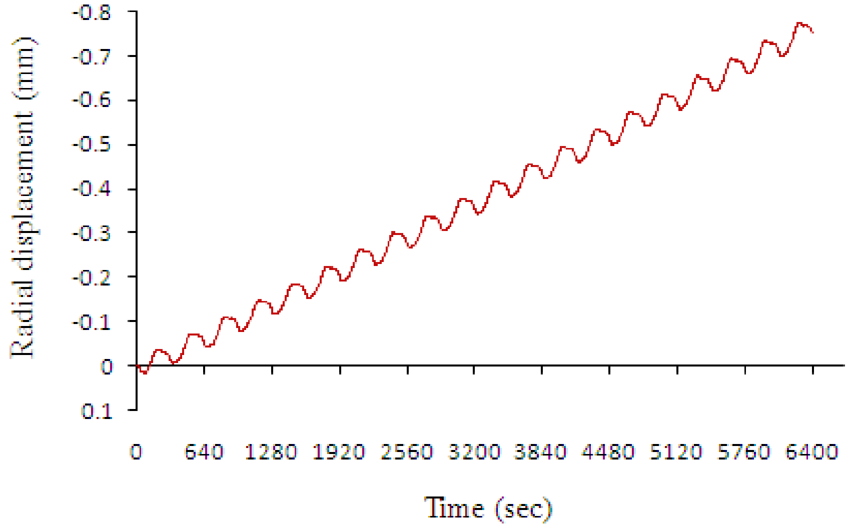

(b)

Figure 3.14 (a) Residual radial displacement with no. of cycles (b) Radial displacement with time (outward direction)

3.4.3 Effect of frequency of free level variation in thermal ratcheting

It is worth noting that progressive deformation behavior requires incorporating time dependent formulation to include visco-plasticity or rate dependence, which may significantly affect ratchet strain [60]. Structures used in nuclear application such as PFBR main vessel, experience loading at various strain/stress rates due to sodium free level fluctuations at different frequencies. Also, sodium free level hold at different elevations, under various operating conditions, effect radial deformation due to creep. The literature on strain accumulation behavior of steels considering time independent and dependent formulations separately for mechanical ratcheting is large. In contrast, literatures covering comparative studies of ratcheting behavior with strain/stress rate contribution and creep contributions under cyclic mechanical loading are few [60]. As far as the authors found, the studies which address relative contribution of these effects for cyclic thermal loading is not available in the literatures hence are valuable. In view of this, effects of sodium free level fluctuations in the main vessel of pool type nuclear reactor are analyzed using time independent and dependent formulations for ratcheting. This revealed the contribution of visco-plasticity in radial strain accumulation during level fluctuations at different frequencies

Table 3.2 Cases for various cycle times (CT)

Model-1 and *Model-2*		
Cases	Time (s)	No. of Cycles
CT-240	240	10
CT-320	320	10
CT-400	400	10
CT-480	480	10

Thermal loading (moving temperature front) as in Figure 3.12 is applied for 10 cycles to compare the material behavior for each model in section 3.4.3.1. Further, the analysis is continued for various cycle time (Table 3.2) in section 3.4.3.2. The temperature cycling due to level fluctuations of 50 mm at various CT is simulated in ABAQUS keeping the axial temperature gradient same throughout the cycle.

3.4.3.1 *Residual radial displacements for Model-1 and Model-2*

The progressive inelastic deformation at the end of each cycle is measured for cycle time of 240 seconds for *Model-1* and *Model-2*. Figure 3.15 (a) and (b) shows residual radial displacements for *Model-1* and *Model-2* for range of 250 mm to 450 mm of cylinder height. The maximum values of residual radial displacements after tenth cycle are −0.30 mm and −0.33 mm for *Model-1* and *Model-2* respectively (−ve sign shows radially outward direction).

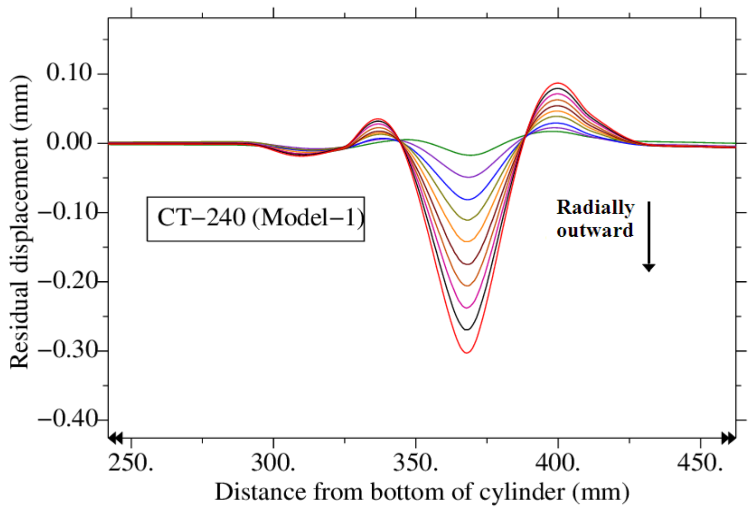

(a)

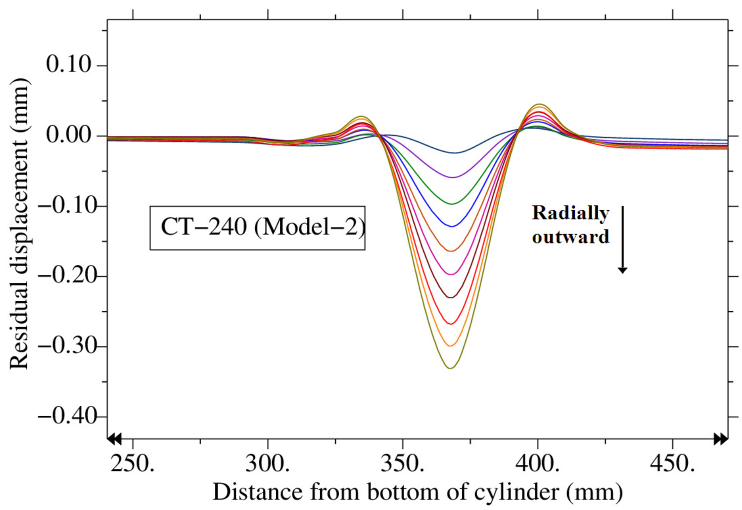

(b)

Figure 3.15 Residual radial displacements for the cycle time 240 seconds for (a) *Model-1* (b) For *Model-2*

3.4.3.2 *Maximum residual radial displacements for various cycle times*

The comparative analysis of time independence and dependence in ratcheting formulation is done with increasing cycle time for each model. The residual radial displacement of the cylinder is recorded after 10 cycles.

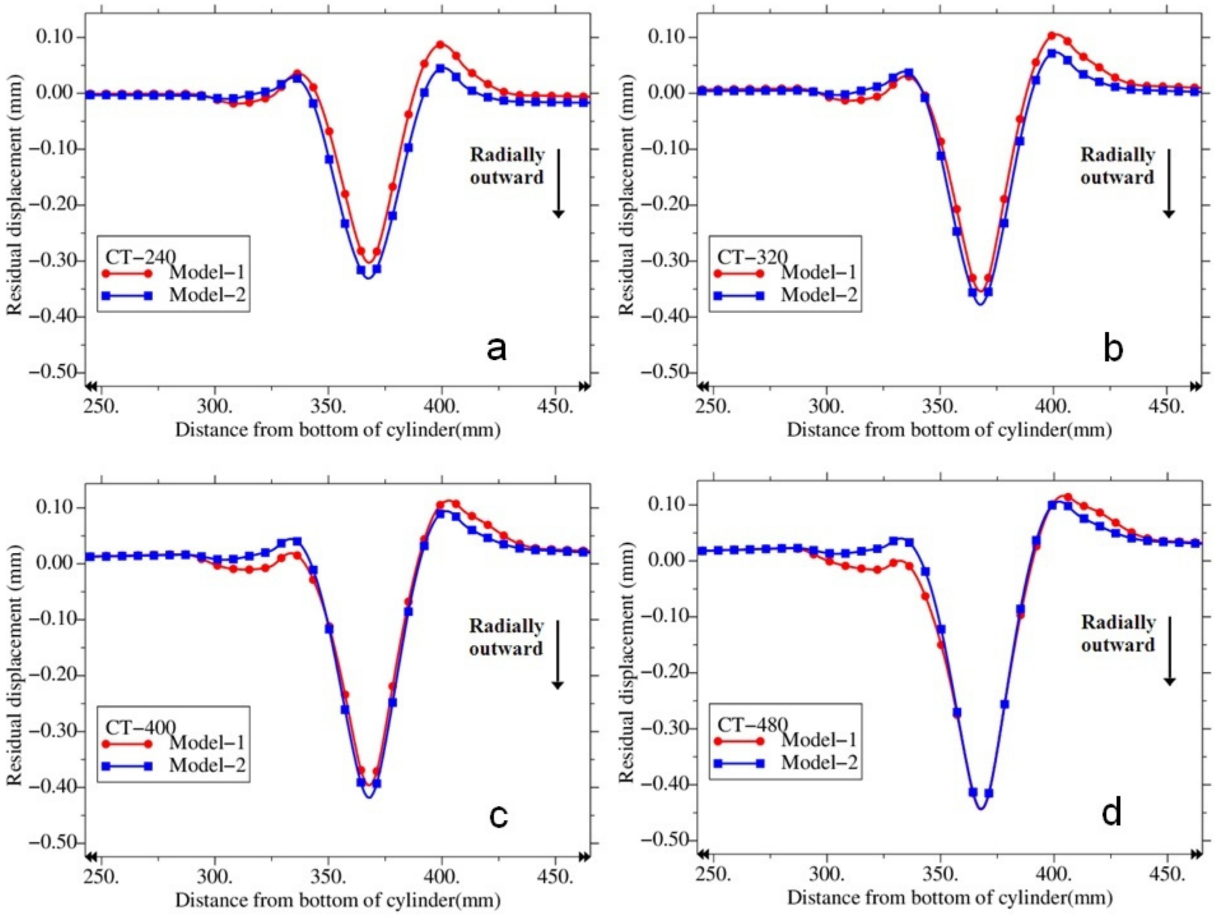

Figure 3.16 Comparison of residual radial displacement (outward) for *Model-1* and *Model-2* after 10^{th} cycle (a) for CT-240 (b) for CT-320 (c) for CT-400 (d) for CT-480.

The profiles of the residual radial displacement along the axis of the cylinder for both models are presented in Figure 3.16 (a), (b), (c), and (d) for various CT to compare the effect of time independence and dependence in ratcheting. Maximum value of residual radial displacements (U1) obtained for CT of 240 s, 320 s, 400 s and 480 s, are given in Table 3.3. The predicted maximum values of residual radial displacement after tenth loading cycles are different for the two models at lower cycle times. The increase in cycle time leads to a decrease in difference in maximum residual displacement observed between the two models. Referring to the case CT-480, Figure 3.16 (d) shows the maximum residual radial displacement is closely matching for both the models, which is −0.44 mm in radially outward direction.

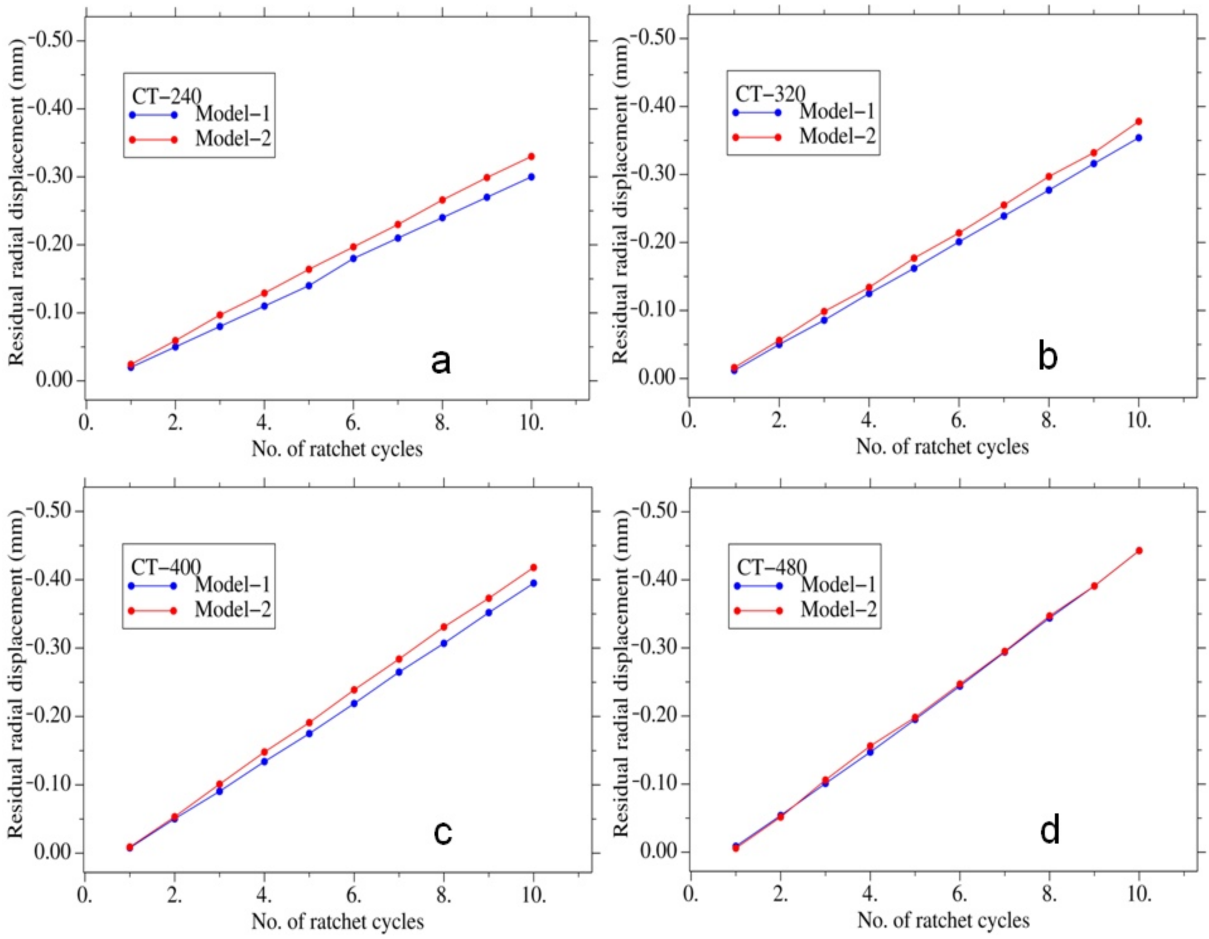

Figure 3.17 Comparison of residual radial displacement with no of ratchet cycles for *Model-1* and *Model-2* (a) for CT-240 (b) for CT-320 (c) for CT-400 (d) for CT-480

Table 3.3 Maximum residual radial displacements (U1) for various cycle times

Models analyzed	Maximum residual radial displacements (U1-mm) for cycle times			
	CT-240	CT-320	CT-400	CT-480
Model-1	−0.30	−0.35	−0.39	−0.44
Model-2	−0.33	−0.37	−0.41	−0.44

Total residual radial displacement in Figure 3.15 (a) and (b) for CT-240 s. reveals the contribution of visco-plasticity in radial strain accumulation that is 0.012 %. This value may increase significantly for higher number of loading cycles. The contribution of visco-plasticity is vanishing at low frequency (cycle time of 480 seconds). The cyclic increase in radial displacement due to progressive accumulation of strain in the cylinder shown in Figure 3.17 clearly distinguishes the effect of cycle time for both the models.

Ratcheting strain increases with number of loading cycles whereas its rate (change in ratcheting strain with number of loading cycles) decreases continuously which may lead to saturation or shakedown. Contrarily, in present analysis, the increase in radial deformation due to thermal ratcheting according to *Model-1* and *Model-2* is not showing any sign of saturation up to ten loading cycles. Moreover, it may lead to infinite ratcheting [59] and collapse may occur due to excessive deformation after large number of cycles. It is inferred from Figure 3.17 (a), (b), and (c), that the rate of strain accumulation for time dependent formulation (*Model-2*) is greater than that of time independent formulation (*Model-1*). The difference in material behavior is observed due to the difference in visco-plastic component (which is accounted in *Model-2* while neglected in *Model-1*) produced at various speed of free level variations in the cylinder analyzed here. Figure 3.17 (d) shows similar progressive deformation behavior for both models at CT-480. Figure 3.18 (a) and (b) show that maximum residual radial displacement of the cylinder increases with increasing cycle time for *Model-1* and *Model-2* respectively.

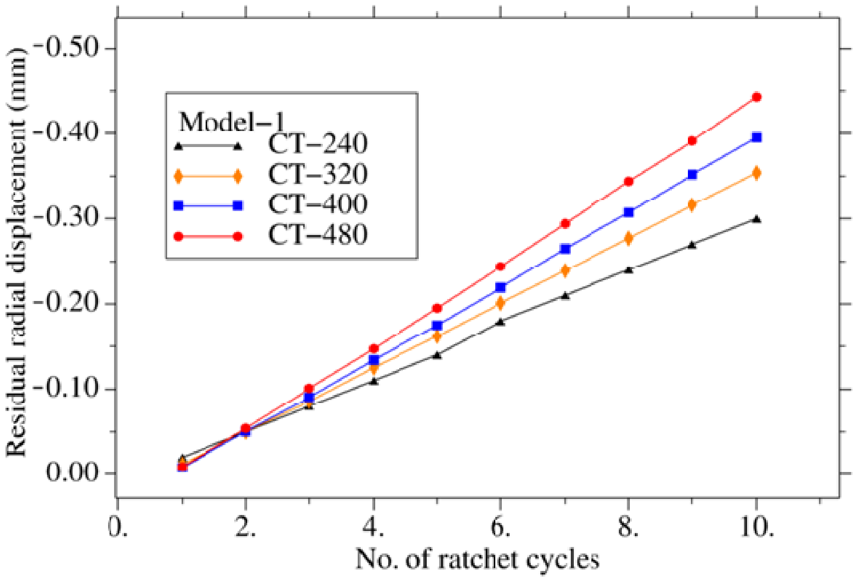

(a)

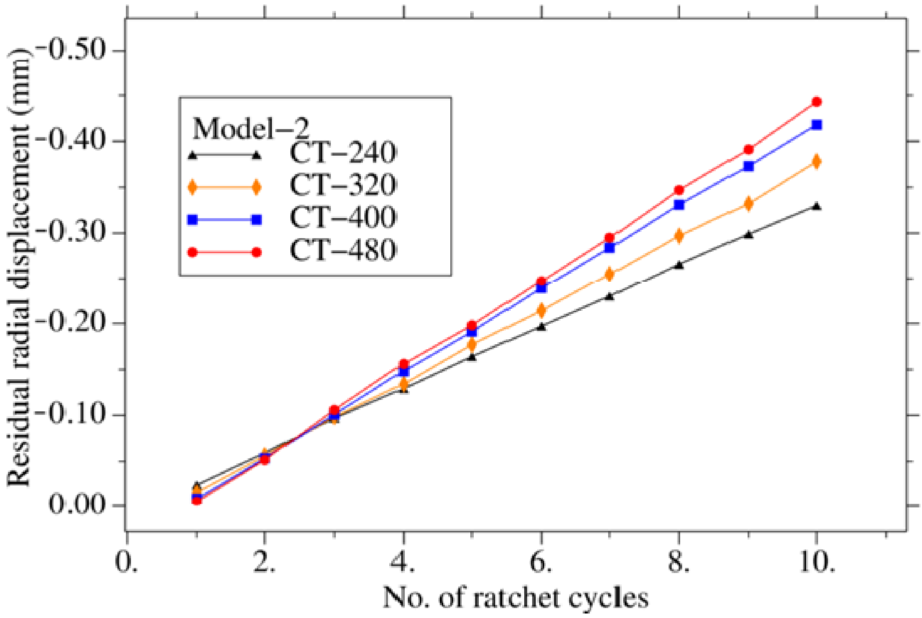

(b)

Figure 3.18 Residual radial displacement (outward) with no. of ratchet cycles at various cycle times (a) For *Model-1* (b) For *Model-2*

3.4.4 Contribution of hold time in thermal ratcheting

Time dependent formulation for progressive deformation as discussed above is suitable for cases where contribution of strain rate effect has to be accounted. Suitability of unified visco-plastic model is limited to describe the ratcheting behavior without peak or valley stress hold. Several researchers [61], [62], [63] have investigated the interaction between plasticity and creep. It was demonstrated earlier [32] that the UVP model satisfactorily simulates the uniaxial ratcheting behavior with negative stress ratio and at moderate stressing rates. However, it yielded poor results at the lower stressing rate at which the creep strain becomes a main part of rate-dependent ratcheting strain. At high temperature, creep deformation (with hold time) dominates, which cannot be described by visco-plasticity (without hold time). The uniaxial ratcheting behavior of SS 304 at high temperature with hold time accounting stress/strain rate effect was experimentally studied [64] and reported that:

- Ratcheting greatly depends on the stress / strain rate and holding time.

- Cyclic creep strain (time dependent ratcheting) should be discriminated from cyclic accumulated plastic strain (time independent ratcheting).

Therefore, the contribution of the material viscous effect as well as peak/valley stress hold at room temperature and at high temperature by superimposing visco-plasticity and creep is important to analyze. In this regard, visco-plasticity-creep superposition model (SVC) that simulates uniaxial time dependent deformation is considered by the superposition of multiaxial visco-plasticity and multiaxial creep law [32] as shown below:

$$\boldsymbol{\varepsilon}_{ij} = \boldsymbol{\varepsilon}_{ij}^{e} + \boldsymbol{\varepsilon}_{ij}^{vp} + \boldsymbol{\varepsilon}_{ij}^{c} + \boldsymbol{\varepsilon}_{ij}^{T} \tag{3.33}$$

$$\dot{\boldsymbol{\varepsilon}}_{ij}^{vp} = \sqrt{\frac{3}{2}} \left\langle \frac{F_y}{K} \right\rangle^{n} \frac{\mathbf{S}_{ij} - \boldsymbol{\alpha}_{ij}}{\left\| \mathbf{S}_{ij} - \boldsymbol{\alpha}_{ij} \right\|} \tag{3.34}$$

$$\dot{\boldsymbol{\varepsilon}}_{ij}^{c} = \frac{3}{2} \frac{\dot{\bar{\varepsilon}}_{c}}{\bar{\sigma}} \mathbf{S}_{ij} \tag{3.35}$$

where $\boldsymbol{\varepsilon}_{ij}^{vp}, \bar{\sigma}, \boldsymbol{\varepsilon}_{ij}^{C}$ and $\dot{\bar{\varepsilon}}_{c}$ are visco-plastic strain, equivalent stress, creep strain and equivalent creep strain respectively. Other terms are same as described in Eqs. (3.10) - (3.13).

The creep response under uniaxial cyclic load was studied and compared with classical ratcheting tests and creep ratcheting tests [60]. Relative quantification of creep with hold time on ratcheting strain shows the significance of peak/valley stress hold in the cyclic evolution of the strain observed in stress controlled experiments. Recognizing this significance, presenting the contribution of hold time in thermal ratcheting behavior is the aim of this section. The analysis is conducted to focus on two points viz. (i) Uniaxial creep deformation of SS 316 L at 550 °C and (ii) Multiaxial cyclic creep ratcheting analysis implementing the proposed formulation procedure. Creep curve generated from creep law as per RCC-MR [44] for uniaxial loading is considered to validate the developed FORTRAN coding for UMAT, in section 4.1. Further, in section 4.2., multiaxial creep formulation is superimposed with multiaxial visco-plastic formulation to reveal the creep or hold time effect in thermal ratcheting.

3.4.4.1 *Uniaxial creep deformation*

Creep curve for uniaxial loading as shown in Figure 3.19 is generated for stress rate 10 MPa/s with peak stress hold for 3600 s. The curves for two stress levels 100 MPa and 120 MPa are compared with the results obtained using the code developed for predicting creep in Figure 3.20 (a) and (b) respectively. Results from UMAT code and creep curve from RCC-MR [44] is in good agreement. Creep law considered for this analysis is shown below:

$$\boldsymbol{\varepsilon}_f = c_1 t^{c_2} \boldsymbol{\sigma}^{n_1} \tag{3.36}$$

Here $\boldsymbol{\varepsilon}_f$ is the % creep strain attained under stress $\boldsymbol{\sigma}$ (MPa) after time t hours. Parameters c_1=1.155, c_2=0.4537 and n_1=3.153 are taken from RCC-MR [44]. Values of creep strain as per Eq. (3.36) are plotted with time axis in seconds to maintain uniformity with previous analysis considering seconds as a unit of time. The present analysis results are in agreement with the generated creep curve from RCC-MR [44].

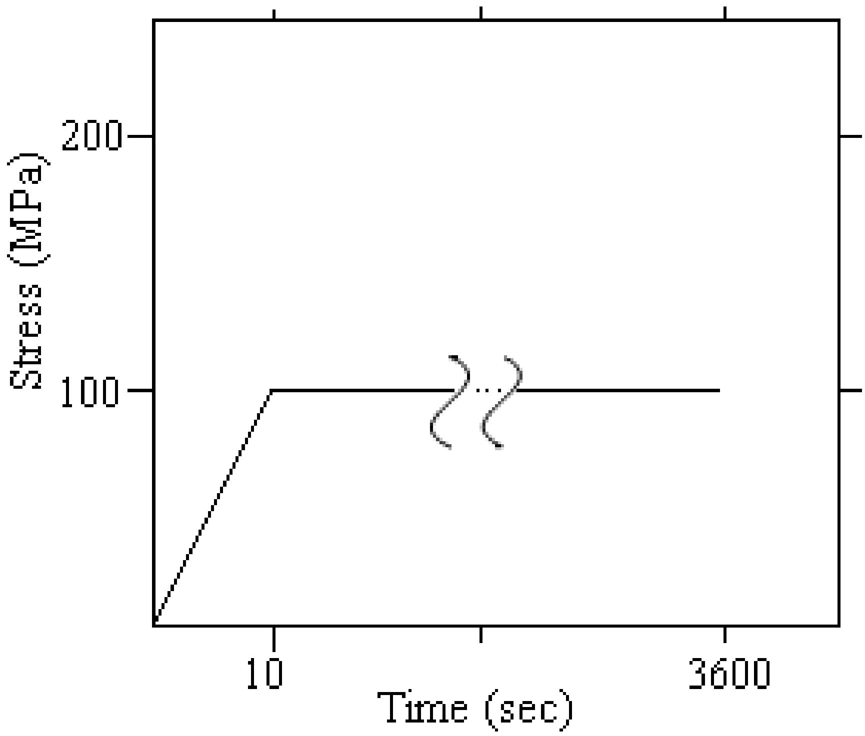

Figure 3.19 Schematic of stress controlled uniaxial loading

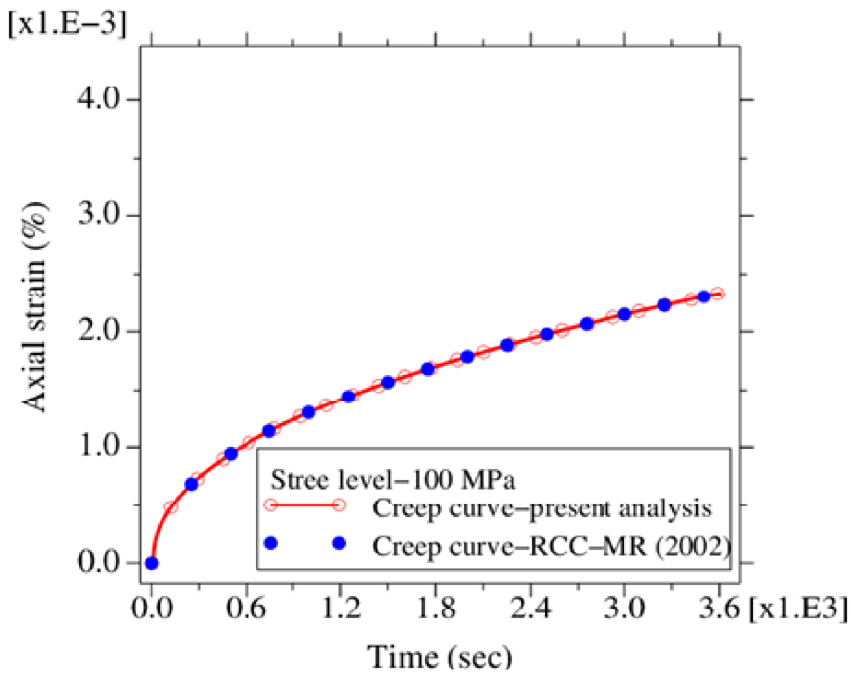

(a)

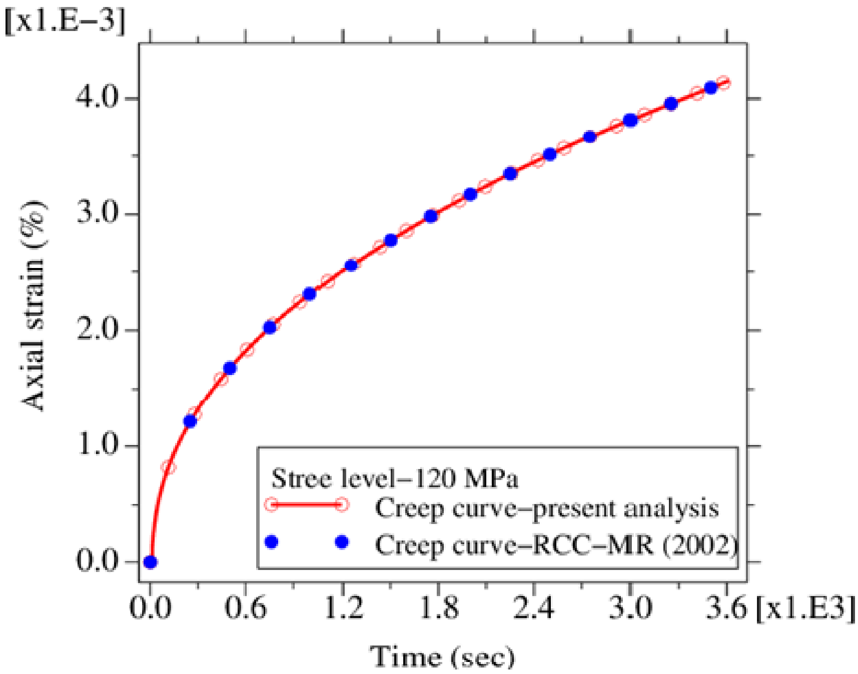

(b)

Figure 3.20 Evolution of creep strain with hold time (a) At 100 MPa stress hold (b) At 120 MPa stress hold

3.4.4.2 *Multi-axial creep deformation superimposed on thermal ratcheting*

Thermal loading as in Figure 3.12 is applied cyclically for two hold times of 5 seconds and 10 seconds at maxima and minima of level fluctuation in the cylinder. New cycle time is 250 s (CT-

250) and 260 s (CT-260) including 5 seconds and 10 seconds of hold time for each case. Residual radial displacement is recorded for ten load cycles Figure 3.21 (a) and (b) show −0.35 mm and −0.38 mm of residual radial displacement for CT-250 and CT-260 cases respectively.

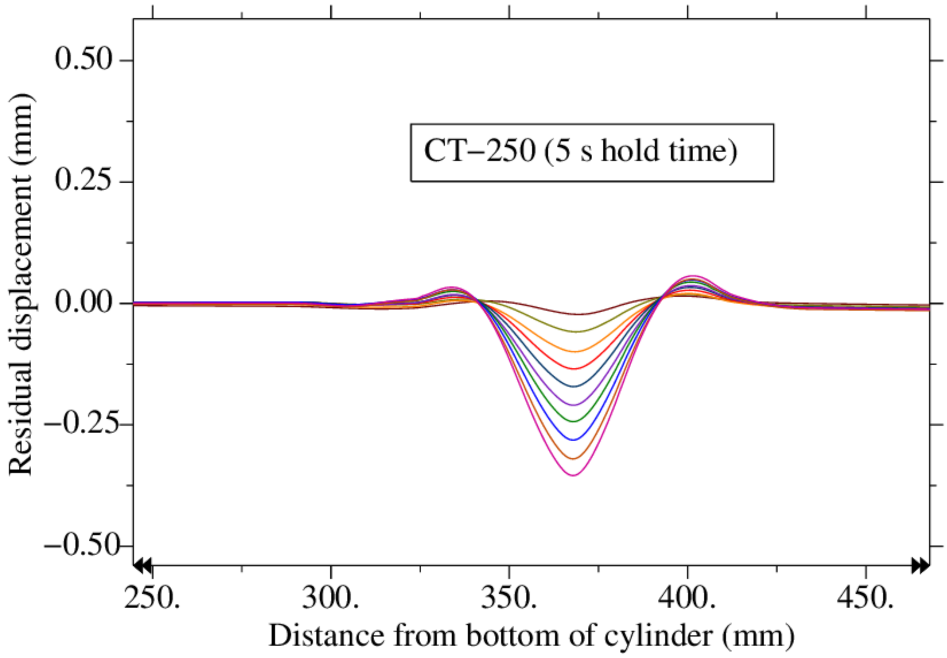

(a)

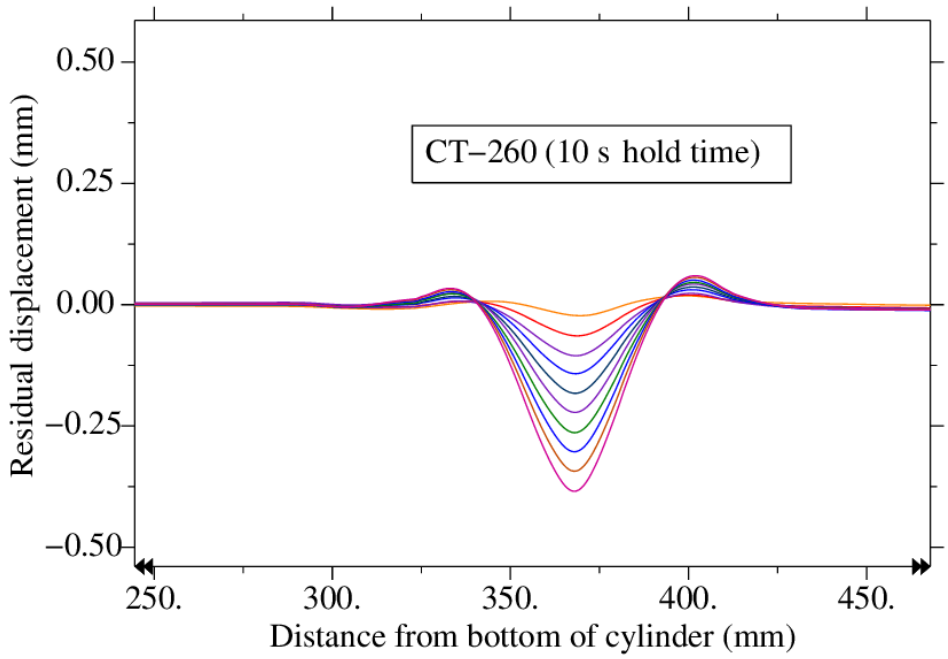

(b)

Figure 3.21 Residual radial displacements for 10 cycles (a) At cycle time 250 seconds (CT-250) with 5 seconds hold time (b) At cycle time 260 seconds (CT-260) with 10 seconds hold time

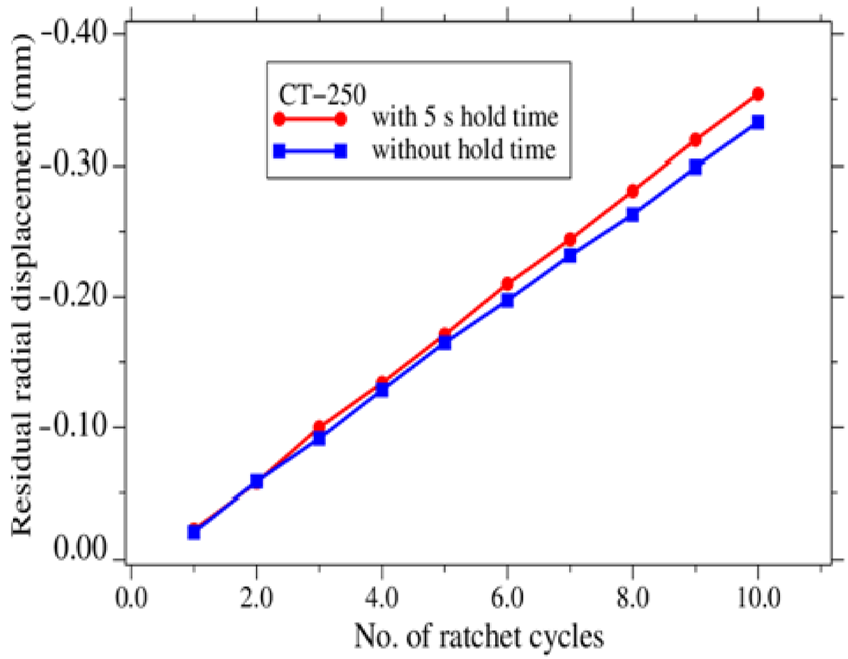

(a)

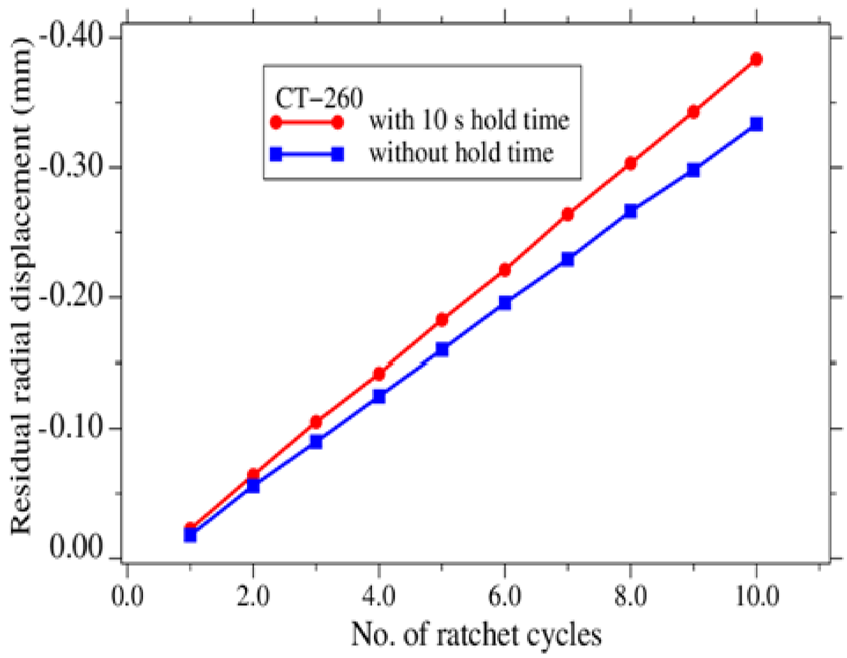

(b)

Figure 3.22 Evolution of radial displacement with hold time and without hold time (a) At cycle time 250 seconds (CT-250) (b) At cycle time 260 seconds (CT-260)

Results of the analysis involving creep formulation with hold time of 5 and 10 seconds shown in Figure 3.22 (a) and (b) reveals the effect of creep (hold time) in progressive deformation. The rate of strain accumulation for 10 s hold time is greater than that for 5 s consequently −0.38 mm and −0.35 mm of residual radial displacement is noticed after 10th cycle.

Information obtained from Figure 3.22 (a) and (b) is the contribution of hold time relative to visco-plastic formulation (no hold time). Using visco-plastic formulation, the maximum residual radial displacement after 10^{th} cycles for CT-250 and CT-260 are −0.3325 mm and −0.3334 mm respectively. Hence, hold time contribution of 0.007 % for 5 s and 0.018 % for 10 s are observed during thermal ratcheting with hold time.

3.5 SUMMARY

A simplified expression for infinitesimal plastic strain increment is discussed. Cyclic hardening behavior of SS 316 L is investigated at various mean stresses under uniaxial cyclic mechanical loading. The corresponding results are aimed to differentiate the cyclic hardening / deformation behavior at room temperature and 550 ºC using time independent (*Model-1*) and time dependent (*Model-2*) constitutive models. Cyclic hardening phenomenon is characterized into Phase-1 and Phase-2 representing rapid and slow hardening zones respectively which further reveals the severity of damage during asymmetric cyclic loading for *Model-1* and *Model-2*.

Further, the thermal ratcheting deformation of a smooth cylindrical shell for two loading cases is evaluated. The aim of the first case is to recognize the shakedown behaviour of the cylinder under applied loading cycles. Alternatively, second case is highlighting the ratcheting behaviour of the cylinder. Based on the loading method in second case, a smooth thin hollow cylinder is considered to simulate the progressive deformation. This condition simulates the $1/25^{th}$ scale down model of the Prototype Fast Breeder Reactor (PFBR) main vessel. After that, results of cyclic strain accumulation behavior of a thin cylindrical shell (SS 316 L) due to thermal ratcheting in the framework of time independent (*Model-1*) and dependent formulations (*Model-2*) is presented. The effect of frequency of free level fluctuations by varying cycle time is compared for *Model-1* and *Model-2*. Contribution of strain due to high frequency and low frequency level fluctuations is quantified. Contribution of hold time in thermal ratcheting strain is evaluated with two different hold times to highlight the effect of free level hold on radial deformation of the cylinder. Improvement in the prediction of ratcheting strain is achieved using SSIP. Implicit plastic increment formulation is derived using Newton’s method and the proposed simplified procedure is found to be very useful for ratcheting analysis under complex loading conditions.

THERMAL RATCHETING ANALYSIS: NON-ISOTHERMAL 4

4.1 INTRODUCTION

Material behavior under stress controlled cyclic thermomechanical loading (here onwards referred as TML) is highly nonlinear and requires understanding of micro to macro mechanics theories to perform calculations not only for life estimation but also to ensure functionality of the components. Literature such as [65], [66] discussed various aspects of strain controlled thermomechanical fatigue (TMF) behavior of austenitic steels. Under TMF condition, with the peak temperature increase, grain boundary sliding becomes pronounced due to unbalanced displacements on the micro level [67] For SS 304 under thermomechanical load, the TMF damage or life is governed by the maximum temperature of cycling while temperature interval and phasing (IP/OP) determine the mechanical response [68]. In most of the available literatures, the TMF analyses of austenitic steels viz. SS 316 L, SS 316 LN were performed with isothermal material parameters neglecting the effect of thermomechanical interactions. Thermomechanical interactions play a significant role in damage accumulation behavior under both strain and stress controlled cyclic loadings. Under asymmetric stress controlled cyclic loadings, the strain accumulation behavior leading to gross plastic deformation and crack initiation is governed by ratcheting fatigue interaction phenomenon. During concurrent ratcheting-fatigue conditions, the consideration of ratcheting damage is extremely important for accurate life prediction since ratcheting strain decreases fatigue life [69]. It is therefore understandable that, the accurate evaluation of overall damage of materials under cyclic loading is largely dependent on the contribution of ratchet damage that relies on the choice of ratcheting prediction models. It was revealed numerically and analytically [70], [71], [72] that introducing temperature rate terms and considering temperature dependent parameters significantly improve the capability of ratcheting prediction models. Therefore, a time dependent ratcheting model with temperature rate terms in hardening rule [73] is chosen to perform non-isothermal ratcheting analysis of the two-bar system and subsequently for cylindrical shell. This chapter highlights the significance of thermal load rate (TLR) in connection with ratcheting response under cyclic TML with coincident and non-coincident peak load conditions. For this purpose, the investigation is performed to describe the macroscopic deformation behavior of SS 316 LN stainless steels under thermal cycling using an FE model of the two-bar system. Further, the study is extended to discuss the thermal ratcheting phenomenon that needs to be considered while designing the main vessel of SFR. The main vessel experiences cyclic TML due to sodium free level variations with concurrent change in sodium temperature. It generates a moving temperature front with concurrent change in peak temperature during the movement. This type of thermal loading condition reported by Chellapandi et al. [49] was simplified in most of the available literature [25], [74] by assuming constant sodium temperature. Hence, for this loading condition, the accumulated radial deformations with and without temperature rate terms (TRT) are compared that emphasize the importance of TRT in modeling thermomechanical loadings.

4.2 NUMERICAL MODELING: DEVELOPMENT OF CODE FOR PREDICTION OF RATCHETING

Numerical modeling for non-isothermal ratcheting analysis is performed implementing the proposed plasticity integration procedure in time dependent framework (i.e. *Model-2*) using the concept of radial return technique as discussed in section 3.2.2.2.

4.2.1 Governing equations

Cyclic evolution of strain in austenitic steels has been researched widely considering various visco-plastic models to account for the strain rate dependence involving several material parameters. The present non-isothermal study has been carried out using nonlinear isotropic hardening and modified kinematic hardening rule having TRT in the framework of unified visco-plasticity [55].

4.2.1.1 *Evolution rules for isotropic and kinematic hardening*

Expression for isotropic hardening considered here is same as in Eq. (3.11). On the other hand, expressions for the kinematic hardening are Eq. (2.11) for without TRT [20] and Eq. (4.1) for with TRT [73] analysis.

$$\dot{\mathbf{X}} = \frac{2}{3}C\mathbf{d}\boldsymbol{\varepsilon}^{\mathbf{P}} - \gamma\mathbf{X}\dot{P} + \frac{\partial C}{\partial T}\frac{\mathbf{X}}{C}\dot{T} + \frac{\partial \gamma}{\partial T}\mathbf{X}P\dot{T} \tag{4.1}$$

4.2.2 Proposed simplified semi-implicit integration procedure

The accuracy of ratcheting predictions is extremely dependent on the constitutive model and the integration scheme adopted for Finite Element (FE) modeling. Therefore, the self-developed SSIP for visco-plastic model using the concept of semi-implicit scheme as explained in the section 3.2.2.2 is also proposed for the present non-isothermal analysis. The expression for the infinitesimal effective plastic strain increment at each iterative step of Newton's method derived for *Model-2* in chapter 3 is used.

4.2.3 Flowchart for the adopted SSIP:Non-isothermal

The computation of stress tensors, strain tensors and hardening variables are based on isothermal material parameters and thus no temperature increment term appeared during the update process of these quantities as illustrated in Figure 3.1. While no temperature increment term was considered in chapter 3, the non-isothermal analyses require temperature increment term and the material parameters are also need to be defined as a function of temperature. The steps of the analysis are detailed in the flowchart shown in Figure 4.1 while the implementations steps are same as given in section 3.2.3.

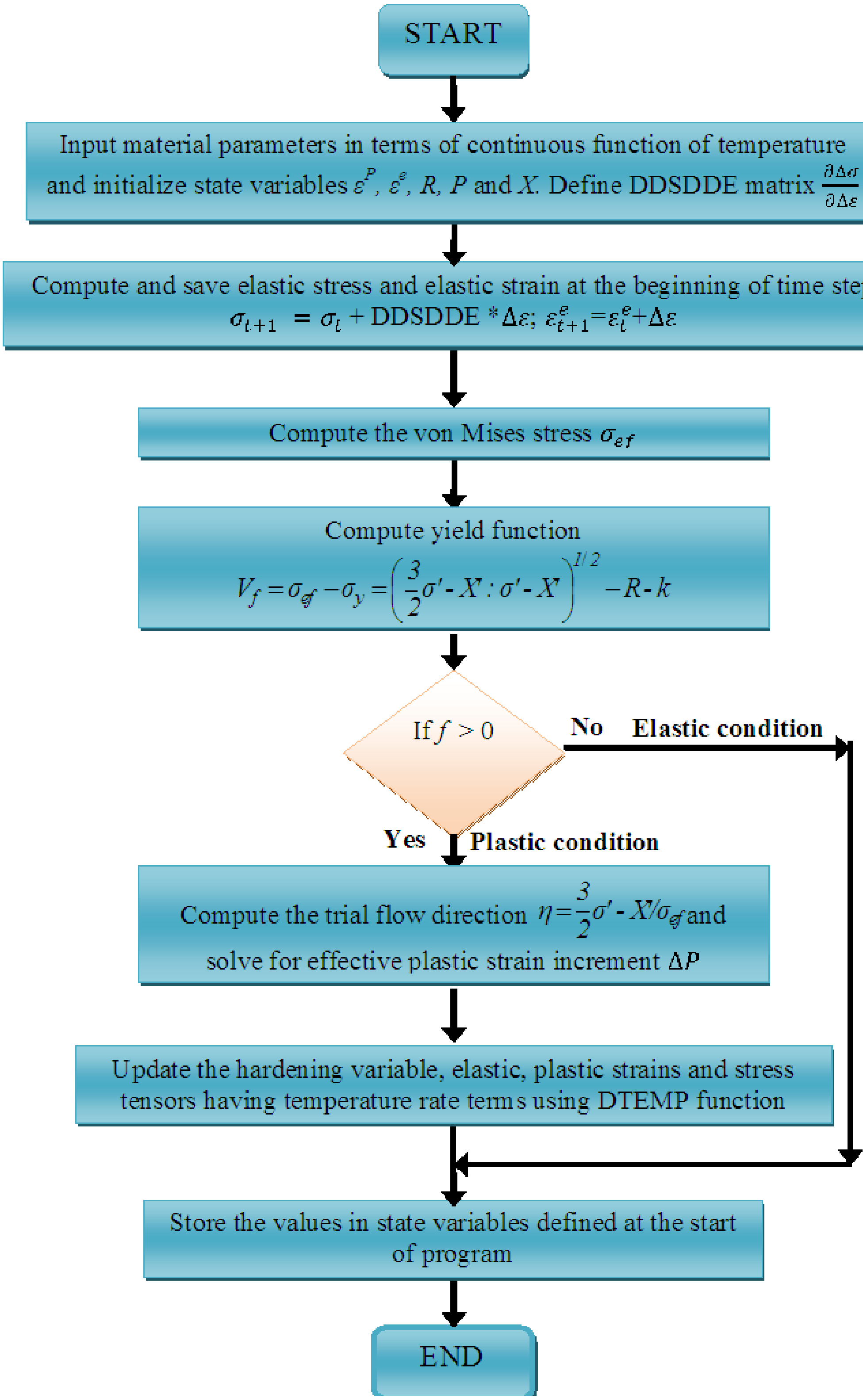

Figure 4.1 Flowchart for the SSIP: Non-isothermal

4.3 BENCHMARK ANALYSIS: TEMPERATURE RATE DEPENDENT MODELING

Under TML, the cyclic hardening characteristics of austenitic steels are highly dependent on TLR that significantly govern the life of components. Delprete and Vercelli [75] have discussed a methodology to predict the life of components under TML using simple nonlinear isotropic and kinematic hardening without temperature rate terms. For time dependent thermal load conditions, not only non-isothermal material parameters, but also TLR dependence needs to be considered while modeling the ratcheting response. To understand the influence of TLR on thermal ratcheting, a two-bar system of SS 316 LN steels in Figure 4.2 (a), analyzed by Kuhner et al. [73] for Test-A and Test-B as shown in Figure 4.2 (b) and (c) is referred. Kuhner’s experiment of the two-bar system had two servo hydraulic MTS 810 testing machines mounting two extensometers on the specimens. Specimen heating was accomplished by induction heaters and cooling by specimen holders through water cooling channels, thermal radiation and convection. Permanent strain accumulation of the two-bar system was recorded to demonstrate the effect of non-isothermal cyclic loading on inelastic material behavior.

For this analysis, the non-isothermal material parameters shown in Table 4.1 are considered. Expressions for material parameters in terms of continuous functions of temperature are defined using polynomial curve fitting technique to calculate their differentials during integration procedure.

Table 4.1 Non-isothermal material parameters for SS 316 LN [73]

T (ºC)	α (1E-5/K)	E (N/mm^2)	n	K (N/mm^{2}s$^{1/n}$)	C (N/mm^2)	γ	$k0$ (N/mm^2)	b	Q (N/mm^2)
200	1.71	170000	3.7	380	35000	550	97	13	100
300	1.75	149700	3.54	354.5	30560	512.2	90.3	12.3	92
400	1.78	140000	3.4	340	28000	490	85	11.7	87
500	1.80	134700	3.3	334	26200	481	80.59	11.3	83
650	1.83	130000	3.2	330	24000	480	75	11	80

As a benchmark analysis, the generalized multiaxial code for UMAT is used to realize cyclic deformation of the two-bar system which has been modeled with two noded truss elements T2D2T for 1 D and four noded CPE4RT beam element for 2 D representation. The two-bar system is a simple self constraint structure compared to cylindrical structure and is widely used for ratcheting analysis. The two-bar system is fixed at top, while it is free to deform axially with a rigid block such that load variations in one bar impose complimentary stresses in the other bar.

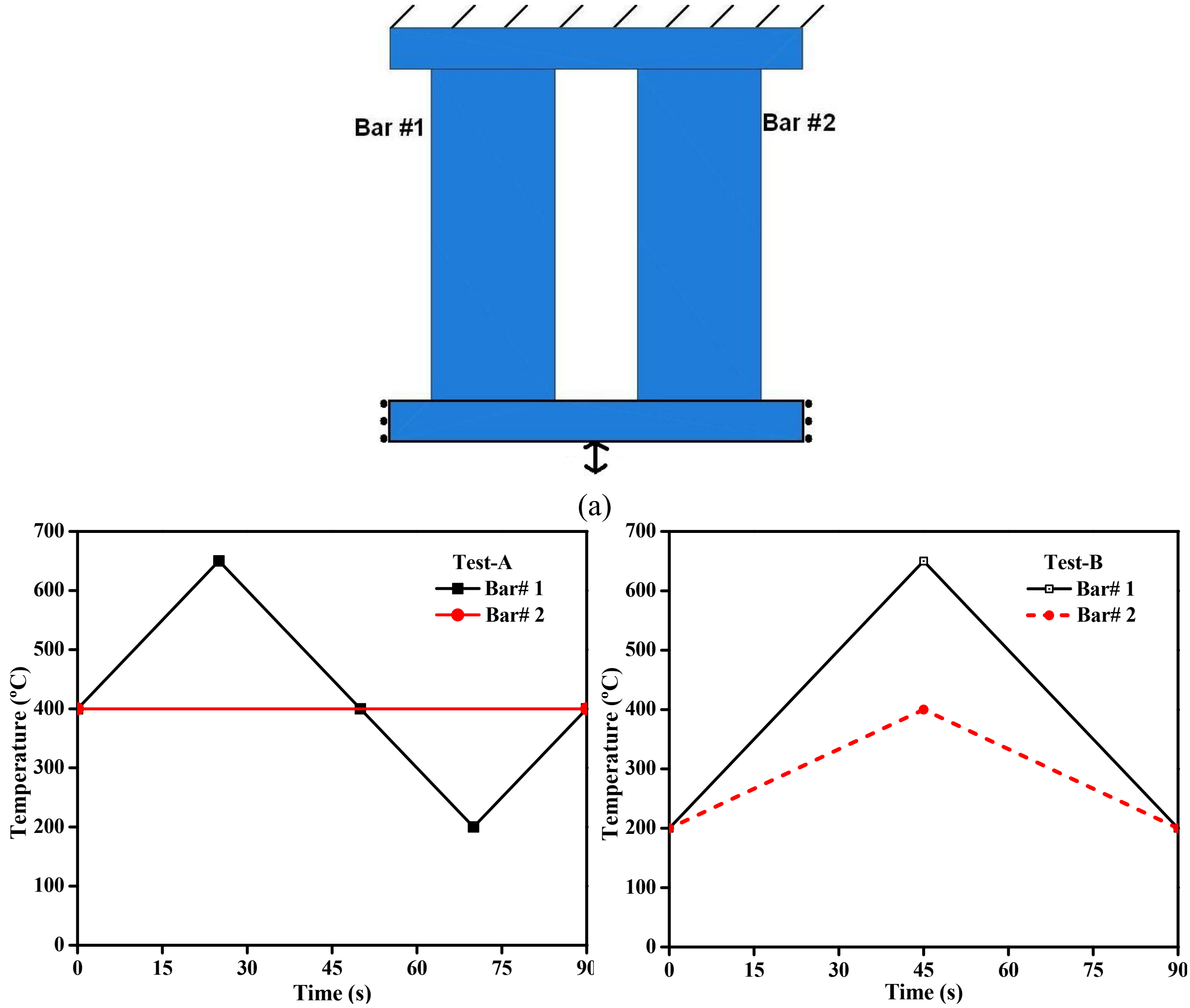

Figure 4.2 (a) Two-bar system (b) Thermal loading for Test-A (c) Thermal loading for Test-B according to Kuhner et al. [73]

The results from the present 1 D and 2 D analyses are compared with the experimental and numerical data from the published results of Kuhner et al. [73]. The evolution of mean strain with load cycles are presented in Figure 4.3 (a) and (b) for Test-A and Test-B respectively, along with the predictions by Kuhner using AF, Sievert and Chaboche rules. It can be noted that the experimental results shows a non-ratcheting behavior, while the predictions by Kuhner using AF, Sievert and Chaboche rules report significant ratcheting.

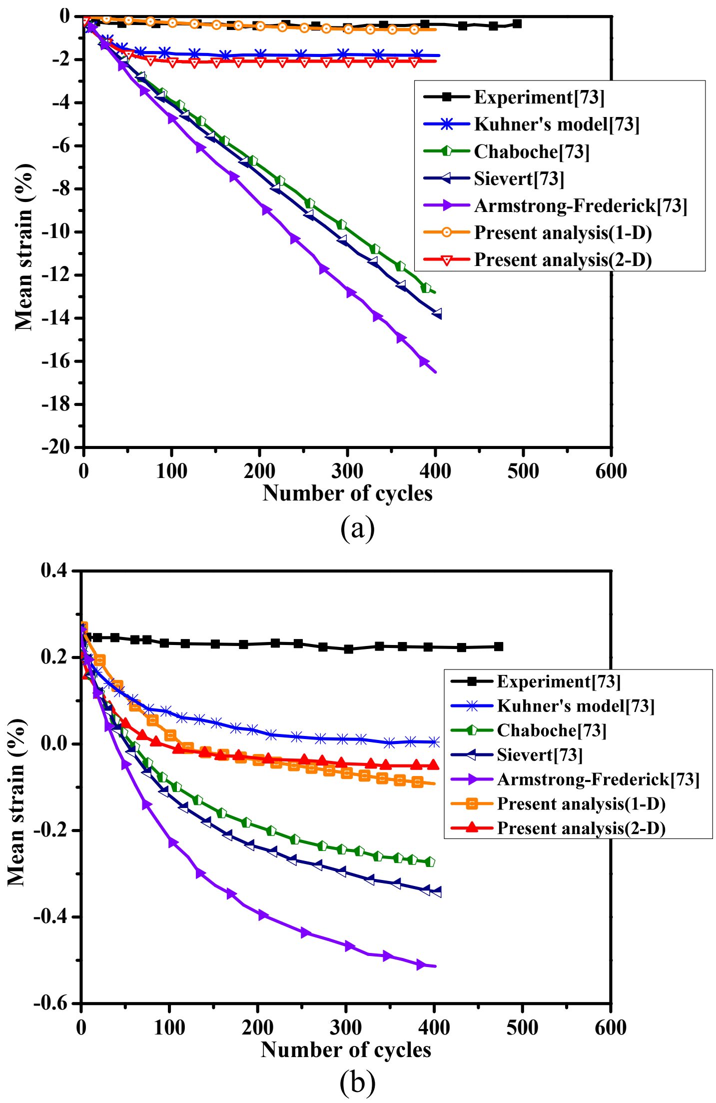

Figure 4.3 Comparison of the present analysis with the ratcheting results of two-bar system obtained by Kuhner et al. [73] experimentally and numerically using AF, Sievert, Chaboche rule and Kuhner's modified model (a) Corresponding to Test-A (b) Corresponding to Test-B

The noticed significant over prediction of ratcheting was controlled by using the modified rule of kinematic hardening having TRT that limits the ratcheting strain produced by the dynamic recovery term under thermal cycling. The TRT grow with inelastic strain influencing little in the beginning of deformation compared to that of the dynamic recovery term. However, it influences inelastic strain significantly compared to the dynamic recovery term during decrease in ratcheting overshoot. The influence of the temperature rate term and the dynamic recovery term is balanced when ratcheting strain is saturated. The similar behavior has been reproduced in the present analysis considering 1 D and 2 D models of the two-bar system. Evolutions of mean strain by 1 D FE analysis are closer to the experimental data which attained stabilization rapidly compared to 2 D FE analysis where poison's ratio plays important role during ratcheting due to thermal cycling. However, both the analysis trends are in reasonably similar to the experimental prediction up to 400 cycles except that 2 D FE analysis has an initial over predictions. This validates the present formulation for non-isothermal ratcheting analysis with the hardening rule expressed by Eq. (4.1). The significant role of TRT in present analysis motivates to perform thermomechanical interaction studies of two-bar system and cylindrical shells under different loading conditions, which are discussed in the following sections.

4.4 THERMOMECHANICAL INTERACTION STUDIES: TWO-BAR SYSTEM

For the thermomechanical interaction studies, symmetric stress load (to analyze ratcheting behavior) is applied and the temperature of the Bar# 1 is varied with time at three different rates for different studies as mentioned in Table 4.2. Values of time to attain maxima of temperature and therefore stress are 15 s, 20 s and 25 s both for *Study-A* and *Study-B*. TML with coincident peaks at each odd thermal cycle for *Study-A*, while coincident valleys at each even thermal cycle for *Study-B* is termed here as IP-loading and OP-loading respectively.

Table 4.2 Thermomechanical loading for various cases

Loading types	*Study-A* (IP-loading)			*Study -B* (OP-loading)			*Study-C*		
	Rate-1	Rate-2	Rate-3	Rate-1	Rate-2	Rate-3	TLR-1	TLR-2	TLR-3
TLR ($\Delta T/\Delta t$ in °C/s)	173/15	173/20	173/25	173/15	173/20	173/25	173/15	173/20	173/25
Stress rate (MPa/s)	50/15	50/20	50/25	50/15	50/20	50/25	50/10	50/10	50/10

In *Study-C,* for non coincident peak load condition, symmetric stress cycling with constant cycle time and asymmetric thermal cycling with three different cycle times are imposed to highlight the effect of TLR. It is to be noted that, the loadings for *Study-A* and *Study-B* are not strictly IP or OP since the cycle times of thermal and mechanical load is kept different. This is done to capture the significance of thermal cycling, which is initially in-phase for IP-loading (*Study-A*) and out of phase for OP-loading (*Study-A*).

4.4.1 Effect of phase shift in thermomechanical loading

Strain accumulation behavior under cyclic TML encompassing the hardening phenomena, noticed in the present analysis for *Study-A* and *Study-B* loadings in Figure 4.4 is discussed here to highlight the effect of phase shift in TML at various rates. Cyclic hardening is an important feature of SS 316 LN that governs the extent of damage. Hence, this section reports the importance of such behavior while predicting TML life under cyclic loading conditions that may cause concurrence of ratcheting and fatigue in engineering components.

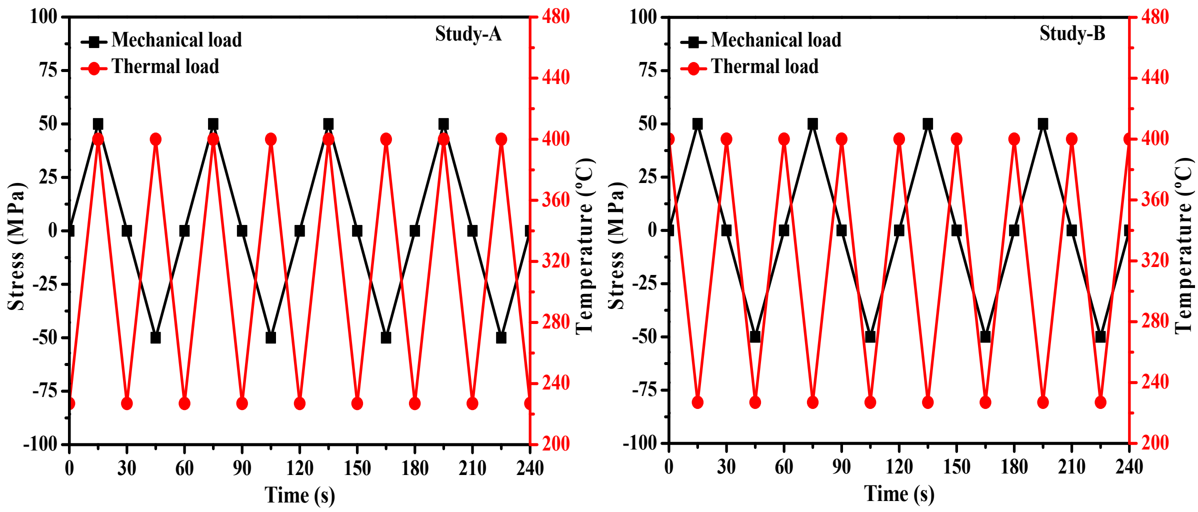

Figure 4.4 Loading schemes for *Study-A* and *Study-B*

Figure 4.5 (a) presents the accumulated strains after 4000 s are 1.9 %, 1.6 % and 1.2 % for Rate-1, Rate-2 and Rate-3 respectively in case of the same phase of thermal load during the first half cycle while opposite phasing in the second half cycle (*Study-A*). The higher the thermal load rate, more is the strain observed which is due to reduced visco-plastic contribution of thermal cycling at high rate. The gross permanent deformation of the bar is noticed under symmetric stress cycling due to the accumulation of residual strain after each expansion and contraction caused by thermal load cycles.

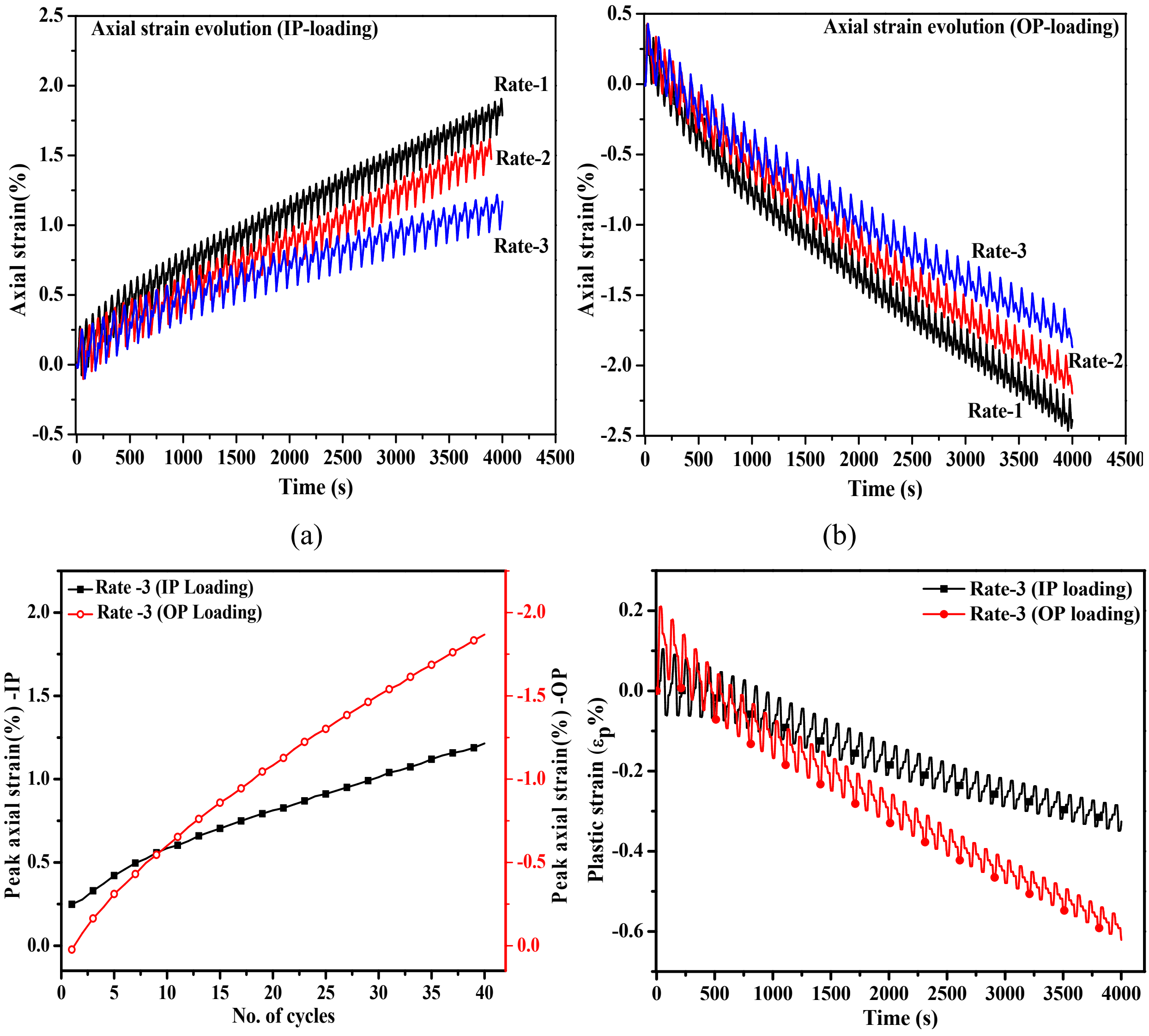

(a) (b)

(c) (d)

Figure 4.5 Evolution of strain for IP/OP loadings (a) for *Study-A* load (b) for *Study-B* load (c) peak strain evolution with no. of cycles (d) plastic strain evolution with time

Mean temperature rise in the Bar# 1 assists axial elongation during first half stress cycle while resisting it during a second half stress cycle resulting in net elongation in both the bars. This is actually a case of non proportional semi in phase load where the effect of initial phasing is responsible for net elongation. Therefore, semi in phase load is referred here as IP-loading. Figure 4.5 (b), shows that the initial OP thermal load producing compressive strain, rapidly exceeds the tensile strain value after tensile yielding, such that net compression is noticed as in case of perfect OP load. The accumulated strain values after 4000 s are −2.4 %, −2.2 % and −1.8 % for Rate-1, Rate-2 and Rate-3 respectively in *Study-B*. Ratcheting damage during IP and OP loading conditions is compared by drawing a dual axis plot (Figure 4.5 (c)) keeping the same scales with peak tensile strain on one axis and peak compressive strain on the other axis for IP and OP predictions respectively. This inference is further supported by the cyclic response in Figure 4.5 (d) indicating higher plastic strain accumulation for OP loading compared to IP for Rate-3. Since net compressive plastic strain during IP-loading condition does not exceed elastic and thermal strain components (tensile) hence net elongation is observed in Bar #1.

4.4.2 Effect of thermal load rates

For non coincident peak load condition in *Study-C*, symmetric stress cycling with constant cycle time and asymmetric thermal cycling with three different cycle times (Table 4.2) are imposed to highlight the effect of TLR. Cyclic response under non coincident peak load as in Figure 4.6 (a) which corresponds to *Study-C*, is shown in Figure 4.6 (b). The contribution of TLR is seen by keeping constant stressing but decreasing the TLR. From the plot, it is evident that the lower the TLR, lesser is the axial strain.

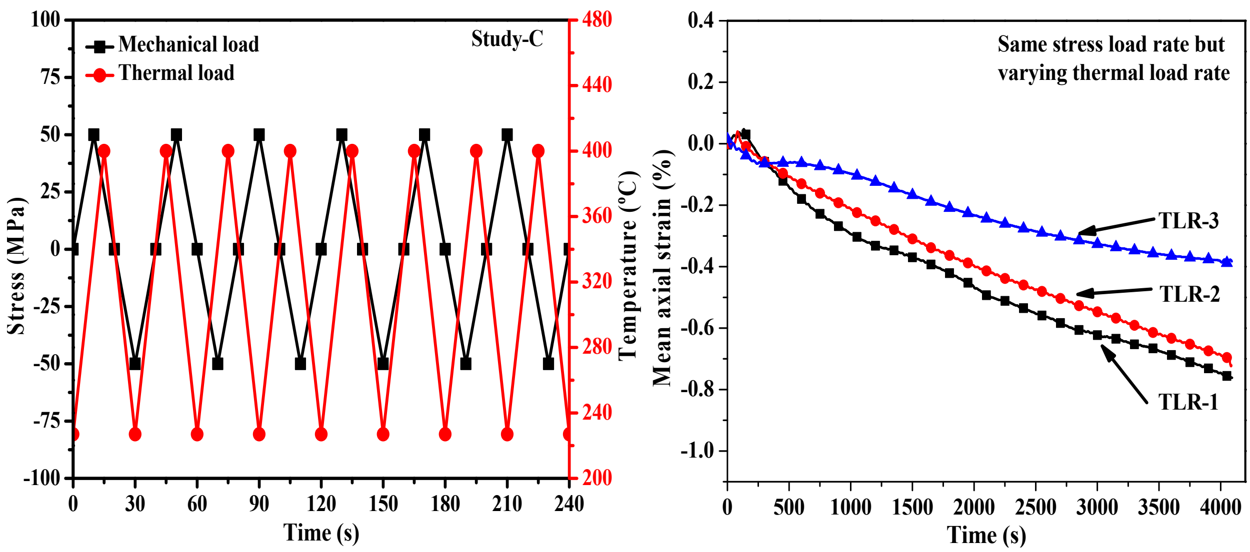

Figure 4.6 Evolution of strain for different thermal load rate (TLR) for *Study-C*

4.5 THERMOMECHANICAL INTERACTION STUDIES: CYLINDRICAL SHELL

Ratcheting in the main vessel of SFR due to free level variations of hot sodium during normal operations and DHR/SGDHR conditions is a complex phenomenon. Additionally, the dynamic behavior of the main vessel experiencing thermomechanical loading during the change in sodium pool temperature with the free level variations is a major concern for the designers. The dynamic behavior of the main vessel under such loadings is due to the heat generation in reactor core, which causes change in temperature and volumetric expansion in sodium pool. Thus, the effect of level variations is further enhanced, which affects the mode of deformation of the main vessel i.e. it may deform inward or outward. The inward or outward deformation may increase or decrease the gap between the main vessel and the safety vessel which may obstruct the free movement of ISI device for inspection. The significance of these transient conditions has not been explored in the existing studies. Focusing on this aspect, the thermomechanical interaction analysis of cylindrical shells has been performed to understand the effect of TLR on the deformation mode of the cylinder. For this purpose, analyses were performed for several rates (TRL) by changing ΔT, out of which, the results for three different TLR (R1, R2 and R3) are presented. The presented results for R2 and R3 indicate the change in the mode of deformation. The results obtained using constitutive models with and without TRT have been compared for R1, R2 and R3. To simulate the loading conditions, an axisymmetric FE model of a thin hollow cylinder of SS 316 LN material with height 600 mm, OD 500 mm and thickness 1 mm is subjected to the thermal load as described below. The boundary conditions are, the top is fixed axially and initial water level is kept at 300 mm (i.e. the mean position).

4.5.1 Imposed thermal loading

A traveling temperature front along the axis is simulated by the up and down movement of the test cylinder in water-filled container as in Figure 4.7 (a) for a cycle time of 320 s, while the temperature of the induction heater is linearly increased and decreased. In the earlier work [50], the temperature of the induction heater was fixed. Thermal loading for the three temperature ranges has been cyclically applied for the 50 mm downward movement of the cylinder. Different thermal load rates are listed in Table 4.3. Temperature front movement for R1 case during free level variation is shown in Figure 4.7 (b) at different instances of time during downward movement of the cylinder. With the downward movement of the cylinder, the temperature front advances in the direction of the arrow with the increasing peak temperature. The same procedure is repeated for the rates R2 and R3 keeping the same mean temperature.

Table 4.3 Loadings for different temperature ranges and corresponding thermal load rates

Temperature ranges	500 °C to 550 °C (525±25 °C)	450 °C to 550 °C (500±50 °C)	400 °C to 600 °C (500±100 °C)
Thermal Load rate (TLR)	**R1**=25/80 (°C/s)	**R2**=50/80 (°C /s)	**R3**=100/80 (°C/s)

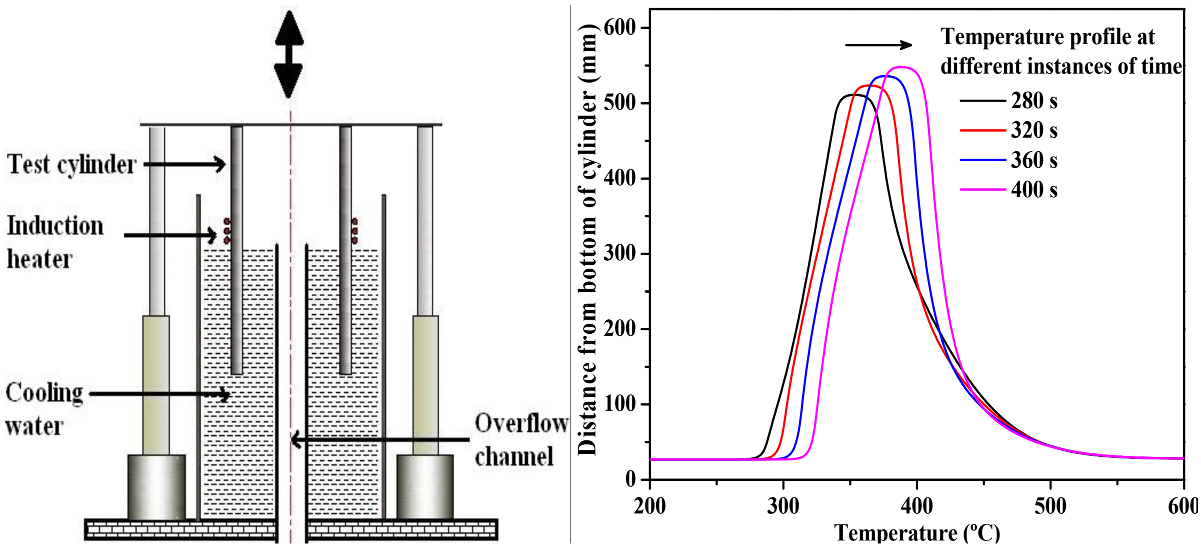

(a) (b)

Figure 4.7 (a) Schematic of thermal ratcheting setup (b) Traveling temperature front along the axis after different time instances of 40 s

4.5.2 Effect of concurrent change in the peak temperature with the moving temperature front

Residual radial displacements due to thermal ratcheting for different thermal loading rates are presented in Figure 4.8. For a TLR of R1, using the present formulation (with temperature rate terms), a radial growth (bulge out or expansion) of 0.52 mm is observed in Figure 4.8 (a), while it is 0.58 mm without temperature rate term (Figure 4.8 (b)). Similarly, the results for the load rates R2 and R3 are presented in Figure 4.8 (c)-(d) and (e)-(f) respectively.

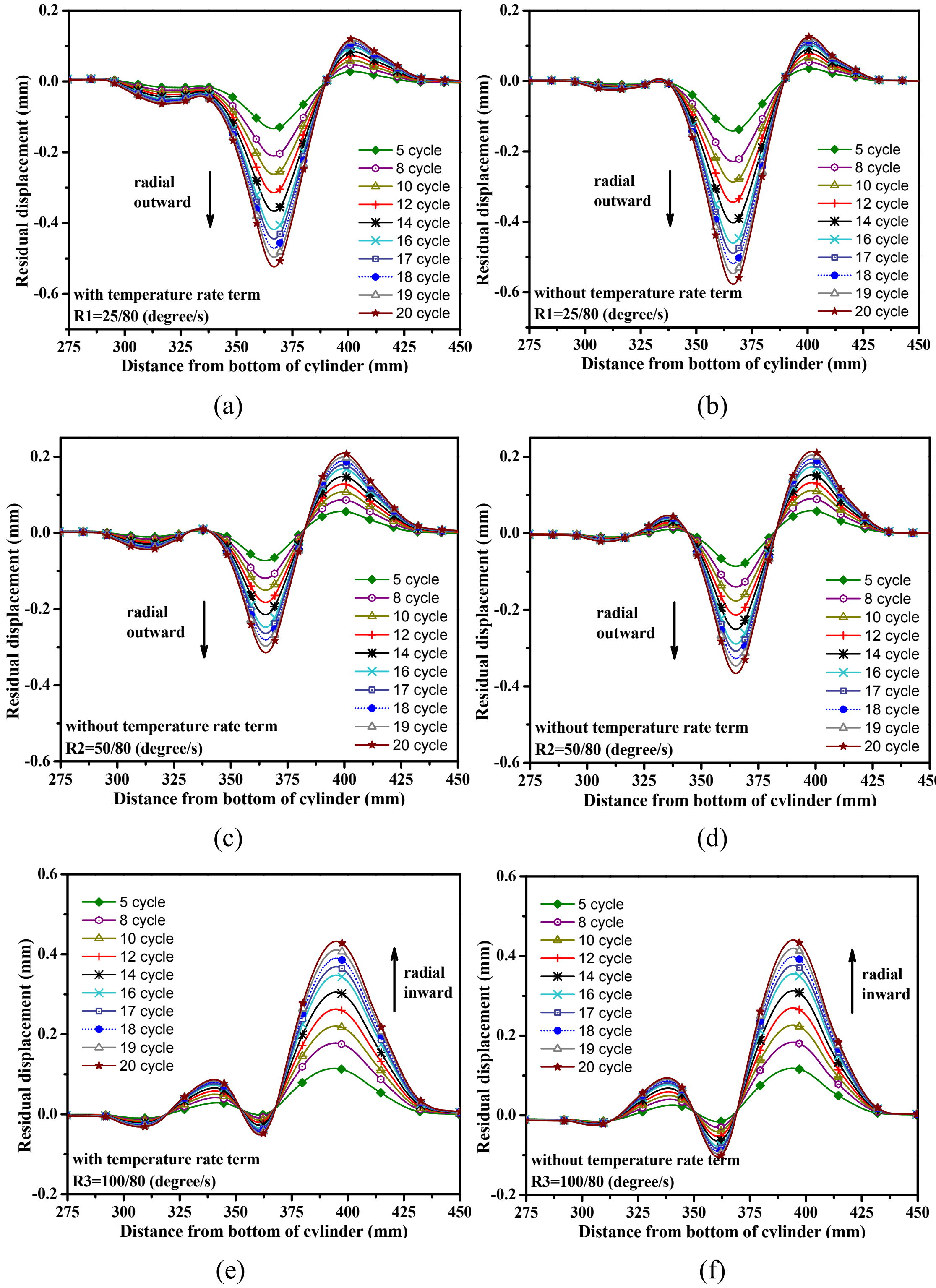

Figure 4.8 Residual radial displacements of cylinder for thermal load rates R1, R2 and R2 using constitutive model with temperature rate term and without temperature rate term

The radial deformation under such type of loading is dependent upon TLR which is clearly seen in Figure 4.9 (a) and (b) where change in deformation mode is noticed for R3. Residual radial displacements observed using non-isothermal material parameters is less than that obtained for isothermal material parameters at maximum temperatures. The lower the mean temperature, i.e. For R2 compared to R1, lesser is the predicted residual radial deformation in the cylinder despite being subjected to higher temperature change from the mean temperature. On the other hand, comparing results for R2 and R3, the significance of temperature change (or TLR is shown, which plays an important role in the thermal ratcheting behavior.

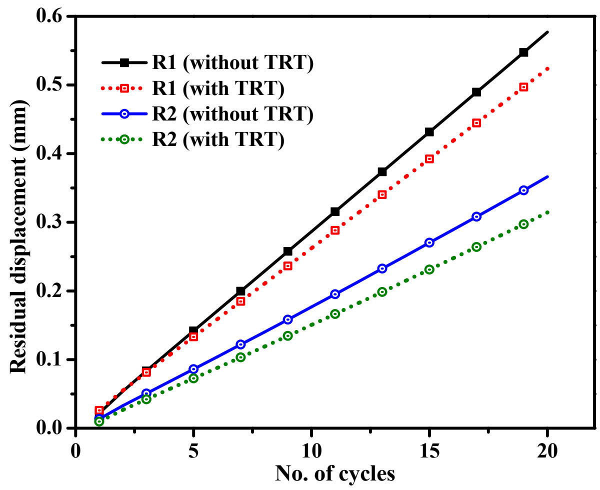

(a)

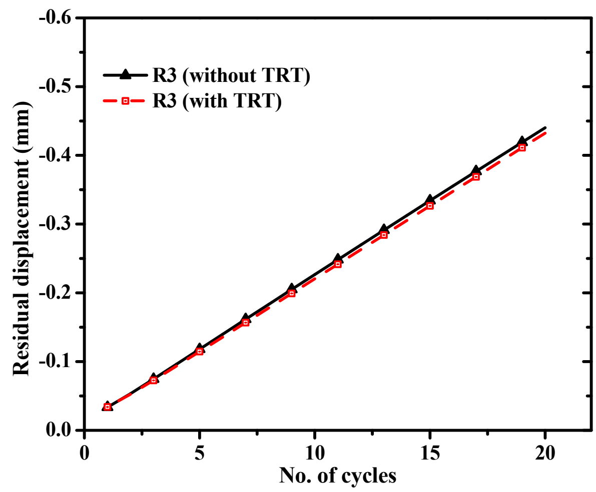

(b)

Figure 4.9 Evolution of residual radial displacements with the number of cycles (a) for rates R1 and R2 showing radial outward growth (b) for rate R3 showing radial inward growth

Noticing an inward deformation from Figure 4.9 (b), it is evident that the deformation mode of expansion or contraction is affected by the change in the temperature from the mean value per unit time i.e. TLR. Additionally, it is observed that TRT has no significant effect on the ratcheting strain for higher TLR i.e. R3. This can be attributed to the negligible change in dynamic recovery term with the temperature change (i.e. 500±100 °C). Furthermore, it can be stated that the change in the mode of deformation is not solely dependent on TLR because no such behavioral change is noticed in Figure 4.9 (a) for R2 being higher than R1. Moreover, no sign of saturation in the radial deformation is observed after 20 cycles, which indicates that the difference between the final radial displacement using both procedures (with and without TRT) may increase further due to progressive ratcheting. Thus, the accuracy of life assessment may significantly be affected by the choice of hardening rule.

4.6 SUMMARY

In this chapter, a constitutive model with temperature rate term is discussed to highlight the effect of TLR during the ratcheting behavior of the two-bar system (SS 316 LN). The influence of TLR is studied for various stress controlled cyclic thermomechanical loadings considering temperature dependent material parameters. Further, the approach is used to reveal the effect of temperature rate term while predicting thermal ratcheting of a thin cylinder caused by change in the peak temperature during temperature front movement. It is to be noted that, the test cylinder moves to simulate the level variation while in the following chapter the cylinder is fixed and level variations are achieved using a level oscillator arrangement. Such thermal loadings are more relevant to the SFR when the pool temperature varies with free level variations as mentioned in the second chapter. Visco-plastic formulation with and without temperature rate term in hardening rule is used to show the differences in the predicted strain. A significant effect of TLR on the deformation mode of the cylinder is also noted while performing this analysis.

EXPERIMENTAL AND NUMERICAL SIMULATIONS / APPLICATIONS 5

5.1 INTRODUCTION

As explained in the previous chapters, ratcheting is a directional cyclic deformation behavior of materials under asymmetric cyclic loading. To deal with the inelastic behavior of materials due to thermal ratcheting, it is necessary to comprehend the capabilities of available constitutive models for the ratcheting prediction. Researchers [12], [53] have investigated the evolution of ratcheting strain with stress cycles. Recently Jian Peng and co-authors [76] discussed the significance of ratcheting during the concurrence of ratcheting and fatigue. Portier et al. [77] studied ratcheting behavior of SS 316 following five sets of constitutive models. They conducted various tests to generate the experimental database for mechanical behavior under uniaxial and multiaxial loadings. Bari and Hassan [19] compared the capabilities of some models. They found Chaboche-type kinematic hardening rules to be suitable to predict nonlinearity due to yield surface translation during multi-axial ratcheting condition. Despite the large number of available reports, the cyclic inelastic behavior of metals under complex loading situations requires further understanding. It is also noticed that most of the constitutive models proposed so far have neglected the thermomechanical interaction effect on ratcheting behavior of material under uniaxial or multiaxial thermomechanical loadings. The studies that highlight the influence of thermomechanical interactions in thermal ratcheting behavior are sparse. Specifically for the cylindrical structures, further thermomechanical studies are needed to understand the suitability of different available hardening rules. It has been emphasized in the previous chapter that the hardening rule must have TRT to improve the accuracy of prediction of ratcheting under thermomechanical loading conditions. In order to adhere to the stringent design rules, the deformation of the main vessel of SFR should be properly estimated considering the realistic loading it is subjected to.

This chapter describes the adequacy of different hardening rules for different loading conditions by predicting the ratcheting or shakedown state and studying the change in the deformation mode of the cylinder. With this aim, the thermal ratcheting experiments are conducted followed by numerical analysis to substantiate the application of the proposed hardening rules with SSIP. The temperature front movement for the following two cases of thermal loadings has been simulated. First case is to demonstrate the suitability of two hardening rules while the second case is to highlight the effect of using TRT with CH3 rule on the deformation mode of the cylinder.

Case-A: Constant sodium pool temperature (by induction heating at fixed temperature) during free level variations with varying axial thermal gradient ($\Delta T/\Delta Z$).

Case-B: Changing sodium pool temperature (by induction heating with linear temperature variations) during free level variations.

Table 5.1 summarizes the different thermal loading conditions that can be achieved by various induction-heating criteria. *Case-A* simulates the loading due to moving temperature front with constant peak temperature as in [50]. *Case-B* simulates loading due to moving temperature front with the concurrent change in the peak temperature. Experiments and numerical simulations with SSIP for *Case-A Type-III* load (Table 5.1) have been undertaken to illustrate the suitability of AF or CH3 rule for different loading conditions. While AF rule is used frequently for the thermal ratcheting prediction, CH3 rule yields better results and is suitable to recognize non saturating ratcheting behavior hence used with TRT in the present chapter. The benchmark study of the two-bar system by Kuhner et al. [73] described in section 4.3 validates the numerical formulations with TRT in AF rule using SSIP. According to Kuhner's study, modified rule with TRT significantly affects the accuracy of prediction of ratcheting with thermomechanical interaction in self-constraint structures, viz., two-bar system and cylindrical shells etc. Hence, to present the effect of thermomechanical interaction on the thermal ratcheting behavior of cylindrical shell under *Case-B* load, TRT in CH3 rule is included as shown in Eq. (5.1).

$$\dot{\mathbf{X}} = \frac{2}{3} C_i \mathbf{d\varepsilon^P} - \gamma_i \mathbf{X}_{\mathrm{i}} \dot{P} + \frac{\partial C}{\partial T} \frac{\mathbf{X}}{C} \dot{T} + \frac{\partial \gamma}{\partial T} \mathbf{X} P \dot{T} \tag{5.1}$$

Table 5.1 Summary of loading cases analyzed

Loading cases	Loading types	Induction-heating criteria	Constitutive model
Case-A	**Type-I**: ΔT/ΔZ varies	**OFF** during cylinder withdrawal. (Test cylinder moves)	Time independent model (analyzed in Chapter 3)
	Type-II: ΔT/ΔZ constant	**ON** during cylinder immersion and withdrawal. (Test cylinder moves)	Time independent model (analyzed in Chapter 3)
	Type-III: ΔT/ΔZ varies	**ON** during level variations (Test cylinder fixed)	Time dependent model (analyzed in this chapter)
Case-B	ΔT/ΔZ varies	**ON** with increasing and decreasing temperature during level variations. (Test cylinder fixed)	Time dependent model with temperature rate terms (analyzed in this chapter)

5.1.1 Experiment and specimen details

To simulate the cyclic thermal loading due to free level variations as in the main vessel of SFR, a thermal ratcheting test facility is developed as shown in Figure 5.1. Specifically, the new thermal ratcheting setup has a test cylinder fixed while a level oscillator arrangement provides the free level variations. Thus, the problem of maintaining a constant gap between the cylinder and the induction heater is resolved, which existed in earlier versions of test setups as mentioned in earlier chapters. This feature helped in the uniform heating throughout the perimeter of the cylinder. The developed setup has an added advantage that the thermal ratcheting in the presence of primary axial load can also be studied in the future.

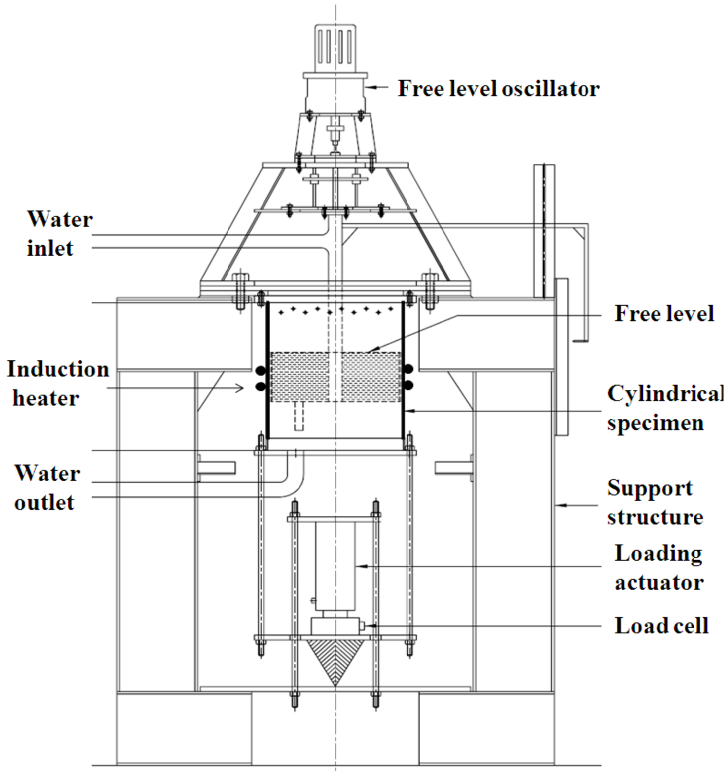

(a)

(b)

Figure 5.1 (a) Schematic of thermal ratcheting test setup (b) Actual thermal ratcheting test setup

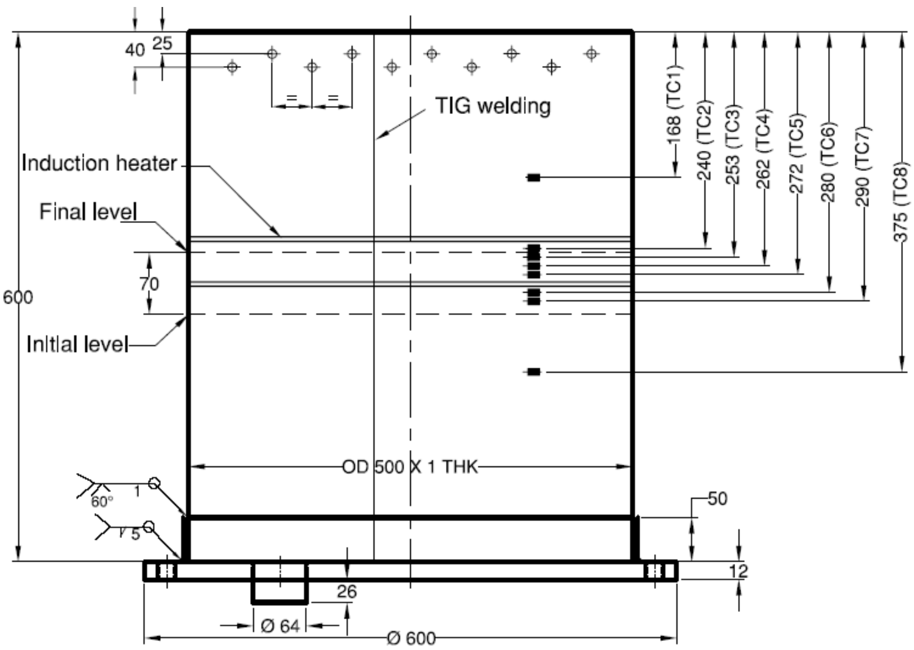

Figure 5.2 Specimen geometry and location of thermocouples for thermal ratcheting test

Thin hollow cylindrical shells of height 600 mm, OD 500 mm and thickness 1 mm were used as test specimens constructed by pre annealed SS 316 L steel. The fixed induction heater provided the required heating from the outside of the specimen. A level oscillator arrangement facilitated the required up and down motion of an empty container (with a hole at bottom) immersed in the circulating water in the cylinder to vary the free level. Level variation was simulated by using a stepper motor arrangement with the appropriate speed reduction gearbox system. The speed of level variation can be adjusted using a variable-frequency drive (VFD) controller. In this experiment, the loading conditions in the main vessel of SFR due to level variation of sodium at constant temperature were simulated by heating the shell locally and varying the water level. To record the transient thermal loading response, thermocouples (TC) were welded outside the cylindrical shell specimens along its height as in Figure 5.2. Non-contact type laser sensors were deployed along the height of the cylinder to capture the radial growth. It is to be noted that the test was performed in the absence of primary axial loading (i.e. Axial loading actuator and load cell arrangement were disengaged). During the experiment, the test cylinder was fixed from the top with the support structure.

5.1.2 Applied thermal loading

The outer surface of the *specimen 1* was heated locally up to 450 °C using induction heater, which was placed above the free level of water. The water level in the cylinder was varied up to 70 mm with a cycle time of 240 s. The temperature variation along the height of the *specimen 1* captured by the thermocouple at different instants of time in Figure 5.3 simulates *Case-A Type-III* load where arrow shows the direction of movement of temperature front. *Specimen 2* was subjected to similar loading with peak temperature of 550 °C, cycle time of 460 s and level variation of 45 mm. The localized heating and cooling were imposed at the vicinity of free level by keeping induction heater switched ON during up and down motion of level oscillator.

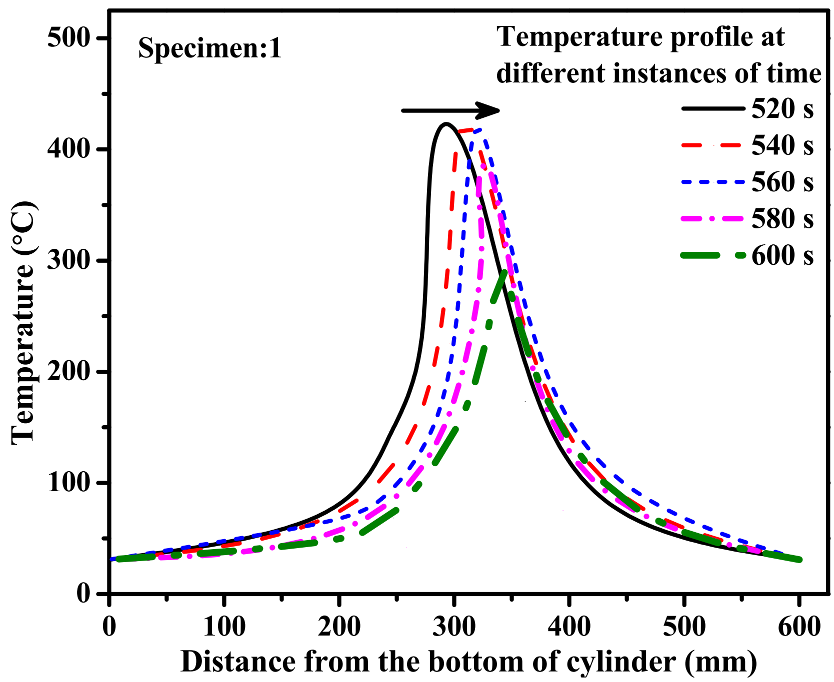

Figure 5.3 Profiles of the moving temperature front recorded by thermocouples (TC) for *specimen 1* (Experimental): *Case-A Type-III* load

5.1.3 Test results

Thermal loading for 20 cycles and 16 cycles were applied and laser sensors were used to capture the radial growth of *specimen 1* and *specimen 2*. Due to high temperature, significant thinning in *specimen 2* was observed so the test was stopped at 16th cycles only The peak residual radial displacement measured for *specimen 1* after 4th, 10th, 14th, 18th and 20th cycles were −0.83 mm,

−1.02 mm, −1.07 mm, −1.20 and −1.30 mm respectively. The peak residual radial displacement for *specimen 2* after 4th, 10th, 12th, 14th and 16th load cycles were −0.75 mm, −1.23 mm, −1.26 mm, −1.31 mm, −1.35 mm respectively. The above values were further confirmed by the manual measurement of the diameter of the specimens at the end of the corresponding cycles measured by the laser sensors. The test results for residual radial displacements along the height from the bottom of the cylinder for the above load cycles are presented in Figure 5.4.

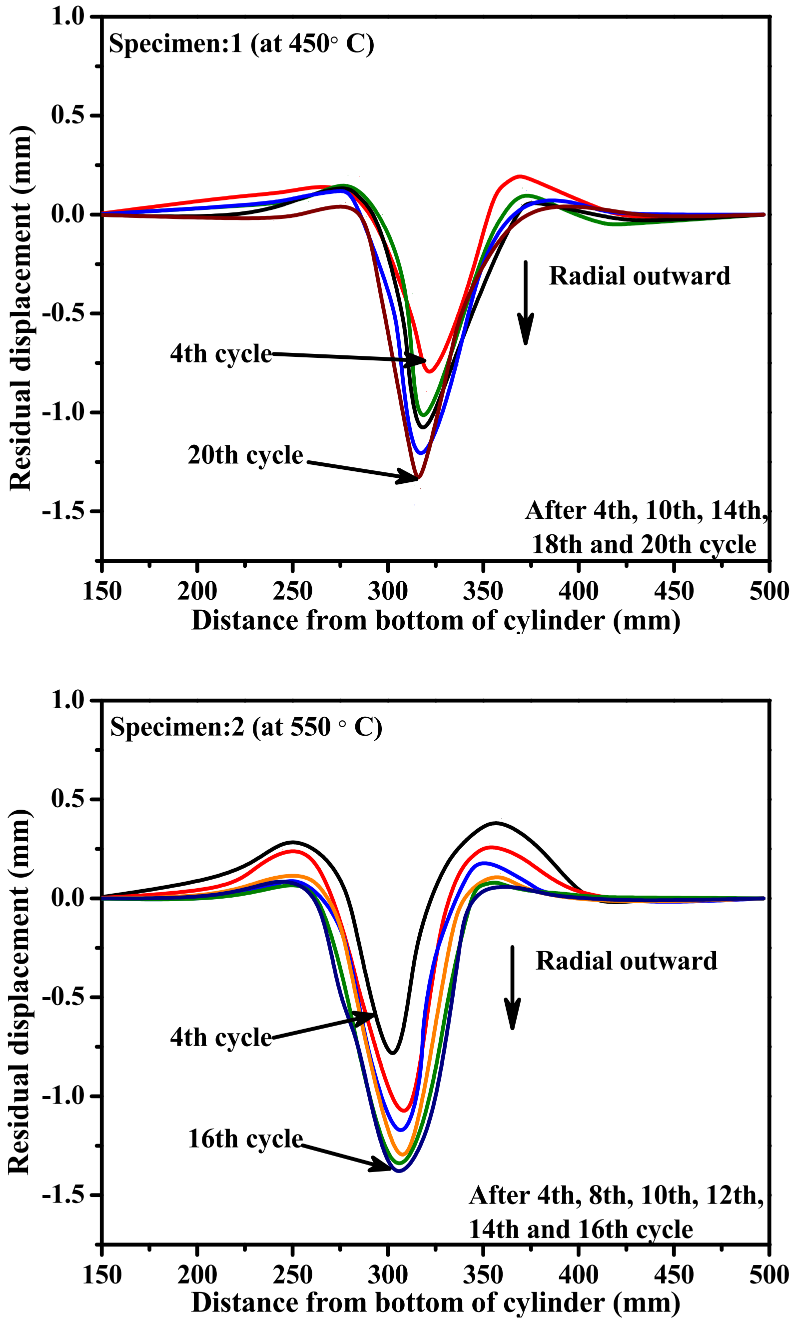

Figure 5.4 Measured residual radial displacements of the cylinder for *specimen 1* and *specimen 2*

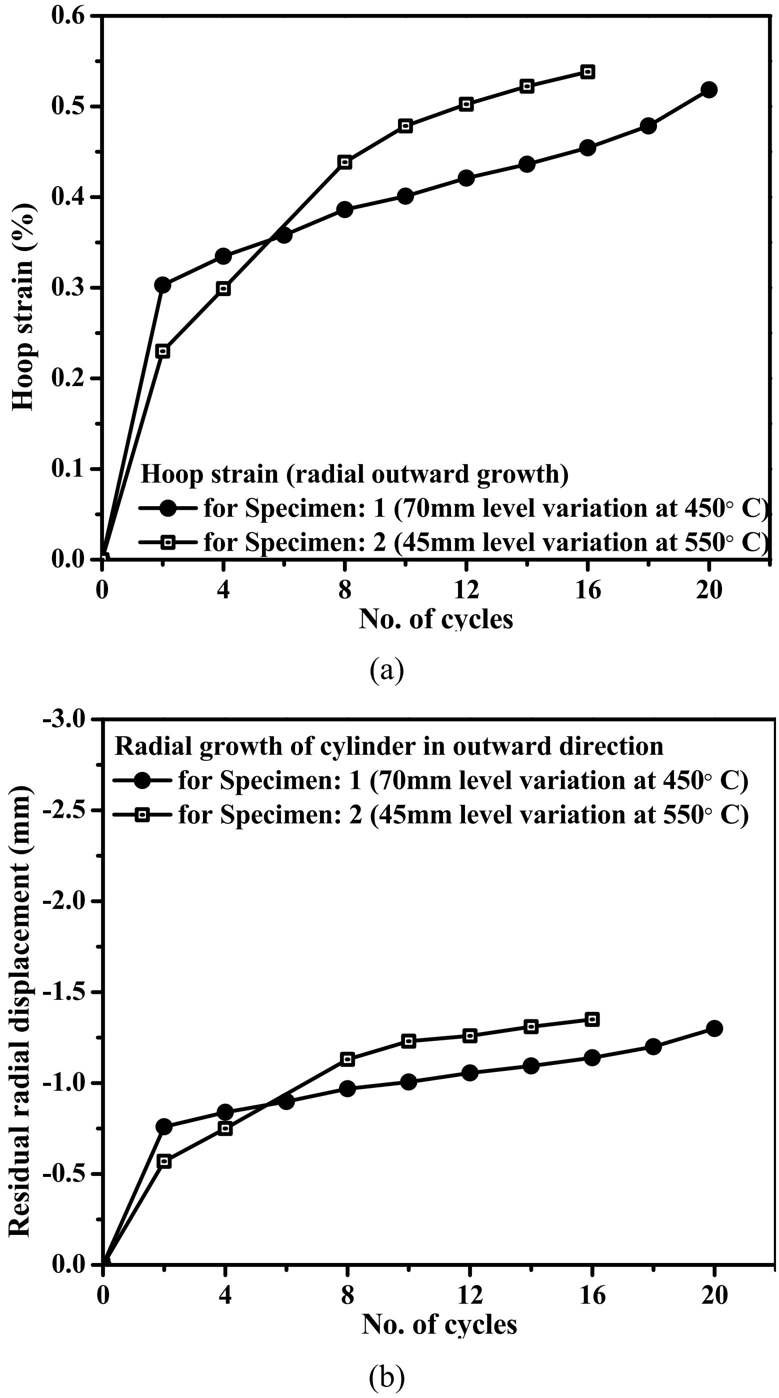

Figure 5.5 (a) Hoop strain evolution for *specimen 1* and *specimen 2* (b) Residual radial displacement for *specimen 1* and *specimen 2*

Hoop strain evolution and residual radial displacement with the number of cycles are shown for both the specimens in Figure 5.5 (a) and (b) respectively. Although, initially, for a few cycles, lower hoop strain is noticed for *specimen 2*, but rapid strain accumulation is observed thereafter compared to *specimen 1* in spite of being operated for reduced level variation (or reduced traveling length of the temperature front). Since the movement of the temperature front is the one of the driving force for thermal ratcheting, hence the traveling length and speed of free level variation both contribute to radial strain accumulation. Therefore, lower strain is observed initially due to the small level variation while higher cycle time and higher operating temperature notably increased the strain after a few cycles approach saturation or shakedown in 16 cycles at a slower rate in case of *specimen 2*. Contrarily, *specimen 1* does not exhibit any sign of saturation and plastic instability may contribute to failure after a higher number of loading cycles. Therefore, *specimen 1* is chosen for FE analysis and the thermal ratcheting behavior observed in the tests, is compared with numerical results to demonstrate the performance of the proposed integration procedure (SSIP) using AF and CH3 rules.

5.2 MATERIAL PARAMETER IDENTIFICATION

To perform the numerical analysis using different hardening rules, the material parameters are identified by conducting the tests as detailed below

5.2.1 Specimen description and applied loading

Uniaxial tests were conducted with SS 316 L obtained from the same batch of material used for the cylindrical shell having a chemical composition (in wt. %): C: 0.027, Mn: 1.7, Ni: 12.2, Cr: 17.53, Mo: 2.49, N: 0.07, Si: 0.22, S: 0.0055, P: 0.013 and Fe as balance. Viscous parameters were identified by conducting strain rate jump test on the specimen (gauge length of 25 mm and diameter 5 mm) at 2×10^{-4}/s and 2×10^{-3}/s. The specimen geometry in Figure 5.6, machined from the heat-treated (solution annealing treatment at 1373 K for 1 hour, followed by water quenching) rods were low cycle fatigue tested at a constant strain rate of 3×10^{-3}/s at strain amplitudes of ±0.4 %, ±0.6 % and ±0.8 %. Cyclic test data for ±0. 8 % (the highest strain rage) were used for identifying the cyclic hardening parameters. The tests were carried out at 450 °C under fully reversed, total axial strain control mode using a symmetrical triangular strain–time waveform using INSTRON servo-electric fatigue testing system.

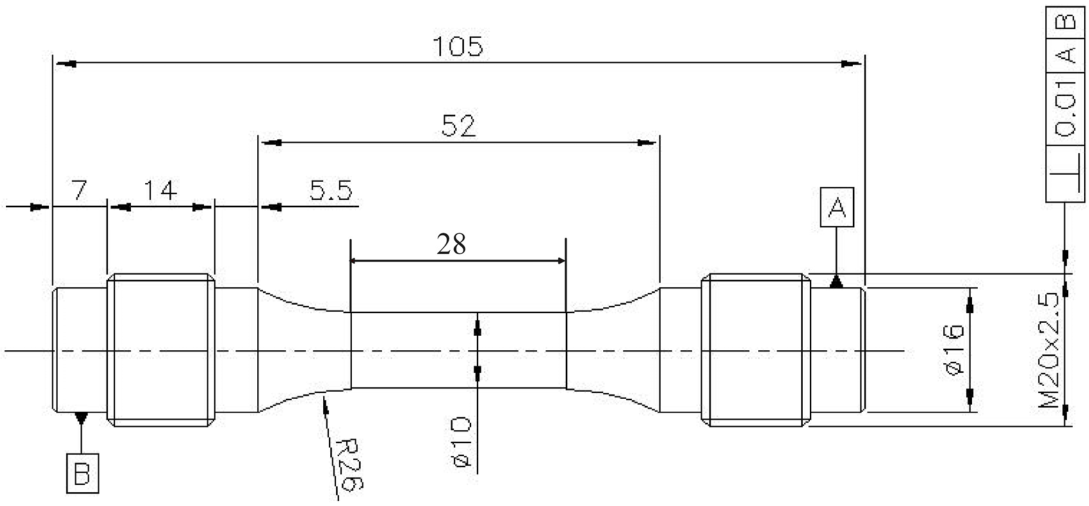

Figure 5.6 Specimen geometry for the LCF tests

5.2.2 Uniaxial tensile and cyclic hardening behavior

Uniaxial stress-strain responses from strain rate jump tests are compared with numerical results obtained using SSIP in Figure 5.7 (a) to identify viscous parameters for AF rule. The numerical results matched well with the experimental results. Stress- strain hysteresis loops obtained from axial strain controlled cyclic tests for ±0.4 % , ±0.6 % and ±0.8 % at 450 ° C are shown in Figure 5.7 (b), (c) and (d).

The same viscous parameters as obtained from the strain rate jump tests are used both for AF and CH3 rules. Further, the optimized cyclic hardening parameters are obtained by the parameter determination methods [19] and comparing the numerical predictions with the test results as shown in Figure 5.7 (e). The nonlinear portion of the stabilized cyclic loop is fairly reproduced by CH3 rule compared to AF rule by reducing the initial yield stress value without compromising maximum stress value due to cyclic hardening. After several iterations and comparisons, the material parameters for AF and CH3 rules identified are shown in Table 5.2. The isothermal parameters for 450 °C are used for thermal ratcheting analysis for *Case-A Type-III* loading and then the same parameters are used for *Case-B* load with TRT in hardening rules.

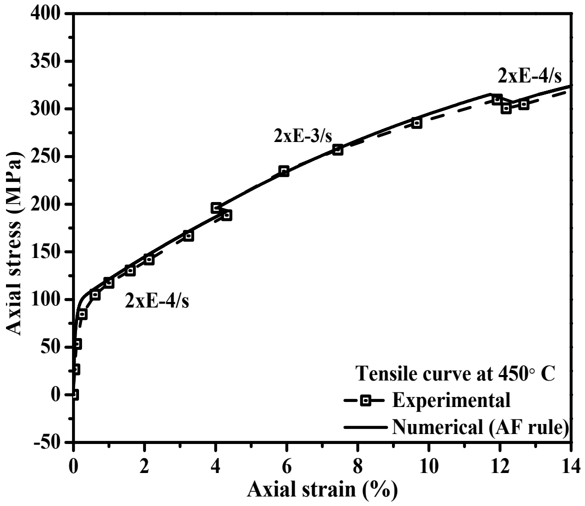

(a)

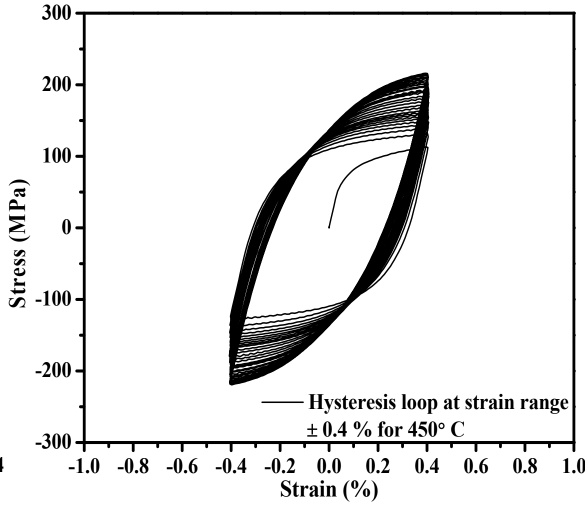

(b)

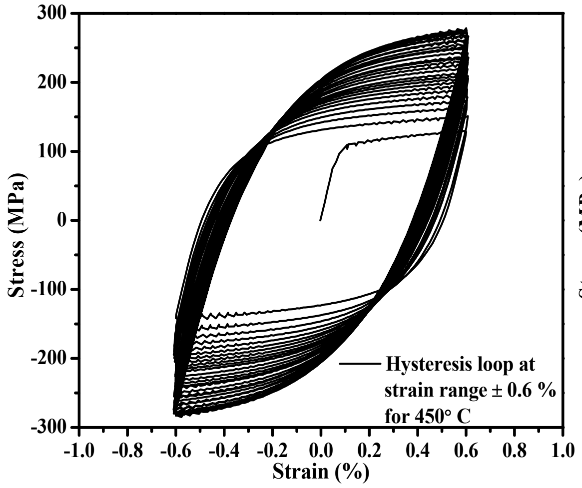

(c)

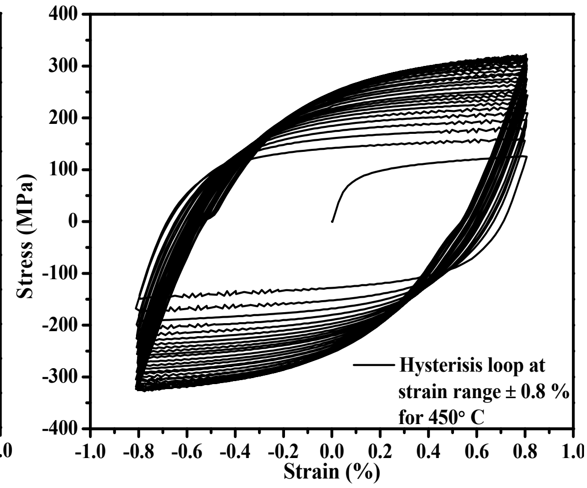

(d)

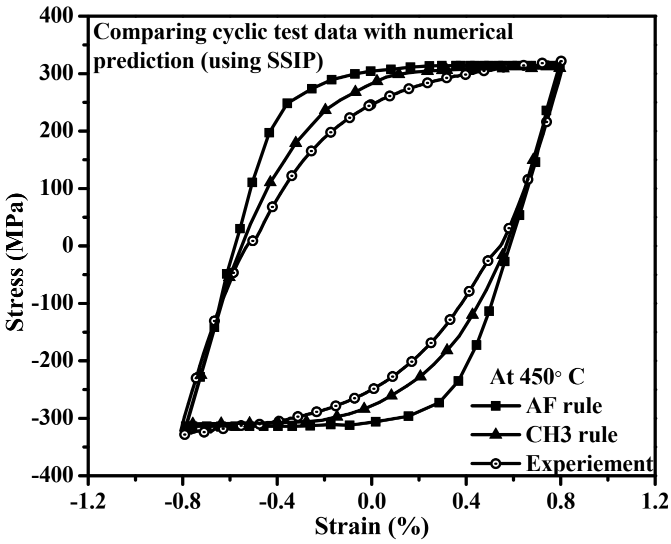

(e)

Figure 5.7 (a) Tensile stress-strain curve (450 °C) (b) Hysteresis loop at ±0.4 % strain range (c) Hysteresis loop at at ±0.6 % strain range (d) Hysteresis loop at ±0.8 % strain range (e) Stabilized hysteresis loop (450 °C) at strain rate 3×10^{-3}/s for ±0.8 % strain range

Table 5.2 Identified material parameters at 450 ºC for AF and CH3 rules

Hardening parameters for AF and CH3 rules											
	$k0$ (N/mm^2)	b	Q (N/mm^2)	C (N/mm^2)	γ	C_1 (N/mm^2)	C_2 (N/mm^2)	$C3$ (N/mm^2)	γ_1	γ_2	γ_3
AF	49	11	206	103200	820	-	-			-	-
CH3	28	6	202	-	-	34200	725	34	172	48	3
Viscous parameters for AF and CH3 rules											
	E (N/mm^2)			n				K (N/mm^{2}s$^{1/n}$)			
	141879			2.5				38			
	141879			2.5				38			

5.3 THERMAL RATCHETING: HARDENING RULES WITHOUT TEMPERATURE RATE TERMS

5.3.1 Numerically simulated thermal loading

An axisymmetric FE model of the cylindrical specimen is used for the numerical analysis by subjecting it to cyclic thermal loading as in Figure 5.8 for 20 cycles. The loading closely simulates experimentally predicted temperature distribution for *specimen 1* in section 2.1. The loading is obtained numerically by using the FILM subroutine [52] whereby varying the film coefficient with time along cylinder height produced the desired temperature profile.

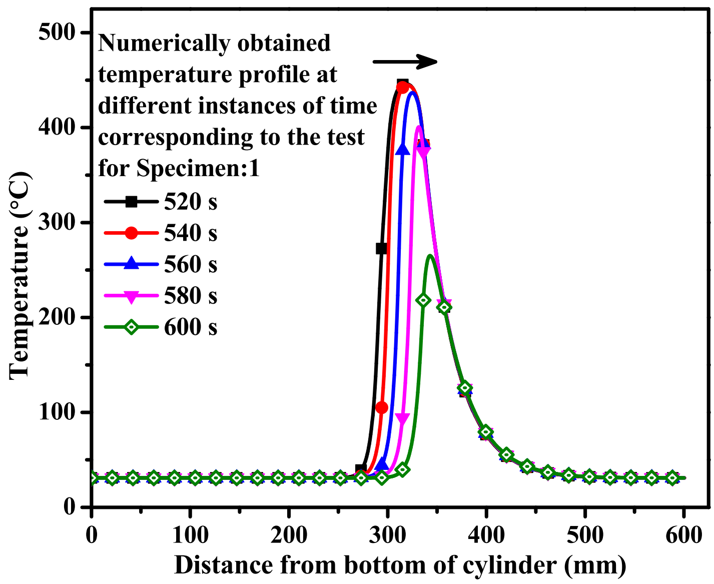

Figure 5.8 Profiles of the moving temperature front at different time instances for s*pecimen 1* (Numerical): *Case-A Type-III* load

5.3.2 Numerical results

A comparison is made between the numerical and experimental predictions of residual radial displacement of the cylinder (*specimen 1*) after the 10th and 20th cycle in Figure 5.9 (a) and (b) respectively.

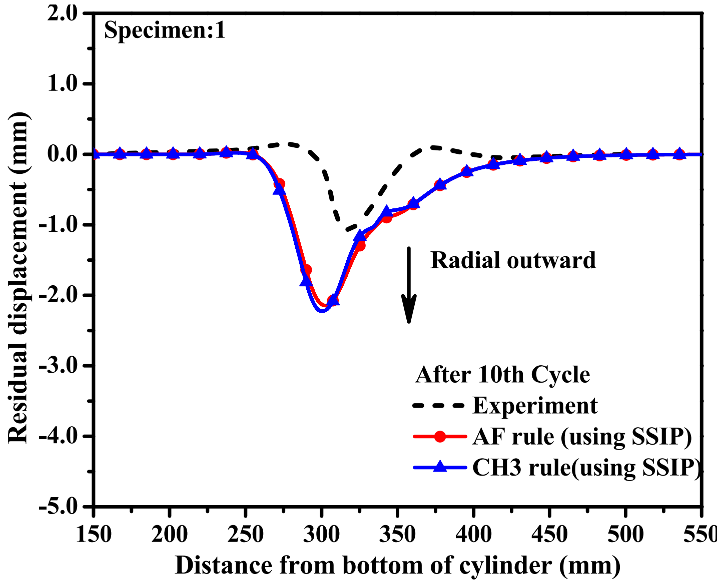

(a)

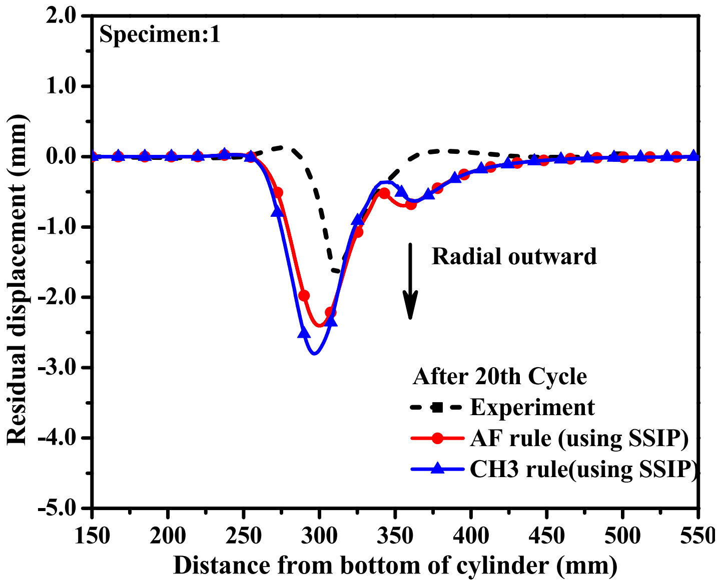

Figure 5.9 Comparison of experimental and numerical prediction of residual radial displacements for *specimen 1* : *Case-A Type-III* load (a) after 10th cycle (b) after 20th cycle

The non-linear kinematic hardening rule by AF and CH3 expressed by Eq. (2.11) and Eq. (2.12) are adopted for numerical analysis. Numerically predicted values of residual radial displacement are −2.15 mm and −2.40 mm after 10th and 20th cycle respectively for AF rule, whereas these are −2.23 mm and −2.80 mm for CH3 rule. Although, slight difference in the location of peak radial deformation is noticed, which is 305 mm obtained numerically and 320 by experimental prediction but the peak radial deformation values are adequately conservative.

The numerical predictions of residual radial displacement using AF and CH3 rules are compared with experimental results as a function of number of cycles (*specimen 1)* in Figure 5.10. It is evident that the numerical predictions from AF rule is approaching shakedown while ratcheting is noticed in case of CH3 rule that recognized the experimental progressive ratcheting (non saturating) behavior aptly, though, initial over prediction by both the model is noticed. Residual displacement in the radially outward direction approached shakedown (using AF rule) at a value of −2.40 mm, whereas progressive finite ratcheting (using CH3 rule) at −2.80 mm is observed for *specimen 1*. The progressive ratcheting is due to a non zero positive value of γ_3 (at γ_3= 3) and shakedown may be achieved if γ_3 is zero.

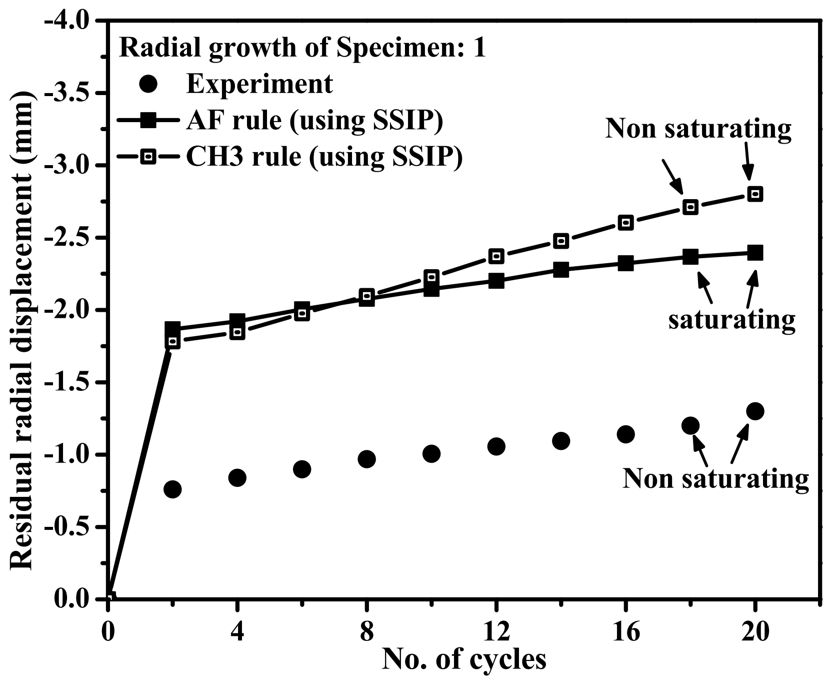

Figure 5.10 Evolution of residual radial displacement with the number of cycles for AF and CH3 rules using SSIP: *Case-A Type-III* load

5.4 THERMOMECHANICAL RATCHETING: HARDENING RULES WITH AND WITHOUT TEMPERATURE RATE TERMS

5.4.1 Effect of concurrent change in the peak temperature with the moving temperature front

The FE model of the *specimen 1* is subjected to a traveling temperature front with the concurrent change in peak temperature simulating a linear increase and decrease of temperature of induction heater with level rise and fall respectively. Peak temperature of moving temperature front (*Case-B* load) varies with time from 250 - 450 °C during free level rise as shown in Figure 5.11. The resulting peak temperature is 362 °C when the temperature front is moved by 70 mm, which simulates the rapid cooling by water with level rise such that the surface of cylindrical shell experiences 362 °C instead of 450 °C. The thermal ratcheting response corresponding to this case of load is analyzed to compare the effect of TRT in CH3 rule, which significantly influenced the deformation mode (expansion/contraction or bulge in/bulge out) of the cylindrical shell.

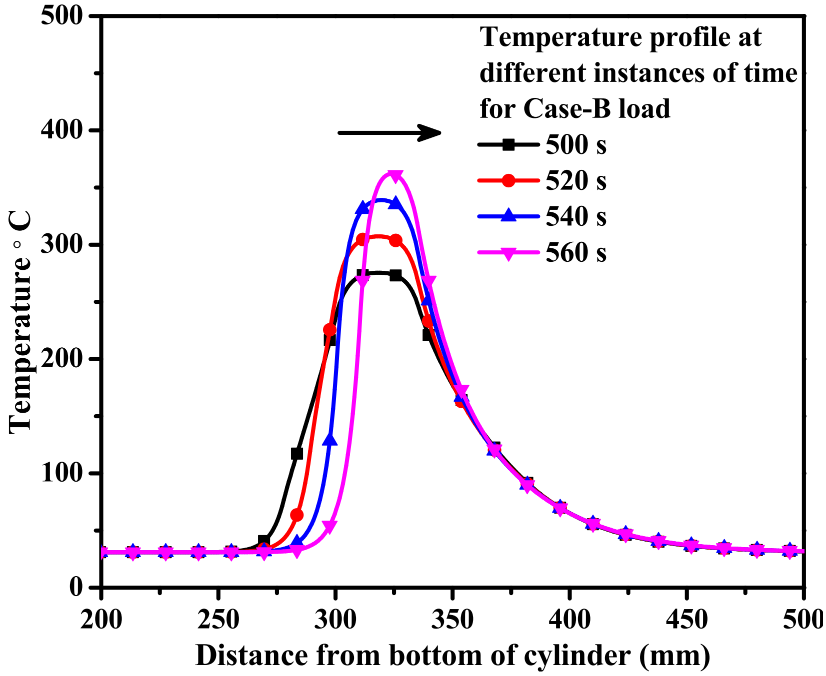

Figure 5.11 Moving temperature front with increasing peak temperature: *Case-B* load

5.4.2 Numerical results

Case-B type of loading condition occurs in real scenario as reported by Chellapandi et al. [49], which mentioned loading with the change in sodium pool temperature during free level changes in the main vessel of SFR. However, several reports [78], [79], [80] have not consider such type of load. This section presents the influence of *Case-B* load on the deformation mode of the cylinder. Because of the significant effect of TRT and linear ratcheting effect of CH3 rule, the thermal ratcheting (non saturating) is predicted under *Case-B* load using CH3 rule with TRT. Corresponding results of progressive deformation in the radial direction using isothermal material parameters for CH3 rule after the intervals of 5 cycles are shown in Figure 5.12. The effect of *Case-B* load is observed, where initial radial outward deformation mode (expansion) changes to radial inward deformation mode (contraction) which is captured by CH3 with TRT. After 15th cycle, no increase in radial growth (expansion) is seen for CH3 with TRT, instead, an increase in radial inward deformation (contraction) is noticed in Figure 5.12 (b).

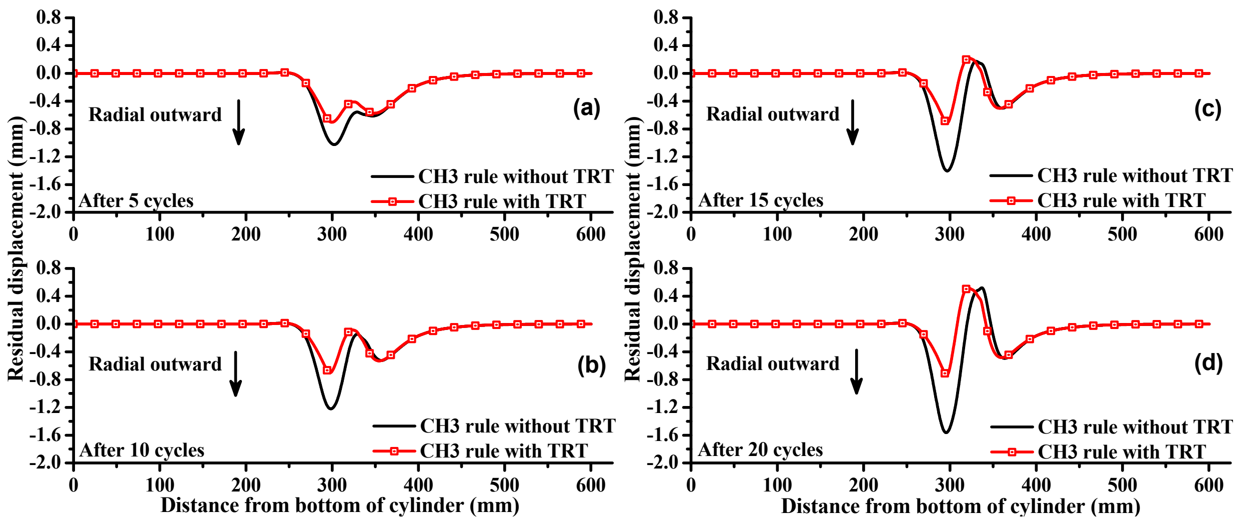

Figure 5.12 Growth in residual radial displacements for *Case-B* load corresponding to CH3 rule with and without TRT after (a) 5 (b) 10 (c) 15 and (d) 20 cycles

The deformed cylinder after 20 cycles due to thermal ratcheting is shown in Figure 5.13 presenting the significance of employing TRT in the constitutive model. The limitation of hardening rules without TRT is clearly visible in these results, which failed to reveal the change in the mode of deformation from expansion to contraction. Contrarily, the inclusion of TRT in CH3 rule as expressed in Eq. (5.1) predicts the change in deformation mode distinctly. After the 20th cycle, the extent of inward growth (contaction) is higher compared to the outward growth (expansion) in Figure 5.13 (b), where U1 is the residual radial displacement in meters.

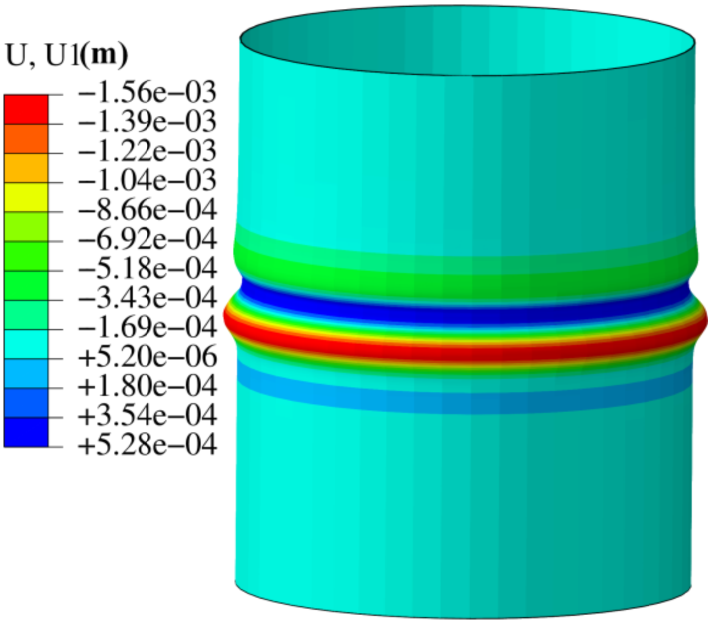

(a)

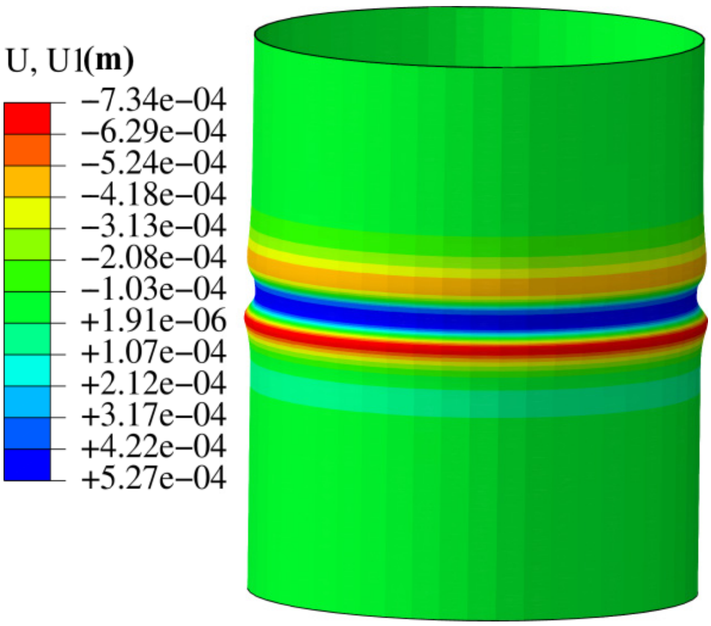

(b)

Figure 5.13 Deformed cylinders after 20 cycles for *Case-B* load (a) corresponding to CH3 rule without TRT (b) corresponding to CH3 rule with TRT

5.5 SUMMARY

Thermal ratcheting behavior of SS 316 L stainless steel cylindrical shells subjected to moving temperature front has been experimentally investigated at 450 °C and 550 °C for different traveling lengths. Numerical analyses considering, Armstrong and Fredrick (AF) and Chaboche three back stress (CH3) rules in the visco-plastic framework have been performed using a proposed plastic strain integration procedure employing identified hardening parameters. Comparison of experimental and numerical results of radial growth in the cylindrical shell highlights the suitability of CH3 rule for predicting progressive ratcheting behavior.

Further, the investigation of thermal ratcheting behavior due to moving temperature front with the concurrent change in peak temperature has been carried out by using temperature rate terms (TRT) in kinematic hardening rule. This situation simulates the changes in sodium pool temperature during free level variations in the main vessel of Sodium Cooled Fast Reactors. Test results of thermal ratcheting behavior of two-bar system from literature are used to validate the capability of the present numerical procedure with TRT in the kinematic hardening rule. The importance of TRT has been demonstrated while predicting the dynamic behavior of the cylindrical shell under thermomechanical loadings. The proposed approach (including TRT in CH3 rule following SSIP) successfully captured the change in deformation mode (expansion to contraction) and can be used for the prediction of ratcheting with thermomechanical interaction.

CONCLUSIONS AND FUTURE SCOPE 6

6.1 CONCLUSIONS

The present study has focused on the development of codes for predicting inelastic deformation behavior of materials under cyclic loadings. It has been well demonstrated in the thesis that the proposed numerical procedure for the considered constitutive models predicted ratcheting with increased accuracy. The important conclusions of the present study are described as below, while the major contributions of this study are provided subsequently in a sub-section 6.1.1.

- The investigation of cyclic hardening behavior shows strong influence of mean stress variation over ratcheting behavior, both at room temperature and at 550 °C. SS 316 L material exhibits considerable rate dependence in monotonic tension. At RT, high strain value is obtained using the *Model-2* compare to *Model-1*. The axial strain is 0.82 % for *Model-2* and 0.69 % for *Model-1* when loading is RT-SL-3: 52±195. Thus, visco-plastic contribution observed is ~0.13 %, which may further reduce for lower stressing rates. Hence *Model-1* may appropriately be used for stressing rates below 26 MPa/s and *Model-2* for higher stressing rates at room temperature. The study presents the suitability of *Model-2* for high temperature ratcheting-fatigue analysis at stressing rate of ~8.5 MPa/s or higher. This appears to be the effect of pronounced positive strain rate sensitivity at high temperature (for a range of 400 °C to 550

°C) which is accounted effectively by employing visco-plastic model in *Model-2* while neglecting in *Model-1*.

- Shakedown studies of thin hollow cylindrical shows that, for *Type-I* load, the residual radial displacement saturates at −3.2 mm and Change in deformation pattern (mode of deformation) for *Type-II* load is obtained which was outward deformation for *Type-I* load. For *Type-II* load, the residual radial displacements of the cylinder are 5.3 mm and 5.6 mm at the end of 14^{th} cycle and 15^{th} cycle respectively which shows ratcheting. At the end of the 15^{th} cycle, excessive geometrical thinning is observed in the region of maximum radial deformation.
- Ratcheting strain for $1/25^{th}$ scale down model of the PFBR main vessel with simplified thermal loading at the end of 50 cycles is 17.25 mm (outward), which is less than the thickness of main vessel (25 mm) of PFBR. This shows that there is no risk of buckling as per the present analysis.
- The study of the effect of frequency of free level variations and hold time shows that radial growth of the cylinder increases with the increase in the cycle time. This shows that more is the dwell time higher is the strain. A significant contribution (0.012 %) of visco-plasticity is noted at lower cycle time. The study further reveals that contribution of visco-plasticity is more at high frequency and its effect decreases with the decrease in frequency of level fluctuations. Rate effect due to visco-plasticity in the cylinder of SS 316 L at 550 °C is vanished for the cycle time of 480 s. Thus, there exists a limit of rate dependence in ratcheting behavior. It can also be noted that time independent and dependent (without creep) ratcheting formulation leads to similar results for higher cycle times. Hence, it may be assumed positively that time independent ratcheting formulation is appropriate (when creep of hold time effect is absent) in case of thermal ratcheting prediction. Significant increase of hold time contribution (from 0.007 % to 0.018 %) during cyclic accumulation of strain is observed when hold time changes from 5 s to 10 s.

- Findings of non-isothermal study of thermal ratcheting presents two different scopes of applications, viz. (a) Predicting cyclic strain accumulation behavior of austenitic steels under phase shift TML conditions and (b) Predicting thermal ratcheting behavior of cylindrical shell under the loading caused by free level variations with linear change in peak temperature. The study demonstrated considerable thermal rate dependence and modeling with the temperature rate terms influence the accuracy of ratcheting prediction under TML.
- Two-bar thermal ratcheting analysis shows that an initial phase shift in thermal and mechanical load governs the deformation behavior significantly because the initial in-phase load caused elongation in Bar# 1 while initial out of phase load caused compression. In case of both IP and OP loading the decrease in accumulated strain is observed with the increase in cycle time of thermal and mechanical load. It can be concluded that under stress controlled TML, the damage observed was more in case of OP (temperature and stress) loading than that of IP loading. Further, the change in a thermal gradient ($\Delta T/\Delta Z$) along the cylinder axis affects the deformation mode, which may bring out a permanent radial outward or radial inward bulge in the cylinder.
- In the case of transient thermal cycling the accuracy of the prediction of thermal ratcheting requires temperature rate terms in the hardening rules. The study also revealed the contribution of TLR during thermomechanical interaction due to moving temperature front with the concurrent change in peak thermal load. The results shows that predictions using CH3 rule are in good agreement with the progressive ratcheting behavior obtained experimentally.
- During free level variation, sodium pool temperature in the main vessel of SFR varies with time, hence noticeable thermal load rate change occurs which require rate dependent or in particular temperature rate dependent modeling. It is also demonstrated that shange in the

thermal gradient ($\Delta T/\Delta Z$) with time along the cylinder height effects deformation mode in addition to the geometry of the specimen, speed and travel length of the temperature front.

6.1.1 Technical and scientific contribution

The major contributions of the present studies on thermal ratcheting behavior are given below:

- A numerical integration scheme for plasticity calculation is derived and a code is developed for UMAT subroutine to perform ratcheting analysis.
- Throughout the study, the constitutive models are implemented in the code following semi-implicit procedure, which has better convergence rate and high accuracy compare to other convention fully implicit or explicit procedure.
- The comprehensive time independent, time dependent (creep and viscoplasticity) modeling approach is very useful for the better understanding of inelastic deformation behavior. It may help the reader while selecting the appropriate models and approach while predicting ratcheting behavior under different loading conditions.
- The non-isothermal studies of inelastic behavior provided a good insight of the significance of temperature rate dependence and hence the present work is very useful for ratcheting, fatigue, thermomechanical fatigue analysis.
- A code is also developed for UMAT which can be effective used for non-isothermal ratcheting or fatigue analysis. The same has been used for predicting thermal ratcheting of thin shells under non-isothermal loadings which is very useful for realistic simulation of ratcheting in main vessel of sodium cooled reactors.
- The present study demonstrate the significance of thermomechanical interaction in thermal ratcheting which affects the mode of deformation of cylinder in addition to dimension of the cylinder, speed of free level variations and loading methods.
- The study proposes a modified constitutive model i.e. CH3 model with temperature rate term and emphasize the need of using it while performing non-linear thermomechanical analysis.

6.2 FUTURE SCOPE

The study showed the ratcheting response of cylindrical shells under different loading conditions and featured the capability of proposed numerical integration procedure for visco-plastic model employing different hardening rules. The proposed approach can widely be implemented for studying the deformation behavior under thermomechanical loading and in especial for the temperature rate dependent studies. This present study is found to have a wide scope in below mentioned areas of research work:

- The deformation behavior studies under concurrent ratcheting and fatigue studies.
- To bring improvement in the accuracy of prediction of ratcheting strain, the proposed SSIP can be derived considering yield distortion hardening and DSA.
- Prediction of thermal ratcheting deformation in the main vessel of nuclear reactors under different operation conditions after establishing the actual thermal loadings during operation.
- Present approach with multiaxial formulation procedure can be widely used in several other applications such as ratcheting in pipe bends, ratcheting in sodium piping.
- The promising feature of the developed thermal ratcheting test facility can be suitably applied to study deformation behavior of cylindrical shells under combine primary load due to weight and secondary thermal load due to high temperature sodiumfree level variation.

REFERENCES

[1] Srinivasan, G., Suresh Kumar, K.V., Rajendran, B. Ramalingam, P.V., "The Fast Breeder Test Reactor-Design and operating experiences," *Nuclear Engineering and Design*, vol. 236, pp. 796-811, 2006.

[2] Chetal, S.C., Balasubramanium, V., Chellapandi, P., Mohanakrishnana, P., Pudhivinayagam, P., Pillai, C.P., Raghupathi, S., Shanmugam, T.K., Sivathanu Pillai, C., "The deisgn of the prototype fast breeder reactor," *Nuclear Engineering and Design*, vol. 236, pp. 852–860, 2006.

[3] Galileo, G., *Discorsi e dimostrazioni matematiche, intorno à due nuove scienze , Leida, Appresso gli Elsevirii*. Leiden: Louis Elsevier, 1638.

[4] Coulumb, C.A., *Essai sur une application des regles de maximis et minimis a quelques problemes de statique relatifs a 1 ‘architecture*, Memoires de Mathematique et de Physique, presentes ed.: Academie Royal des Science par divers savants, 1776.

[5] Tresca, H., *Mémoire sur l'écoulement des corps solides, par M. H. Tresca*. Paris: Impr. impériale, 1868.

[6] Saint Venant, de B., *Relatif à l'écoulement des corps solides malléables poussés hors d'un vase cylindrique par un orifice circulaire*. Paris: Académie des Sciences, 1870.

[7] Levy, M., *Mémoire sur les équations générales des mouvements intérieurs des corps*

solides ductiles au-delà des limites où l'élasticité pourrait les ramener à leur premier état. Paris: Académie des Sciences, 1870, vol. 70.

[8] Mises, von R., "Nachrichten von der Gesellschaft der Wissenschaften zu Göttingen, Mathematisch-Physikalische Klasse," *The European Digital Mathematics Library*, vol. 4, pp. 582-592, 1913.

[9] Hencky, H., "On the theory of plastic deformation and thereby in the material caused re-tensioning," *Journal of Applied Mathematics and Mechanics*, vol. 4, pp. 323-334, 1924.

[10] Khan, A.S., Huang S., *Continuum theory of plasticity*.: Wiley, 1995.

[11] Chaboche, J.L., Nouailhas D., "Constitutive modeling of ratcheting effects: Part I. Experimental facts and properties of classical models.," *Journal of Engineering Materials and Technology*, vol. 111, pp. 384-392, 1989.

[12] Hassan, T., Kyriakides, S., "Ratcheting of cyclically hardening and softening materials: I. Uniaxial behavior," *International Journal of Plasticity*, vol. 10, pp. 149-184, 1994.

[13] Hassan, T., Kyriakides, S., "Ratcheting of cyclically hardening and softening materials: II. Multiaxial behavior," *International Journal of Plasticity*, vol. 10, pp. 185-212, 1994.

[14] Dieter, G. E., *Mechanical metallurgy*. London: McGraw-Hill Book company, 1996.

[15] Lemaitre, J., Chaboche, J.L., *Mechanics of solid materials*. Cambridge: Cambridge University Press, 1990.

[16] Chaboche, J.L., "A review of some plasticity and viscoplasticity constitutive theories," *International Journal of Plasticity*, vol. 24, pp. 1642-1693, 2008.

[17] Abdel-Karim, M., "Shakedown of complex structure according to various hardening

rules," *International Journal of Pressure Vessel And Piping*, vol. 82, pp. 427-458, 2005.

[18] Prager, W., "A new method of analyzing stresses and strains in work hardening plastic solids.," *ASME Journal of Applied Mechanics*, vol. 23, pp. 493-496, 1956.

[19] Bari, S., Hassan T., "Anatomy of coupled constitutive models for ratcheting simulation," *International Journal of Plasticity*, vol. 16, pp. 381-409, 2000.

[20] Armstrong, P.J., Frederick C.O., "A mathematical representation of the multiaxial Bauschinger effect," *Materials at High Temperatures*, vol. 24, pp. 1-26, 2007.

[21] Araujo, M.C., "Non-linear kinematic hardening model for multiaxial cyclic plasticity," Faculty of the Louisiana State University, Brazil, Ph.D. dissertation 2002.

[22] Chaboche, J.L., Dang-Van K.; Cordier, G., "Modelization of the strain memory effect on the cyclic hardening of 316 stainless steel," in *Proceedings of the 5th International Conference on SMIRT*, vol. Div. L, 1979.

[23] Chaboche, J.L., "Time-independent constitutive theories for cyclic plasticity," *International Journal of Plasticity*, vol. 2, pp. 149-188, 1986.

[24] Ohno, N., Wang, J.D., "Kinematic hardening rules with critical state of dynamic recovery, Parts I and II," *International Journal of Plasticity*, vol. 9, pp. 375–403, 1993.

[25] Kobayashi, K., Ohno, N., "Thermal ratcheting of cylinder subjected to a moving temperature front: Effect of kinematic hardening rules on the analysis," *International Journal of Plasticity*, vol. 12, pp. 255-271, 1996.

[26] Sievert, R., Olschewski, J., "Modellierung thermisch-mechanischen visco-plastichen Verfestigugnsverhaltens and Lebensdauerabschatzung bei mehrachsiger Hochtemperaturemudung am Beispiel von IN738LC," in *Karaman- Auditorium*,

RWTH Aachen, Germany, 1997.

[27] Paul, S.K., Sivaprasad, S., Dhar, S., Tarafder, S., "Ratcheting and low cycle fatigue behavior of SA333 steel and their life prediction," *Journal of nuclear materials*, vol. 401, pp. 17–24, 2010.

[28] Gao, Q., Kang, G. Z., Yang, X. J., "Uniaxial ratcheting of SS304 stainless steel at high temperatures: visco-plastic constitutive model," *Theoretical and Applied Fracture Mechanics*, vol. 40, pp. 105-111, 2003.

[29] Suresh Kumar, R., Lakshmana Rao, C., Chellapandi, P., "Biaxial Ratcheting Response of SS316 Steel ," *Applied Mechanics and Materials*, vol. 24-25 , pp. 207-211, 2010.

[30] Chaboche, J.L. , "On some modifications of kinematic hardening to improve the description of ratchetting effects," *International Journal of Plasticity*, vol. 7, pp. 661–678, 1991.

[31] Kang, G.Z., Gao, Q., "Uniaxial and non-proportionally multiaxial ratcheting of U71Mn rail steel: Experiments and simulations," *Mechanics of Materials*, vol. 34, pp. 809–820, 2002.

[32] Kang, G.Z., Kan, Q.H., "Constitutive modeling for uniaxial time-dependent ratcheting of SS304 stainless steel," *Mechanics of Materials*, vol. 39, pp. 488-499, 2007.

[33] Sarkar, A., Nagesha, A., Sandhya, R., Mathew, M. D., "On the dynamic strain aging effects during elevated temperature ratcheting of type 316 LN stainless steel," *High Temperature Materials and Processes*, vol. 32, pp. 475-484, 2013.

[34] Ortiz, M., Simo, J. C., "An analysis of a new class of integration algorithms for elastoplastic constitutive relations," *International Journal for Numerical Methods in*

Engineering, vol. 23, pp. 353-366, 1986.

[35] Kan, Q.H., Kang, G.Z., Guo, S.J., "Finite element implementation of a super-elastic constitutive model for transformation ratchetting of NiTi alloy," *International Journal of Computational Methods*, vol. 9, p. 1240022, 2012.

[36] Kang, G.Z., Kan, Q.H., Zhang, J., "Time-dependent ratcheting experiments of SS304 stainless steel," *International Journal of Plasticity*, vol. 22, pp. 858-894, 2006.

[37] Abdel-Karim, M., Ohno, N., "Kinematic hardening model suitable for ratchetting with steady-state," *International Journal of Plasticity*, vol. 16, pp. 225–240, 2000.

[38] Bree, J., "Elastic-plastic behaviour of thin tubes subject to internal pressure and intermittent high-heat fluxes with application to fast nuclear reactor fuel elements," *Journal of Strain Analysis*, vol. 2, pp. 226-238, 1967.

[39] Bradford, R. A. W., "The Bree problem with primary load cycling in-phase with the secondary load," *International Journal of Pressure Vessels and Piping*, vol. 99-100, pp. 44-50, 2012.

[40] Wada, H., Igari, T., Kitade, S., "Prediction of plastic ratcheting of cylinder subjected to axially moving temperature distribution," in *Proceedings of the 10th International Conference on SMIRT*, vol. Div L, 1989.

[41] Igari, T., Kitade, S., Ueta, M., Ichimiya, M., Kimura, K., Satoh, Y., Take, K., "Advanced evaluation of thermal ratchetting of FBR components," *Nuclear Engineering and Design*, vol. 140, pp. 341-348, 1993.

[42] Cabrillat, M.T., Gatt, J.M., Schoulguine, P., Skiara, A., "Evaluation of thermal ratchetting on axisymmetric thin shells at the free level of sodium: Experimental results and elastic analysis," in *Proceedings of the 12th International Conference on SMIRT*, vol. Div E, 1993.

[43] R5., Design and construction rules for mechanical components of FBR nuclear Islands, 2002.

[44] RCC-MR., Assessment procedure for the high temperature response of structures, 2003.

[45] ASME Section III., Rules for construction of nuclear power plant components. Division 1- Subsection NH: Class 1 components in elevated temperature services, 2004.

[46] Wada, H., Odani, T., Fujioka, T., "The ratcheting evaluation methods in Japanese demonstration FBR design," in *Proceedings of the 14th International Conference on SMIRT*, vol. Div F, 1997.

[47] DDS., Demonstration fast breeder reactor high temperature structure design rules., 1998.

[48] Igari, T., Kobayashi, M., Yoshida, F., Imatani, S., Inoue, T., "Inelastic analysis of new thermal ratcheting due to a moving temperature front," *International Journal of Plasticity*, vol. 18, pp. 1191-1217, 2002.

[49] Chellapandi, P., Chetal, S.C., Bhoje, S.B., "Theoretical and experimental simulation of thermal ratchetting of thin vessels in," *Transactions of the Indian Institute of Metals*, vol. 53, pp. 391-399, 2000.

[50] Lee, H.Y., Kim, J.B., Lee, J.H., "Thermal ratcheting deformation of a 316L stainless steel cylindrical structure under an axial moving temperature distribution.," *International Journal of Pressure Vessel And Piping*, vol. 80, pp. 41-48, 2003.

[51] Badnava, H., Farhoudi, H. R., Fallah Nejad, K., Pezeshki, S. M., "Ratcheting behavior of cylindrical pipes based on the Chaboche kinematic hardening rule," *Journal of Mechanical Science and Technology*, vol. 26, pp. 3073-3079, 2012.

[52] ABAQUS version 6.10., Dassault Systèmes. Simulia Corp., Providence, RI, USA., 2010.

[53] Chaboche, J.L., Rousselier G., "On the plastic and visco-plastic constitutive equations. Part I. Rules developed with internal variable concept," *Journal of Pressure Vessel and Technology*, vol. 105, pp. 153-58, 1983.

[54] Chaboche, J.L., Rousselier, G., "On the plastic and visco-plastic constitutive equations. Part II. Application of internal variable concept to the 316 stainless steel," *Journal of Pressure Vessel and Technology*, vol. 105, pp. 159-164, 1983.

[55] Chaboche, J.L., "Modeling of ratcheting: evaluation of various approaches," *European Journal of Mechanics A /Solids*, vol. 13, pp. 501-518, 1994.

[56] Dunne, F., Petrinic, N., *Introduction to Computational Plasticity*. U.K.: Oxford University Press, 2005.

[57] Kang, G.Z., Gao, Q., "Uniaxial ratcheting of SS316 L stainless steel at high temperature: Experiments and simulations," in *Proceedings of the 18th International Conference on SMIRT*, vol. Div F, 2005.

[58] Kan, Q.H., Kang, G.Z., Zhang, J., "Uniaxial time-dependent ratchetting: Visco-plastic model and finite element application," *Theoretical and Applied Fracture Mechanics*, vol. 47, pp. 133-144, 2007.

[59] Hubel, H., "Basic conditions for material and structural ratcheting," *Nuclear Engineering and Design*, vol. 162, pp. 55-65, 1996.

[60] Taleb, L., Cailletaud, G., "Cyclic accumulation of the inelastic strain in the 304L SS under stress control at room temperature: Ratcheting or creep?," *International Journal of Plasticity*, vol. 27, pp. 1936-1958, 2011.

[61] Kawai, M., Ohashi, Y., "Couple effect between creep and plasticity of type 316

stainless steel at elevated temperature," in *Second International Conference on Constitutive Laws for Engineering Materials: Theory and Applications*, Tucson, Arizona, U.S.A, 1987.

[62] Krempl, E., "An experimental study of room temperature rate-sensitivity, creep and relaxation of AISI Type 304 stainless steel," *Journal of the Mechanics and Physics of Solids*, vol. 27, pp. 363–375, 1979.

[63] Yoshida, F., "Uniaxial and biaxial creep-ratcheting behavior of SUS 304 stainless steel at room temperature," *International Journal of Pressure Vessel And Piping*, vol. 44, pp. 207-223, 1990.

[64] Kang, G.Z., Zhang, J., Sun, Y., Kan, Q.H., "Uniaxial time-dependent ratcheting of SS304 stainless steel at high temperatures," *Journal of Iron and Steel Research, International*, vol. 14, pp. 53-59, 2007.

[65] Fujino, M., Taira S., "Effect of thermal cycling on low cycle fatigue life of steels and grain boundary sliding characteristics," in *Proceeding of ICM 3*, 1979.

[66] Chaboche, J. L., "Life time predictions and cumulative damage under high temperature conditions," in *ASTM STP 770*, Philadelphia, 1982.

[67] Nagesha, A., Valsan, M., Kannan, R., Bhanu Sankara Rao, K., Bauer, V., Christ, H.-J., Vakil Singh., "Thermomechanical fatigue evaluation and life prediction of 316L(N) stainless steel," *International Journal of Fatigue*, vol. 31, pp. 636-643, 2009.

[68] Zauter, R., Christ, H-J., Mughrabi, H., "Some aspects of thermomechanical fatigue of AISI 304L stainless steel: Part I. creep- fatigue damage," *Metallurgical and Materials Transactions A*, vol. 25, pp. 401-406, 1994.

[69] Dutta, K., Sivaprasad, S. Tarafder, S. Ray, K. K., "Influence of asymmetric cyclic

loading on substructure formation and ratcheting fatigue behaviour of AISI 304LN stainless steel," *Material Science and Engineering: A*, vol. 527, pp. 7571-7579, 2010.

[70] Mucke, R., Bernhardi, O-E., "On temperature rate terms for viscoplastic constitutive models with applications to high temperature materials," *Computer Methods in Applied Mechanics and Engineering*, vol. 195, pp. 2411-2431, 2006.

[71] Hasbroucq, S., Oueslati A., Saxce, G., "Inelastic responses of a two-bar system with temperature-dependent elastic modulus under cyclic thermomechanical loadings," *International Journal of Solids and Structures*, vol. 47, pp. 1924-1932, 2010.

[72] Hasbroucq, S., Oueslati, A., Saxce, G., "Analytical study of the asymptotic behavior of a thin plate with temperature-dependent elastic modulus under cyclic thermomechanical loadings," *International Journal of Mechanical Sciences*, vol. 54, pp. 95-104, 2012.

[73] Kuhner, R., Aktaa, J., Angarita, L., Lang, K-H., *The role of temperature rate terms in viscoplastic modelling: theory and experiments , Kuhner, R., Aktaa, J., Angarita, L., Lang, K-H., 200*, H., Maier H.J. Sehitoglu, Ed. Conshohocken: ASTM STP 1371, 2000, vol. 3.

[74] Kobayashi, M., Ohno, N., Igar,i T., "Ratchetting characteristics of 316 FR steel at high-temperature, Part-II-Analysts of thermal ratchetting induced by spatial variation of temperature," *International Journal of Plasticity*, vol. 14, pp. 373-390, 1998.

[75] Delprete, C., Vercelli, A., "A methodology to predict residual life in LCF regime," *Journal of Physics: Conference Series*, vol. 181, p. 012037, 2009.

[76] Jian Peng, Chang-Yu Zhou, Qiao Dai Xiao-Hua He Xiaochun Yu., "Fatigue and ratcheting behaviors of CP-Ti at room temperature," *Materials Science \& Engineering: A*, vol. 590, pp. 329-337, 2014.

[77] Portier, L., Calloch, S., Marquis, D., Geyer, P., "Ratcheting under tension-torsion loadings: Experiments and modelling," *International Journal of Plasticity*, vol. 16, pp. 303-335, 2000.

[78] Wada, H., Kaguchi, H., Ueta, M., Ichimiya, M., Kimura, K., Fukuda, Y., Suzuki, M., "Proposal of a new estimation method for the thermal ratchetting of a cylinder subjected to moving temperature distribution.," *Nuclear Engineering and Design*, vol. 139, pp. 261-267, 1993.

[79] Wada, H., Ueta, M., Ichimiya, M., Ueno, T., Hirayama, H., Takahashi, S., "Proposal of a new estimation method of thermal ratchetting behavior of fast breeder reactor components," *Nuclear Engineering and Design*, vol. 155, pp. 519-526, 1995.

[80] Cabrillat, M.T., Gatt, J.M., "Evaluation of thermal ratchetting on axisymmetric thin shells at the free level of sodium-Inelastic Analysis," in *Proceedings of the 12th International Conference on SMIRT*, vol. Div E, 1993.